https://doi.org/10.5194/egusphere-2026-492
Preprint. Discussion started: 23 April 2026

Improving the CLASSIC (v1.8) Snow Model to Better Simulate Arctic Snowpacks

Mickaël Lalande[1, 2], Alexandre Roy[1, 2], Libo Wang[3], Diana Verseghy[4,*], Vincent Vionnet[5], Florent Dominé[2, 6, 7], and Christophe Kinnard[1, 2]

[1]Centre for Research on Watershed-Aquatic Ecosystem Interactions, Department of Environmental Sciences, Université du Québec à Trois-Rivières, Trois-Rivières, QC, Canada
[2]Centre for Northern Studies, Université Laval, Québec, QC, Canada
[3]Climate Research Division, Environment and Climate Change Canada, Toronto, ON, Canada
[4]Formerly at Climate Research Division, Environment and Climate Change Canada, Toronto, ON, Canada
[5]Meteorological Research Division, Environment and Climate Change Canada, Dorval, QC, Canada
[6]Takuvik Joint International Laboratory, Université Laval (Canada) and CNRS-INSU (France), Québec, QC, Canada
[7]Department of Chemistry, Université Laval, Québec, QC, Canada
[*]retired

Correspondence: Mickaël Lalande (mickael.lalande.phd@gmail.com)

Abstract. This study enhances the snow model of the Canadian Land Surface Scheme including Biogeochemical Cycles (CLASSIC), with a particular focus on Arctic environments. Key snow model physics improvements include adjustments to the thermal conductivity at the top of the first soil layer, a revised computation of the temperature at the snow–soil interface (hereafter, bottom snow temperature), and the addition of a windless exchange coefficient in sensible heat flux calculations. Arctic-specific adaptations include blowing-snow sublimation losses, a new snow compaction scheme, and snow thermal conductivity parameterization. Evaluations at seven mid-latitude and alpine sites (SnowMIP sites) and three Arctic sites (Bylot Island, Umiujaq, and Trail Valley Creek) show that these enhancements improve the overall simulated snowpack characteristics and soil temperatures across both SnowMIP and Arctic sites. The revised bottom snow temperature yields better agreement between simulated and observed snow and bottom snow temperatures. The new windless exchange coefficient reduced the surface temperature RMSE from 3.50 °C to 1.93 °C on average across all sites. The improved snow compaction scheme reduces the snow depth biases from 12.0 cm to 0.1 cm on average across the Arctic sites and improves the simulated snow densities while not degrading the overall model performance at the SnowMIP sites. Blowing-snow sublimation had a negligible effect at most sites, except at the wind-exposed sites of Umiujaq, Trail Valley Creek, and Senator Beck, decreasing snow depth on average by 2-4 cm. Adding a new snow thermal conductivity parameterization—combined with all previous developments—reduces the RMSE of the simulated soil temperatures from 5.3 °C to 3.0 °C on average at all Arctic sites. Our new developments demonstrate the ability of a single-layer snow model to reasonably reproduce Arctic bulk snowpack characteristics, while maintaining good performance at the SnowMIP sites. Inherent uncertainties remain in the forcing datasets, especially due to the harsh Arctic environment characterized by strong winds, snow redistribution, frost, and polar night. Future model developments will focus on spatial-scale simulations across the whole Arctic, with particular attention to snow cover fraction parameterizations to better capture sub-grid-scale spatial heterogeneity in Arctic environments.

https://doi.org/10.5194/egusphere-2026-492
Preprint. Discussion started: 23 April 2026

1 Introduction

During winter, snow covers up to 40 % of the Northern Hemisphere (NH) land surface, predominantly in mid- to high-latitude regions (Robinson and Frei, 2000; Lemke et al., 2007). Its presence and characteristics profoundly impact regional and global climate dynamics (e.g., Vernekar et al., 1995; Xu and Dirmeyer, 2011; Cohen et al., 2012), as snow plays a critical role in land-atmosphere interactions, particularly due to its high albedo, which reflects a large portion of incoming shortwave radiation (Flanner et al., 2011). Due to its low thermal conductivity, snow insulates the underlying soil in winter, which strongly influences the soil temperature regime and thus the thermal state of permafrost and its carbon balance (Groffman et al., 2001; Zhang, 2005; Vavrus, 2007; Cook et al., 2008; Gouttevin et al., 2012; Park et al., 2015; Campbell and Laudon, 2019; Mavrovic et al., 2023). In addition, snow influences the ecosystems by protecting low vegetation in winter from frost damage (Sturm et al., 2001), conditioning the springtime onset of the growing season (Pulliainen et al., 2017), and affecting Arctic animals such as caribou and lemmings (e.g., Domine et al., 2018b; Pedersen et al., 2021). It also significantly contributes to the hydrological cycle in cold regions, where its accumulation and melt control the timing and magnitude of spring runoff, impacting water resources and ecosystem dynamics (e.g., Barnett et al., 2005; Bring et al., 2016).

Climate change is altering snow conditions, particularly in the Arctic regions, which are warming significantly faster than the global average (Stuecker et al., 2018; Rantanen et al., 2022). These changes affect the hydrological cycle, infrastructures, and ecosystems (Bokhorst et al., 2016; Bring et al., 2016). Carbon stocks in the Arctic permafrost are important because they contain nearly twice as much carbon as the atmosphere, and their thawing could release large amounts of greenhouse gases, amplifying climate change (Schuur et al., 2022). This stresses the need to better simulate carbon fluxes of these ecosystems in response to climate change, including the snow cover, which greatly affects these fluxes through its impact on soil temperature (Natali et al., 2019; Miner et al., 2022; Mavrovic et al., 2023). Noticeable reductions in global snow mass and extent have been documented over the last decades, albeit with marked regional variability (Liston and Hiemstra, 2011; Pulliainen et al., 2020; Mohammadzadeh Khani et al., 2022), and are projected to continue into the 21st century (Bring et al., 2016; Mudryk et al., 2018, 2020). It is therefore crucial to adequately simulate snow cover across all environments, particularly in the Arctic, where amplified warming and the vulnerability of substantial permafrost carbon stocks pose significant climate feedback risks (e.g., Burke et al., 2017; Comyn-Platt et al., 2018; Yokohata et al., 2020).

Snow models have been developed with varying degrees of complexity depending on the intended application (e.g., Magnusson et al., 2015; Terzago et al., 2020). Land surface models (LSMs) embedded in general circulation models (GCMs) include snow schemes varying from simple single-layer snow models (Manabe, 1969; Verseghy, 1991; Douville et al., 1995) to medium-complexity multi-layer ones taking into account additional processes such as snow compaction, water percolation, and refreezing (e.g., Loth et al., 1993; Lynch-Stieglitz, 1994; Sun et al., 1999; Boone and Etchevers, 2001; Dai et al., 2003; Yang and Niu, 2003; Xue et al., 2003; Dutra et al., 2010; Shrestha et al., 2010; Best et al., 2011; Wang et al., 2013; Decharme et al., 2016). However, most of these models have been designed for alpine snowpacks and do not adequately simulate Arctic snowpack characteristics (Domine et al., 2019).

https://doi.org/10.5194/egusphere-2026-492
Preprint. Discussion started: 23 April 2026

Arctic snowpacks are exposed to extreme weather conditions with low precipitation, cold temperatures, and high wind speeds over exposed landscapes. This results in a shallow snowpack shaped by wind-induced compaction of the upper layers, forming a dense "wind slab" at the top of the snowpack. Meanwhile, strong vertical temperature gradients arise within the snowpack—especially during autumn, when unfrozen soils coexist with very cold air temperatures—inducing an upward moisture flux leading to the formation of depth hoar in the lower part of the snowpack with low-density and large snow grain size (Sturm et al., 1997; Domine et al., 2015, 2016; Gouttevin et al., 2018). In contrast, snowpacks in mid-latitude alpine environments are generally thicker and characterized by smaller vertical temperature gradients, such that compaction of the lower snow layers under the weight of the overlying snow becomes the dominant process. Consequently, even the most detailed snow models developed for alpine environments, such as Crocus (Vionnet et al., 2012), SNOWPACK (Bartelt and Lehning, 2002; Lehning et al., 2002b, a), and SnowModel (Liston et al., 2020) fails in simulating the vertical profile of snow properties in Arctic snowpacks (e.g., Barrere et al., 2017; Gouttevin et al., 2018; Royer et al., 2021b).

Solutions have been explored, such as introducing explicit moisture fluxes within the snowpacks (e.g., Jafari et al., 2020; Simson et al., 2021; Jafari et al., 2022; Brondex et al., 2023). However, this option is still under exploration, as it presents significant challenges related to computational scheme and cost arising from the complexity of coupling the moisture fluxes with snowpack dynamics and thermodynamics. Alternatively, modifications have been introduced to overcome the lack of water vapor transport, such as increasing the maximum density of wind-induced snow compaction of the upper snowpack layers and reducing the density of the lower layers. This considerably improved the simulated density profiles and made them more comparable to observations at site scales (e.g., Barrere et al., 2017; Gouttevin et al., 2018; Royer et al., 2021b; Lackner et al., 2022; Woolley et al., 2024). However, these modifications remain site-specific, having often been calibrated to one or a few Arctic sites, and have not been designed for global applicability.

Whether multiple snow layers are needed to accurately simulate bulk snowpack properties and the thermal regime of underlying soil in climate models, and if so, how many, remains an open question in the snow modelling community (e.g., Essery et al., 2013; Augas et al., 2020; Cristea et al., 2022). Domine et al. (2019) have shown with an ideal snow modeling case study that as long as the bulk thermal resistance of the snowpack is well simulated, having an inverted density profile has little impact on ground and surface temperatures (averaged over several days). However, Gouttevin et al. (2018) and Royer et al. (2021b) showed that the adaptations made to simulate Arctic snowpacks in Crocus and SNOWPACK tended to modify the bulk snow density and thermal conductivity, thus impacting soil temperatures.

The Canadian Land Surface Scheme including Biogeochemical Cycles (CLASSIC; Melton et al., 2020; Seiler et al., 2021) is the LSM used within the Canadian Earth System Model (CanESM; Swart et al., 2019) used for climate change impact assessments (e.g., Eyring et al., 2016; IPCC, 2021; Mudryk et al., 2020). CLASSIC includes a one-layer snow model that demonstrates comparable performance to the most detailed snow models in terms of bulk snow properties according to the Snow Models Intercomparison Project (SnowMIP; Etchevers et al., 2004; Krinner et al., 2018; Menard et al., 2021). However, the SnowMIP evaluation sites do not include "true" Arctic sites—apart from Sodankylä in Finland (67.368° N; Essery et al., 2016), which lies at the border of the boreal forest and is not characterized by typical Arctic snowpack conditions. Therefore,

https://doi.org/10.5194/egusphere-2026-492
Preprint. Discussion started: 23 April 2026

evaluating the CLASSIC snow model at Arctic sites is crucial in order to ascertain whether its simple single-layer snow scheme can capture key snowpack processes in this environment.

This study aims to evaluate and improve the current 1D physics of the CLASSIC snow model worldwide, with a particular focus on the Arctic, using offline land simulations driven by observed meteorological forcing at seven SnowMIP sites and three additional Arctic sites. We aim to address the following questions: (1) Can a single-layer snow model reproduce the bulk characteristics of Arctic snowpacks? (2) What effect do the adaptations for Arctic conditions have on the model performance elsewhere (e.g., mid-latitude Alpine snowpacks)? (3) How do those adaptations impact the simulated soil temperatures and carbon fluxes? The data and methods are presented in Sect. 2. The results are presented in Sect. 3, and discussed in Sect. 4. The conclusion is presented in Sect. 5.

2 Data and Methods

2.1 SnowMIP and Arctic sites

CLASSIC requires the following seven meteorological forcings: incoming short- and long-wave radiation, near-surface air temperature, wind speed, specific humidity, total precipitation rate (and optionally snowfall rate), and air pressure. Both total precipitation and snowfall rates were prescribed at all sites to minimize uncertainties related to snow accumulation. The quality-controlled and standardized SnowMIP data are used, which combine meteorological forcings and snow measurements such as snow depth, snow water equivalent, albedo, surface and soil temperatures, depending on sites (Krinner et al., 2018; Ménard et al., 2019; Menard et al., 2021). Additionally, three Arctic sites are considered in this study: Bylot Island (Domine et al., 2021a), Umiujaq TUNDRA (Domine et al., 2024b), and Trail Valley Creek (Dutch et al., 2022) (Fig. 1). The boreal SnowMIP sites (Old Aspen, Old Black Spruce, and Old Jack Pine) are excluded from our study because of the uncertainties due to snow canopy processes, which are out of the scope of this work. All sites are described in Table 1. More information about site initialization and variables is available in the Supplement Tables S1, S2, and S3.

The relative humidity at Umiujaq and TVC was converted to specific humidity as an input for CLASSIC (see Sect. 2 of the Supplement). The data from Umiujaq FOREST were not used because of the uncertainties related to snow trapping by tall vegetation (tall shrubs and black spruce) (Domine et al., 2024b). At the Umiujaq TUNDRA, soil data are available separately for the shrub and lichen subareas but were averaged here, as the snow measurements and meteorological forcing are based on a single location between the two subareas. To best match the observations, the plant functional type at this site was prescribed in the model as 50 % broadleaf deciduous cold shrub (*Betula glandulosa*) and 50 % bare soil, as lichen is not currently represented as a plant functional type in CLASSIC (Table S1). At all Arctic sites, a fibric peat layer (Letts et al., 2000) was prescribed in the uppermost soil layer (top 10 cm) to partially alleviate the absence of explicit lichen and moss representations in CLASSIC and to mimic the insulating properties of the lichen or moss layers present at these sites. This imperfect solution is further discussed in Sect. 4.5. The thickness of the peat layer (10 cm) was set to best match the observed amplitude of summer soil temperatures and soil water content (not shown). When needed, the simulated soil variables (soil temperature and soil water

https://doi.org/10.5194/egusphere-2026-492
Preprint. Discussion started: 23 April 2026

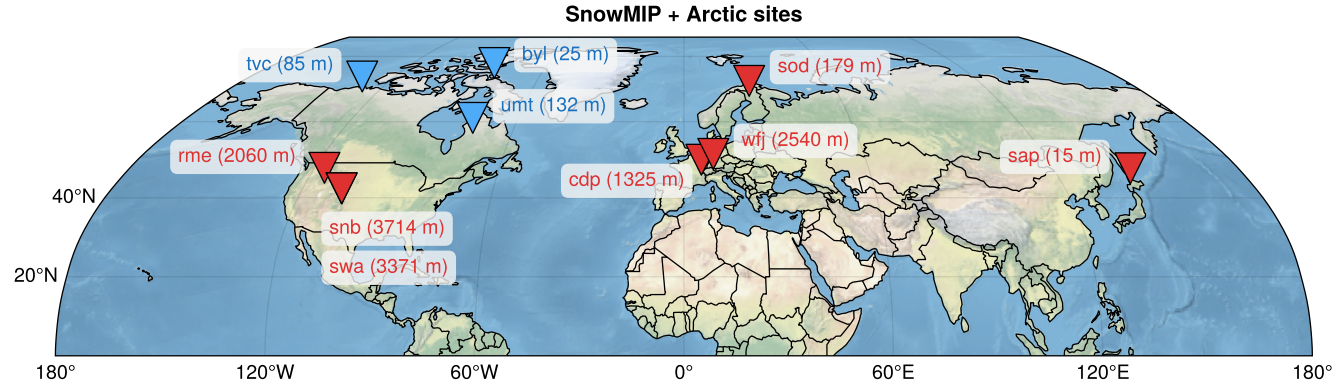

Figure 1. Map showing the locations of the SnowMIP (red; cdp: Col de Porte, rme: Reynolds Mountain East, snb: Senator Beck, swa: Swamp Angel, sap: Sapporo, sod: Sodankylä, wfj: Weissfluhjoch) and Arctic sites (blue; byl: Bylot Island, umt: Umiujaq TUNDRA, tvc: Trail Valley Creek) with the Natural Earth background (license: public domain). Site elevations are indicated in brackets. See Table 1 for further information about the sites.

content) were linearly interpolated to the first observational measurement depth greater than or equal to 5 cm (corresponding to the center of the first model soil layer) for comparison with observations.

At TVC, the dataset used in Woolley et al. (2024) was not publicly available at the time of this study; therefore, we relied on the forcing data from Dutch et al. (2022), which span a two-year period. As only total precipitation was provided, rainfall and snowfall rates were estimated using the suggested temperature threshold of 1 °C from Woolley et al. (2024). The station location itself may act as a local snow accumulation zone, leading to measured snow depths that are likely larger than those representative of the surrounding tundra (Brampton Dakin and Georgina Woolley, personal communication, 2023). Furthermore, since the initial simulated snow depth was too low, and the snow density underestimated compared to snow pit measurements, we adjusted the snowfall rate in Dutch et al. (2022) to match the snow depth at peak snow accumulation in our simulations including our new Arctic snow model developments (corresponding to a scaling of the snowfall rates by a factor of two; Fig. S1a–d blue and green lines in Sect. 3 of the Supplement), which will be further discussed in Sect. 4.4. The updated dataset used in Woolley et al. (2024) is expected to provide improved forcing data and may help resolve these snowfall rate uncertainties in future studies.

The precipitation at Umiujaq was measured only from 2016 onward, and ERA5 data are used prior to that (Domine et al., 2024b). Therefore, only the period after 2016 is considered for the model evaluation. The albedo at the Arctic sites can be retrieved from the incoming and outgoing shortwave radiation measurements. However, due to frost-related issues with the instruments, some data are inaccurate and gap-filled, often leading to unrealistic values; therefore, the simulated albedo will not be assessed against observations at those sites. All data provided are quality-controlled and use snowfall wind undercatch corrections. Further in-depth discussion on the measurement uncertainties is addressed in Sect. 4.4. The snow depth time series at all sites are shown in Fig. A1.

https://doi.org/10.5194/egusphere-2026-492
Preprint. Discussion started: 23 April 2026

Table 1. SnowMIP (cdp, rme, snb, swa, sap, sod, wfj) and Arctic (byl, umt, tvc) sites. More information about site initialization and variables is available in the Supplement Tables S1, S2, and S3, respectively. Further information about SnowMIP sites is available at: https://www.geos.ed.ac.uk/~ressery/ESM-SnowMIP/ESMSnowMIP_Reference_sites.pdf (last access: 12 March 2024).

Site	Site (short)	Latitude	Longitude	Elevation	Period used	Type	Reference
Col de Porte, France	cdp	45.30° N	5.77° E	1325 m	1994—2014	Alpine	Morin et al. (2012); Lejeune et al. (2019)
Reynolds Mountain East, USA	rme	43.06° N	116.75° W	2060 m	1988—2008	Alpine	Reba et al. (2011)
Senator Beck, USA	snb	37.91° N	107.73° W	3714 m	2005—2015	Alpine	Landry et al. (2014)
Swamp Angel, USA	swa	37.91° N	107.71° W	3371 m	2005—2015	Alpine	Landry et al. (2014)
Sapporo, Japan	sap	43.08° N	141.34° E	15 m	2005—2015	Maritime	Niwano et al. (2012)
Sodankylä, Finland	sod	67.37° N	26.63° E	179 m	2007—2014	Taiga	Essery et al. (2016)
Weissfluhjoch, Switzerland	wfj	46.83° N	9.81° E	2540 m	1996—2016	Alpine	Wever et al. (2015); Wever (2017)
Bylot Island, Canada	byl	73.15° N	80.00° W	25 m	2014–2019	Arctic	Domine et al. (2021a)
Umiujaq TUNDRA, Canada	umt	56.56° N	76.48° W	132 m	2016–2021	Arctic	Domine et al. (2024b)
Trail Valley Creek, Canada	tvc	56.55° N	76.47° W	82 m	2017–2019	Arctic	Dutch et al. (2022); Boike et al. (2023)

https://doi.org/10.5194/egusphere-2026-492
Preprint. Discussion started: 23 April 2026

2.2 CLASSIC and model developments

This study introduces three snow model physics improvements: (1) a correction of the computation of the thermal conductivity at the top of the first soil layer (Sect. 2.3.1), (2) a revised computation of the bottom snow temperature (Sect. 2.3.2), and (3) the addition of a windless exchange coefficient within the sensible heat flux calculation (Sect. 2.3.3). Furthermore, three Arctic-specific snowpack adaptations are proposed: (1) the inclusion of blowing-snow sublimation losses (Sect. 2.4.1), (2) a revised compaction scheme (Sect. 2.4.2), and (3) a modification of the snow thermal conductivity parameterization (Sect. 2.4.3). All details about the code implementation are available in Sect. 4 of the Supplement.

2.2.1 General model description

In this study, we use the Canadian Land Surface Scheme Including Biogeochemical Cycles (CLASSIC v1.8; Melton et al., 2020) that is based on the coupled Canadian Land Surface Scheme (CLASS; Verseghy et al., 2017) and the Canadian Terrestrial Ecosystem Model (CTEM; Melton and Arora, 2016). The physical component (formerly CLASS) operates at a time step of up to 30 minutes and includes 20 soil layers up to 61 m depth. The vertical energy and water fluxes are modeled separately for four subareas in each grid cell: vegetated, bare soil, vegetated with snow cover, and bare soil with snow cover. The biogeochemistry component (formerly CTEM) provides the model physics with dynamically simulated vegetation structural attributes—such as leaf area index (LAI), vegetation height, and rooting depth. The model represents vegetation using twelve plant functional types (PFTs) for biogeochemical processes (including three PFTs—sedges and evergreen/cold-deciduous shrubs—introduced by Meyer et al. (2021) in addition to the 9 PFTs used in CLASSIC v1.0), which are aggregated into five PFTs for the physical component.

2.2.2 Snow model description

Snow in CLASSIC is modeled as a single layer, with thermal properties distinct from the underlying soil. A fitted quadratic temperature curve is assigned within the snow layer as a first-order method of accounting for the characteristic sharp near-surface temperature gradient in snowpacks. The snow albedo decreases, and the snow density increases exponentially with time from fresh snow values according to empirically derived functions (Brown et al., 2006; Verseghy et al., 2017). The fresh snow density is determined as a function of the air temperature (Pomeroy and Gray, 1995). The snow thermal conductivity is derived from the snow density (Sturm and Benson, 1997). Melting of the snow layer can occur either from above (in response to surface energy fluxes) or from below (in response to conduction from the underlying soil); if melting occurs at the top, percolation and refreezing of meltwater in the snowpack occur until the snow is isothermal at 0 °C, after which meltwater can infiltrate into the soil. Water retention in snowpacks is taken into account (Bruce and Clark, 1966). The interception of snowfall by vegetation is explicitly modeled, with the interception capacity depending on the vegetation leaf area index (Hedstrom and Pomeroy, 1998; Bartlett et al., 2006; Bartlett and Verseghy, 2015). The snow cover fraction (SCF) is considered complete (100 %) when the average snow depth (d_s) reaches 0.1 m. When d_s is lower than this threshold, the SCF is calculated as $\frac{d_s}{0.1}$ and d_s is reset to 0.1 m over the subfraction covered by snow (following snow mass conservation). More details on the previous

https://doi.org/10.5194/egusphere-2026-492
Preprint. Discussion started: 23 April 2026

CLASS snow model developments and evaluations are available in Bartlett et al. (2006); Brown et al. (2006); Langlois et al. (2014); and Verseghy et al. (2017).

2.3 Snow model: physics improvements

2.3.1 Thermal conductivity at the top of the first soil layer

In CLASSIC, the effective thermal conductivity at the top of the first soil layer (λ_0) below the snowpack is computed as the harmonic mean of the thermal conductivity at the top of the first soil layer ($\lambda_{1,t}$) and that of the snowpack (λ_s) as follows:

$$\lambda_0 = \frac{1}{\frac{0.5}{\lambda_s} + \frac{0.5}{\lambda_{1,t}}}. \quad (1)$$

However, when snow cover is partial ($0 < SCF < 100$ %), Eq. 1 was applied uniformly across all grid-cell subareas, including both snow-covered and snow-free fractions. As a result, the effective thermal conductivity at the top of the first soil layer over snow-free areas was underestimated, leading to an overestimated insulating effect under snow-free conditions when $SCF < 100$ %. This issue was corrected in this study: Eq. 1 is applied only to snow-covered subareas, while $\lambda_0 = \lambda_{1,t}$ is prescribed for snow-free subareas. More details are available at: https://gitlab.com/cccma/classic/-/issues/119 (last access: 10 October 2025).

2.3.2 Bottom snow temperature

The bottom snow temperature $T_{s,b}$—defined as the temperature at the interface between the snowpack and the soil—was estimated as an average of the first soil layer T_1 and snow T_s temperature weighted by their depth d_1 and d_s respectively, as follows (https://gitlab.com/cccma/classic/-/blob/CLASSICv1.0/src/snowTempUpdate.f90?ref_type=tags#L139; last access: 10 October 2025):

$$T_{s,b} = \frac{d_s T_s + d_1 T_1}{d_s + d_1}. \quad (2)$$

This bottom snow temperature serves as the boundary condition for computing the ground heat flux and then updating the snow and soil temperatures via the quadratic temperature profile (https://cccma.gitlab.io/classic/snowTempUpdate_8f90.html and https://cccma.gitlab.io/classic/soilHeatFluxPrep_8f90.html, last access: 10 October 2025). However, this equation tended to underestimate the simulated bottom snow temperature and induce an overestimated snow temperature compared to observations (see results in Sect. 3.1.2). Indeed, as the snowpack thickens, its insulating effect increases; as a result, the bottom snow temperature becomes less influenced by the snowpack's bulk (average) temperature and instead approaches the temperature of the underlying soil layer (fixed thickness of 10 cm). The underestimated simulated bottom snow temperature induces, in turn, an overestimated conductive heat flux from the soil into the snowpack (especially at the beginning of the winter). A better option was implemented by weighting the soil and snow temperatures with the inverse depth of the snow and

https://doi.org/10.5194/egusphere-2026-492
Preprint. Discussion started: 23 April 2026

soil layers, respectively (improved results are presented in Sect. 3.1.2 and Appendix B):

$$T_{s,b} = \frac{\frac{T_s}{d_s} + \frac{T_1}{d_1}}{\frac{1}{d_s} + \frac{1}{d_1}}. \tag{3}$$

2.3.3 Windless exchange coefficient

Brown et al. (2006) reports that "*a number of studies have shown that the traditional Monin-Obukhov similarity theory is unable to explain turbulent energy exchanges over snow and ice surfaces under stable atmospheric conditions (King, 1990; Morris et al., 1994; Yen, 1995; Martin and Lejeune, 1998). Under these conditions, turbulence does not shut down completely and is characterized by intermittent bursts. [...] This has prompted a range of solutions, including the introduction of a "windless transfer coefficient" into sensible heat calculations (Jordan et al., 1999)*". For a comprehensive review of this issue, see Sect. 4e of Brown et al. (2006). This deficiency led to a cold bias in simulated snow surface temperatures, particularly during nighttime temperature inversions, reaching up to about 10 °C in CLASS v3.1 (Fig. 11 of Brown et al. (2006), thin solid line). A similar behavior was observed in CLASSIC at most SnowMIP sites (not shown), resulting in an average cold bias of approximately 2 °C in daily simulated snow surface temperature (see results in Sect. 3.2.2). Brown et al. (2006) alleviated this bias by introducing a windless transfer coefficient (E_0) into the sensible heat flux formulation (Q_H) as follows:

$$Q_H = (\rho_{\text{air}}\, c_P\, C_H\, U + E_0)\,(T_s - \theta_a)\,, \tag{4}$$

where ρ_{air} is the density of air (kg m^{-3}), c_P is the specific heat capacity of air (set to $1.00464 \cdot 10^3$ J kg^{-1} K^{-1} in CLASSIC), C_H is the surface drag coefficient (unitless), U the wind speed at reference height (m s^{-1}), T_s the surface temperature (K), and θ_a the potential air temperature at the reference height (K). E_0 is set to 2 W m^{-2} K^{-1} when $T_s < \theta_a$ (i.e., for atmospheric stable condition) and 0 W m^{-2} K^{-1} otherwise. This correction is applied only over non-vegetated subareas. Following Brown et al. (2006)'s study, this windless transfer coefficient was not activated by default in CLASSIC, as it was tested at only a limited number of sites. The present study extends this evaluation to the selected SnowMIP and Arctic sites.

2.4 Snow model: Arctic adaptations

2.4.1 Blowing-snow sublimation losses

The blowing-snow sublimation loss parameterization of Gordon et al. (2006) is implemented. It computes the blowing-snow sublimation rate as a function of near-surface meteorological conditions when the wind speed exceeds the threshold for snow transport. This empirical formulation was derived by averaging sublimation rates from several existing models and parameterizations—including the Prairie Blowing Snow Model (PBSM; Pomeroy et al., 1993). The total sublimation rate Q_s [kg m^{-2} s^{-1}] is defined as:

$$Q_s = 0.0018 \left(\frac{T_0}{T_{\text{air}}}\right)^4 U_t\, \rho_a\, q_{si}\, (1 - RH_i) \left(\frac{U_{10}}{U_t}\right)^{3.6}, \quad \text{for } U_{10} > U_t \text{ and } T_{\text{air}} < T_0, \tag{5}$$

https://doi.org/10.5194/egusphere-2026-492
Preprint. Discussion started: 23 April 2026

with:

$$U_t = 6.98 + 0.0033\,(T_{\text{air}} - 245.88)^2\,, \tag{6}$$

where U_t [m s^{-1}] is the threshold wind speed at 10 m for the initiation of blowing snow, T_{air} is the near-surface air temperature [K], T_0 is the freezing point of water (defined as 273.16 °K in CLASSIC), ρ_a is the density of air [kg m^{-3}], q_{si} is the saturation specific humidity of ice at reference height [kg kg^{-1}], RH_i is the relative humidity with respect to ice [fraction], U_{10} is the wind speed at 10 m above the snow surface [m s^{-1}]. This equation is applied only to bare-ground subareas covered with snow (i.e., to bare ground and to subareas where snow buries vegetation). The blowing-snow sublimation losses from the intercepted snow on the canopy are not considered.

2.4.2 Snow compaction

The aim of modifying the compaction scheme is to represent first-order Arctic snow densification processes, including depth hoar and wind slab formation, in a "bulk" approach. Initial results revealed that CLASSIC tended to underestimate snow density and overestimate snow depth at the Arctic sites (see results in Sect. 3.1.3). Indeed, Arctic snowpacks tend to be characterized by shallow snow depth (usually less than 0.5 m) composed of a low-density depth hoar layer ($\simeq$ 250 kg m^{-3}) overlain with denser wind slabs (>300 kg m^{-3}), while the average bulk snow densities tends to have high values ranging from about 250 to 400 kg m^{-3} (e.g., Gouttevin et al., 2018; Domine et al., 2021a; Royer et al., 2021a). Consequently, several parameters controlling snow compaction—such as fresh snow density, maximum snow density, and compaction rate—can be adjusted to better represent Arctic bulk snow densities.

Fresh snow density

CLASSIC's fresh snow density ρ_i is based on the equations of Pomeroy and Gray (1995) and Pomeroy et al. (1998) for temperatures above and below 0 °C respectively:

$$\rho_i = \begin{cases} 67.92 + 51.25 \exp\left(\dfrac{T_{\text{air}}}{2.59}\right), & T_{\text{air}} \leq 0°\text{C}, \\ \min(200,\, 119.17 + 20.0\,T_{\text{air}})\,, & T_{\text{air}} > 0°\text{C}. \end{cases} \tag{7}$$

New parameterizations such as the ones based on CROCUS (Vionnet et al., 2012), SNOWPACK (Lehning et al., 2002b), or SnowTran-3D (Liston et al., 2007) based on relative humidity, (wet-bulb) air temperature, and/or wind speed were tested, including their "Arctic-tuned" versions (e.g., Royer et al., 2021b; Walter et al., 2024). However, none of those new, fresh snow density equations brought significant improvements over time in CLASSIC at the Arctic sites, and they worsened its performance at the SnowMIP sites (not shown). Indeed, they mostly increase the fresh snow density at the start and end of the season for the Arctic sites when air temperatures are in the range of -10 to 0 °C, but have a negligible impact over most of the snow season, because the temperature term dominates over the wind term under very cold (below -20 to -30 °C) conditions. So Eq. 7 was kept unchanged in this study despite its non-consideration of the wind speed.

https://doi.org/10.5194/egusphere-2026-492
Preprint. Discussion started: 23 April 2026

Maximum snow density

The snow density ρ_s in CLASSIC increases exponentially towards a maximum snow density $\rho_{\max}$ as follows:

$$\rho_s(t+1) = [\rho_s(t) - \rho_{\max}] \exp\left(-\frac{0.01\Delta t}{3600}\right) + \rho_{\max}, \tag{8}$$

with:

$$\rho_{\max} = 450 - \frac{204.7}{d_s}\left[1.0 - \exp\left(-\frac{d_s}{0.673}\right)\right] \quad \text{for } T_s < 0°\text{C and,} \tag{9}$$

$$\rho_{\max} = 700 - \frac{204.7}{d_s}\left[1.0 - \exp\left(-\frac{d_s}{0.673}\right)\right] \quad \text{for } T_s = 0°\text{C,} \tag{10}$$

where d_s is the snow depth [m], T_s the snow temperature [°C], and Δt the model time step [s]. The maximum snow density formulations are based on Tabler et al. (1990), with additional temperature threshold and enhanced settling rates determined empirically (Brown et al., 2006, unpublished manuscript, 2001). However, the maximum snow density values for dry snow (Eq. 9) do not reflect actual measured snow densities in Arctic environments under strong wind conditions, where values can reach 250–400 kg m^{-3} for thin snowpacks (< 1 m) (e.g., Domine et al., 2021a; Royer et al., 2021a). Indeed, those observed values are above the maximum snow density defined by Brown et al. (2006): e.g., 235.4 kg m^{-3} for a typical Arctic snowpack height of 50 cm (Fig. 2, shaded blue curve). The following equations are thus proposed to take into account the effect of wind on the maximum snow density for dry snow:

$$\rho_{\max} = 430 - \frac{204.7}{d_s}\left[1.0 - \exp\left(-\frac{d_s}{0.673}\right)\right] \quad \text{for } T_s < 0°\text{C and } U < 2.5\ \text{m s}^{-1}\ (= \rho_{\text{no wind}}) \text{ and,} \tag{11}$$

$$\begin{aligned}\rho_{\max} &= \rho_{\text{no wind}} + (\rho_{\text{wind}} - \rho_{\text{no wind}}) \exp\left[-\frac{(d_s - d_0)^2}{2\sigma^2}\right] \quad \text{for } T_s < 0°\text{C and } U \geq 2.5\ \text{m s}^{-1} \\ &= 430 - \frac{204.7}{d_s}\left[1.0 - \exp\left(-\frac{d_s}{0.673}\right)\right]\left\{1 - \left[1 - \exp\left(-\frac{U}{U_0}\right)\right]\exp\left[-\frac{(d_s - d_0)^2}{2\sigma^2}\right]\right\},\end{aligned} \tag{12}$$

with:

$$\rho_{\text{wind}} = 430 - \frac{204.7}{d_s}\left[1.0 - \exp\left(-\frac{d_s}{0.673}\right)\right]\exp\left(-\frac{U}{U_0}\right), \tag{13}$$

where U is the wind speed at 2 m above the snowpack [m s^{-1}], $U_0 = 2.5$ m s^{-1} (or 3.5 m s^{-1} for the TVC adjusted version; see Sects. 2.5 and 2.6), $d_0 = 0.8$ m, and $\sigma = 1.0$ m. The constant 450 is reduced to 430 to better fit the observations across all sites, given the increased wind compaction during wind events. The wind-induced compaction is only applied over the bare ground subfraction (i.e., over non-vegetated subareas and/or when the snow entirely buries the vegetation) as we consider that there is no further snow compaction within the canopy. Over the vegetated subarea $\rho_{\text{no wind}}$ (Eq. 11) is maintained regardless of the wind speed. We adjust the wind speed provided at specific measurement heights to 2 m above the snowpack in the model using a logarithmic wind profile (Sect. 5 in the Supplement). For wet snow, Eq. 10 is kept unchanged.

https://doi.org/10.5194/egusphere-2026-492
Preprint. Discussion started: 23 April 2026

Figure 2 shows Eqs. 9 (shaded blue), 11 (blue), 12 (red), and 13 (green) for different wind speed and U_0 values. The wind-induced compaction term (Eq. 13; green curves) increases the snow density for thin snowpacks proportionally to the wind speed. However, it also affects thick snowpacks, where gravitational and metamorphic compaction dominate over wind effects, and, when used as is, it degrades model skill at SnowMIP sites (not shown). Eq. 12 (red curves) introduces a Gaussian formula that peaks around an optimized value of 80 cm towards this wind-induced compaction term ρ_{wind} (Eq. 13) and tends towards $\rho_{\text{no wind}}$ (Eq. 11) for values lower and higher than 80 cm of snow depth. This enables the indirect consideration of depth hoar in very thin snowpacks, while affecting less snowpacks with a thickness greater than 2 to 3 m.

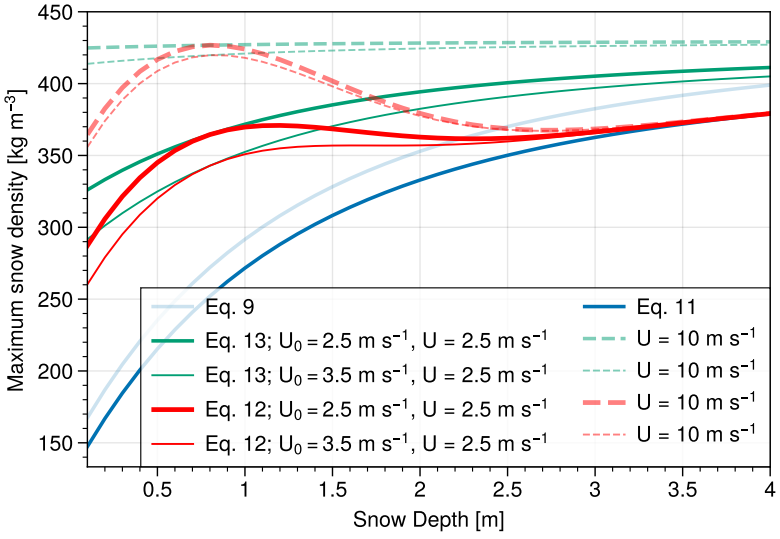

Figure 2. Maximum snow density with respect to snow depth for dry snow of Eqs. 9 (shaded blue), 11 (blue), 12 (red), and 13 (green). The solid and dashed green lines represent wind speeds of 2.5 and 10 m s^{-1} respectively, as an example. The thick and thin red and green lines represent, respectively, the U_0 values of 2.5 and 3.5 m s^{-1} optimized without or with TVC (see Sects. 2.5 and 2.6).

Compaction rate

Alternatively, the compaction rate could also be increased, either alone or in combination with increasing the fresh snow density and/or the maximum snow density (e.g., Royer et al., 2021b; Woolley et al., 2024). However, no further improvements were observed compared to increasing the maximum snow density alone, which can indirectly account for these processes. This will be further discussed in Sect. 4.3.

https://doi.org/10.5194/egusphere-2026-492
Preprint. Discussion started: 23 April 2026

2.4.3 Snow thermal conductivity

The current CLASSIC snow thermal conductivity parameterization is based on Sturm and Benson (1997):

$$\lambda_s = \begin{cases} 0.234 \times 10^{-3}\,\rho_s + 0.023, & \rho_s < 156\ \mathrm{kg\,m^{-3}}, \\ 3.233 \times 10^{-6}\,\rho_s^2 - 1.01 \times 10^{-3}\,\rho_s + 0.138, & \rho_s \geq 156\ \mathrm{kg\,m^{-3}}, \end{cases} \tag{14}$$

with λ_s the snow thermal conductivity [W m^{-1} K^{-1}], and ρ_s the snow density [kg m^{-3}]. We propose a more recent formulation based on Calonne et al. (2011):

$$\lambda_s = 2.5 \times 10^{-6}\,\rho_s^2 - 1.23 \times 10^{-4}\,\rho_s + 0.024, \tag{15}$$

This new parameterization has the advantage of having been calibrated with high-resolution three-dimensional images of snow microstructure, covering a wide range of seasonal snow types—including wind slabs and depth hoar. The sample size in Calonne et al. (2011) is smaller than in Sturm and Benson (1997); however, this approach provides a more reliable, physics-based representation of snow properties by directly capturing the microstructural geometry, compared to the heated-needle probe method, which has known limitations (Fourteau et al., 2022).

2.5 Simulation setup

This study uses CLASSIC v1.8 (Melton et al., 2020). The meteorological forcings at all sites described in Sect. 2.1 were used to force the model in 1D point-scale simulations and were linearly interpolated from 1h to the chosen 30-minute model physics time step. CLASSIC requires full-year forcing files; therefore, the forcing data were extended at both the beginning and end of the time series by replicating the first and last available full years over any missing periods, and analyses were carried out only on the available data period. All the forcing files were provided in local time or were converted to local time.

The soil texture (sand, clay, and organic matter content) was prescribed based on site information when available (Tables 1 and S2 in the Supplement) and complemented with the global gridded dataset SoilGrids250m version 1 (Hengl et al., 2017) when needed. Soil permeable depth and soil color index were prescribed with the nearest grid cell of the gridded dataset from Hengl et al. (2017) and Shangguan et al. (2017). The PFTs were prescribed with site information (Table 1 and S1 in the Supplement). The proportions of C3 and C4 grasses were derived from Still et al. (2003). The model was run with the biogeochemistry component (CTEM) enabled, allowing vegetation to evolve dynamically and CO_2 fluxes to be simulated. The methane and nitrogen cycle, fire, competition, and dynamic tiling options were not activated in our run (the default options in the current CLASSIC version). The CO_2 forcing was derived from Friedlingstein et al. (2023). Further information is available in Sect. 1 of the Supplement.

A first spin-up phase was performed at all sites over 100 to 300 years by looping over the forcing files (with an accelerated carbon pool storage—*spinfast* parameter set to 10) until reaching the equilibrium in the carbon pools. A final spin-up phase was performed on the same duration with the *spinfast* parameter set to 1 to ensure the conservation of carbon (see Sect. 6 of the Supplement for further details on the spin-up procedure). During the spin-up phases, the CO_2 concentration was held constant

https://doi.org/10.5194/egusphere-2026-492
Preprint. Discussion started: 23 April 2026

at the value corresponding to the first year of the meteorological forcing file specific to each station; then, for the runs, the CO_2 concentration evolved on an annual basis, following the values from Friedlingstein et al. (2023).

Table 2 presents the set of experiments conducted at the SnowMIP and Arctic sites, designed to sequentially test the improvements and modifications introduced above in the CLASSIC snowpack scheme (Sect. 2.3 and 2.4).

Table 2. Description of all experiments.

Experiment	Description
DEF	Default model version
TCZERO	*DEF* with the thermal conductivity at the top of the first soil layer bug correction (Sect. 2.3.1).
TSNBOT	*TCZERO* with the improvement on the bottom snow temperature (Sect. 2.3.2).
EZERO (*PHYS*)	*TSNBOT* with the addition of the windless exchange coefficient (Sect. 2.3.3). Alias *PHYS*, as it includes all the snow physics improvements.
SUBLI	*PHYS* with the blowing-snow sublimation losses (Sect. 2.4.1).
COMPAC	*SUBLI* with the improved snow compaction scheme for the Arctic (Sect. 2.4.2; Eq. 12 with $U_0 = 2.5$ m s^{-1}).
CL11 (*ALL*)	*COMPAC* with the Calonne et al. (2011) snow thermal conductivity parameterization. Alias *ALL*, as it includes all the physics and Arctic model developments.
ALL_TVC	*ALL* with the adjusted maximum snow density parameters including TVC (Sect. 2.4.2; Eq. 12 with $U_0 = 3.5$ m s^{-1}). Note that the threshold at which the maximum snow compaction is increased due to wind speed remains at 2.5 m s^{-1}.

2.6 Evaluation metrics

Model skill is evaluated using observed manual and automatic snow depth and SWE, snow albedo (excluding Arctic sites; see Sect. 2.1), surface temperature, soil temperature in the upper soil layers (1–30 cm, depending on the site), and snow cover duration (SCD), which is derived as the number of days within a snow season (September to August) with snow depth exceeding 10 cm. Table S3 in the Supplement lists the measurements available at each site. To avoid uncertainties arising from patchy snow in both the model and observations, the metrics are computed for snow depth greater than 10 cm. In addition, observed snow albedo values are constrained to be between 0.4 and 0.9, and snow surface temperature to be less than or equal to 0°C, to ensure that they remain within a realistic physical range and to avoid potential artifacts or errors from observational measurements. For the soil temperatures, the first soil layer measurement at a depth greater than or equal to 5 cm is used for comparison with the model.

The following mean bias (MB), normalized mean bias (NMB), root-mean-square error (RMSE), and normalized RMSE (NRMSE) are used for each site:

$$\mathrm{MB} = \frac{1}{d}\sum_{t=1}^{d}(M_t - O_t)\,, \tag{16}$$

https://doi.org/10.5194/egusphere-2026-492
Preprint. Discussion started: 23 April 2026

$$\mathrm{NMB} = \frac{\mathrm{MB}}{\sigma_O}, \tag{17}$$

$$\mathrm{RMSE} = \sqrt{\frac{1}{d}\sum_{t=1}^{d}(M_t - O_t)^2}, \tag{18}$$

$$\mathrm{NRMSE} = \frac{\mathrm{RMSE}}{\sigma_O}, \tag{19}$$

where M_t and O_t denote the daily modelled and in situ observed values at time t, d is the number of days available within the analysis period for each variable and site, and σ_O is the standard deviation of the daily observed values over the corresponding period. The normalized RMSE and MB allow for better comparison among sites and variables.

In addition, we define an overall score over all sites and variables as follows:

$$\mathrm{Score} = \frac{1}{\sum_{i=1}^{n} m_i}\sum_{i=1}^{n}\sum_{j=1}^{m_i}\frac{\sigma_{O,ij} - \mathrm{RMSE}_{ij}}{\sigma_{O,ij}}, \tag{20}$$

where n is the number of variables, m_i the number of available sites for each variable i, RMSE_{ij} is the root-mean-square error for the variable i at site j, and $\sigma_{O,ij}$ is the standard deviation of the corresponding observations. The score is equal to 1 when the model perfectly matches the observations, equal to 0 when the RMSE equals the observational standard deviation, and becomes negative when the RMSE exceeds the observational variability. Each variable enumerated before is counted (snow depth, SWE, snow albedo, surface temperature, soil temperatures, and SCD). The snow depth and SWE include both the automatic and manual measurements, giving slightly more weight to those variables.

2.7 Optimization process

The snow model physics developments (Sect. 2.3) were mainly carried out independently of each other, guided by physical considerations and evaluated against available observations, without aiming to optimize scores or overall model performance. The snow Arctic adaptations (Sect. 2.4) were developed upon the physics developments by testing various formulations with manual iteration and exploration of the parameter space. All sites except TVC were used in this process in order to preserve TVC as an independent validation site—and given the substantial uncertainties associated with the snowfall rates at this site (see Sect. 2.1). Nevertheless, we also propose an adjusted version that includes TVC (experiment *ALL_TVC*; Table 2), motivated by the distinct behavior observed at this site and the limited number of available Arctic sites (see details below).

This study presents only the optimal solutions, although additional combinations of parameters and parameterizations were tested (not shown). The key tuning process was focused on the dry maximum snow density (Eq. 12). The following spaces of parameters were tested: $0.5 < d_0 < 2$ with increments of 0.1 m, $0.5 < \sigma < 1$ with increments of 0.1 m, $1 < U_0 < 5$ with increments of 0.1 m s^{-1} and the maximum constant of 430 (Eqs. 11 and 12) was tested between 400 and 450 with increments

https://doi.org/10.5194/egusphere-2026-492
Preprint. Discussion started: 23 April 2026

of 5 kg m^{-3}. The threshold wind speed at which wind-induced compaction is triggered was tested as U_0 (independently). Modifications to the constant 700 in the wet maximum snow density Eq. 10 were tested but did not yield any enhancements; therefore, this value was left unchanged. Note that snow density can exceed this value through melting and refreezing processes, but the snowpack will not undergo further compaction.

The overall score presented in Eq. 20 was used as the most objective metric to tune those parameters across all sites and variables, but when similar scores occurred (difference lower than 0.1), further investigation was carried out at individual sites to choose the most physically-based option (considering consistency between the simulated snow depth, soil temperatures, and snow density) and/or favoring best performances at the Arctic sites (Bylot and Umiujaq), because of their underrepresentation. Even though the simulations and results are presented stepwise, we calibrated the effects of the three Arctic model enhancements by systematically testing each possibility back and forth to ensure consistent tuning.

TVC was excluded from the tuning process and only added in the *ALL_TVC* experiment by adjusting the U_0 parameter in Eq. 12—by exploring the same parameter space described above—to get the best score at all sites (including TVC), but without redoing the whole tuning process mentioned above. Despite the large uncertainties associated with TVC (snowfall rates, limited number of years, etc.), this approach allows us to provide a range of possible values for the U_0 parameter. Furthermore, given the limited number of Arctic sites currently available and the uncertainties inherent to Arctic environments (such as drifting snow, frost on sensors, and snowfall rate measurements), this allows us to retain a parameter to fine-tune for future spatial simulations.

3 Results

Section 3.1 presents the annual cycles at all sites for each variable in a qualitative manner, for the *DEF* experiment (Sect. 3.1.1), the physics improvements (Sect. 3.1.2), and the Arctic adaptations (Sect. 3.1.3). Section 3.2 provides quantitative analyses and comparisons of the different experiments based on the metrics introduced in Sect. 2.6. Some experiments are superimposed in certain figures owing to similar model responses; each figure therefore provides complementary insights, supported by the main text and by additional clarifying plots in the Appendix and Supplement.

3.1 Annual cycles

3.1.1 *DEF* experiment

Figure 3 shows the annual cycles of the snow depth, SWE, snow albedo, surface temperature, and soil temperatures for all experiments at all sites. Generally, the default model version (*DEF*; dark blue line) demonstrates good skills in representing the annual cycle of the snow depth (first column) and SWE (second column) at most of the SnowMIP sites compared to the observations (black line). However, the *DEF* experiment overestimates and underestimates the snow depth at the Senator Beck and Swamp Angel sites, respectively (panels k and p). These discrepancies may be related to wind-driven snow redistribution and are further discussed in Sect. 4.1. At Weissfluhjoch, the simulated snowpack melts too early, with a decrease in snow

https://doi.org/10.5194/egusphere-2026-492
Preprint. Discussion started: 23 April 2026

depth starting in mid-March, almost 1 month earlier than in the observations (panel ee). This problem may be related to an underestimated simulated albedo (of about 0.05 from November to April; panel gg) or issues with light-absorbing particles (LAPs). Arctic sites exhibit thinner snowpacks in general, with a maximum snow depth of about 50 cm (Bylot and TVC; panels jj and tt) to 1 m (Umiujaq; panel oo). In the *DEF* experiment, simulated snow depth at the Arctic sites is overestimated by about 10–20 cm.

Overall, snow albedo (third column) is reasonably well simulated, except at several sites where it is overestimated by about 0.1–0.2 toward the end of the snow season (e.g., panels c, m, r, and w). This bias may be related to the lack of representation of light-absorbing particles (LAPs) in the simulations and is further discussed in Sect. 4.1. The simulated snow surface temperature (fourth column) tends to be underestimated by a few degrees at all SnowMIP sites in the *DEF* experiment compared to observations. In contrast, soil temperatures remain close to the 0 °C curtain at most SnowMIP sites in both the observations and simulations. At the Arctic sites (Bylot, Umiujaq, and TVC), larger discrepancies are observed between the model and the observations. In particular, simulated soil temperatures are overestimated by about 5–10 °C in the *DEF* experiment relative to observations, which reach -10 to -25 °C in winter (panels nn, ss, and xx). Given the strong temperature gradients between the atmosphere and the soil—particularly in autumn and spring—and the relatively thin snowpacks (< 1 m) at these sites, the overestimation in simulated snow depths likely leads to an excessive insulating effect and can partly explain the discrepancies in simulated soil temperatures.

3.1.2 Physical improvements

The inclusion of the new physics (*PHYS*; orange line in Fig. 3) leads, in general, to a slight degradation of the overall model performance. The impacts of the individual physical improvements are detailed below and in Fig. C1 of the Appendix. The correction of the thermal conductivity at the top of the first soil layer (*TCZERO*; orange line in Fig. C1) does not lead to substantial differences relative to the *DEF* experiment (blue line) at most sites. An exception is observed at Bylot, where a slight decrease in simulated soil temperature occurs at the beginning of winter (Fig. C1nn). This behavior is consistent with the strong atmosphere–soil temperature gradients during early winter and partial snow cover conditions, under which snow-free subareas cool more efficiently once the overestimated insulating effect is resolved (Sect. 2.4.3). Aside from this site-specific response, changes are limited and mainly occur during periods of partial snow cover and strong temperature gradients at other sites, but do not persist throughout the snow season (not shown). Further investigation will be carried out in future spatial studies, where larger impacts are expected.

The implementation of the new bottom snow temperature computation (Eq. 3; Sect. 2.3.2) substantially reduces biases in simulated snow temperatures. At Col de Porte over the 2002–2014 period, the mean snow temperature bias decreases from 0.8 to 0.3 °C (with the RMSE decreasing from 1.4 to 1.2 °C), while the bottom snow temperature bias is reduced from -0.4 to -0.1 °C (RMSE from 0.5 to 0.3 °C). Figures 4g–j and B1g–j illustrate these improvements on specific snow seasons reflected by the *PHYS* experiment (orange line; affected mainly by the bottom snow temperature change) compared to the *DEF* experiment (blue line). At Bylot, we assessed the estimation of the theoretical bottom snow temperature—not to get affected by the initial poor performance of the *DEF* experiment—, which is markedly improved with the RMSE decreasing from 4.2

https://doi.org/10.5194/egusphere-2026-492
Preprint. Discussion started: 23 April 2026

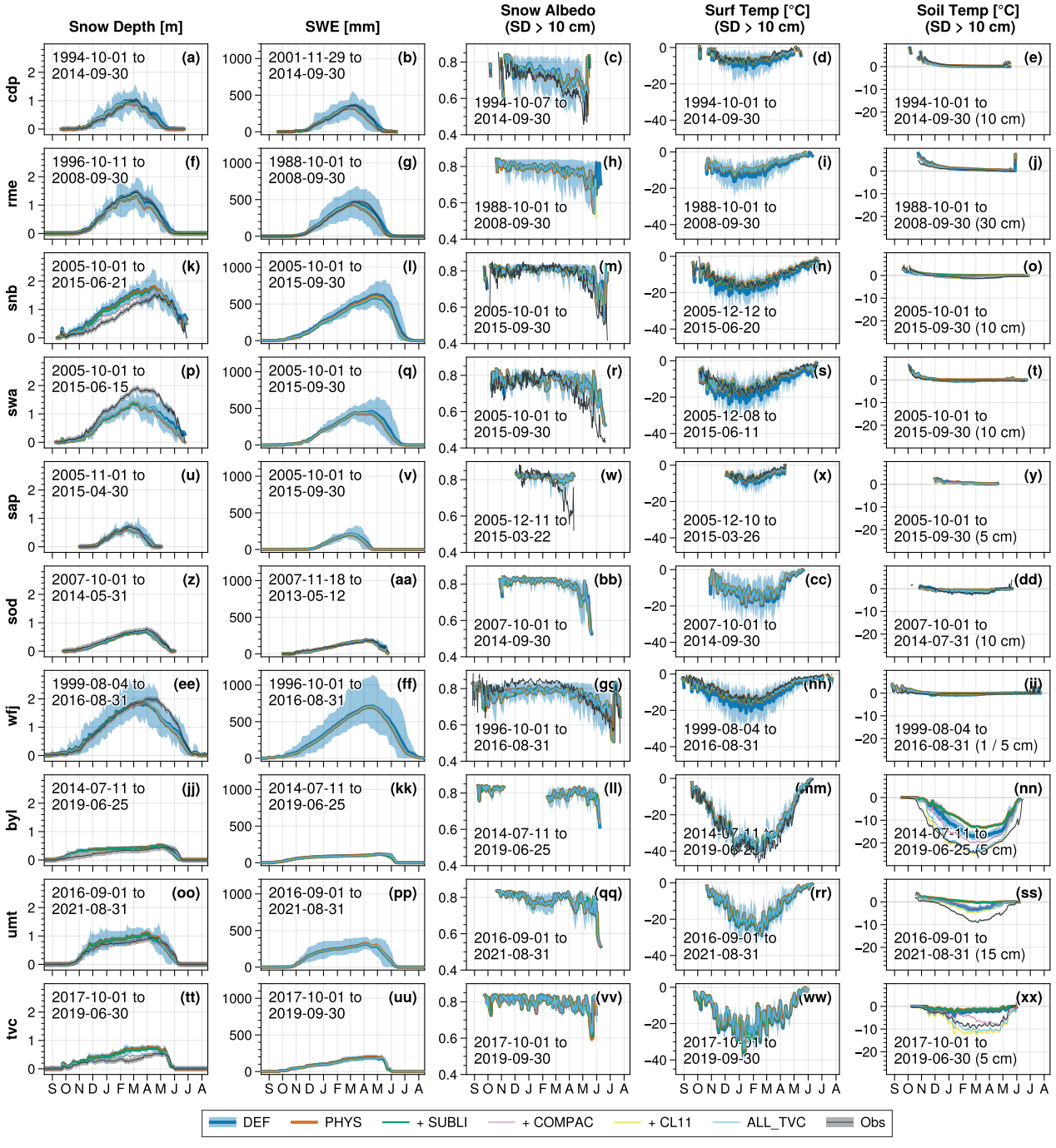

Figure 3. Annual cycles at all sites (rows) of the snow depth (automatic measurement), SWE (automatic measurement), snow albedo, surface temperature, and soil temperature at first measured depth (columns) of the daily time series of the experiments described in Table 2 over the available analysis period (shown in each panel). The blue shading corresponds to the 10–90 % quantile range of the interannual daily variability of the *DEF* experiment, and the black shading corresponds to the observational uncertainties estimated at Col de Porte (Lejeune et al., 2019) and shown at the other sites as an indicative reference. Values for the last three variables (snow albedo, surface temperature, and soil temperature) are considered only when snow depth is larger than 10 cm.

https://doi.org/10.5194/egusphere-2026-492
Preprint. Discussion started: 23 April 2026

to 0.9 °C (Fig. B2 in the Appendix). Appendix B provides additional information on the method used to compute the bottom snow temperature.

These improvements to the new estimate of temperature at the base of the snowpack alone, however, worsen the simulated soil temperatures at several sites, particularly at Arctic sites (*TSNBOT*; green line in the last column of Fig. C1nn and ss). Indeed, because the simulated bottom snow temperature tended to be underestimated in the *DEF* experiments for most of the snow season (e.g., Figs. 4i, B1i and B2 blue line), it was leading to an overestimated soil heat loss toward the snowpack, inducing an overestimated snow temperature (e.g., Figs. 4g and B1g blue line). Changing the snow thermal conductivity from Sturm et al. (2001) to Calonne et al. (2011) allows the soil temperature to revert to similar performances to the *DEF* experiment (see next Sect. 3.1.3). Indeed, the parameterization proposed by Calonne et al. (2011) leads to higher snow thermal conductivity values than that of Sturm et al. (2001) (see Fig. 1 of Calonne et al., 2011), which enhances heat exchange between the soil and the atmosphere without significantly affecting snow or bottom snow temperatures (differences < 0.5 °C; Figs. 4g—j and B1g—j, orange and yellow lines). Consequently, the current model performance of the simulated soil temperatures in the *DEF* experiment was likely induced by a bias compensation related to the bottom snow temperature computation and snow thermal conductivity.

The addition of the windless exchange coefficient in the sensible heat flux during stable atmospheric conditions (*EZERO*; pink line in Fig. C1) leads to a slightly earlier melt at Col de Porte and Reynolds Mountain East, with underestimated snow depths and SWE during the ablation period (panels a, b, f, and g). On the other hand, it alleviates the surface temperature bias at all SnowMIP sites, leading to simulated surface temperatures within the range of observations (Fig. C1 fourth column). The *EZERO* experiment does not affect simulated soil temperatures, which remain comparable to those of the *TSNBOT* experiment (green line; Fig. C1, last column).

3.1.3 Arctic adaptations

Introducing the new physics (*PHYS* experiment) alone is not sufficient to improve the model skills at the Arctic sites. Indeed, Arctic environments are subjected to strong winds and high temperature gradients, which involve other processes such as blowing-snow sublimation and the formation of wind slabs and depth hoar. The impacts of the Arctic-specific model developments are detailed below.

Applying the blowing-snow sublimation loss parameterization of Gordon et al. (2006) (*SUBLI*; green line in Fig. 3) has little impact at most sites, except at Umiujaq and TVC, where the snow depth is decreased by about 2–4 cm (Figs. 3oo and tt, and D1 and D2a and b). Large snow depth biases still persist at Bylot and TVC, with overestimations of about 7 and 18 cm, respectively. A slight improvement is also observed at Senator Beck, with a reduction in snow depth of a few centimeters (Fig. 3k). The impacts on soil temperature are negligible.

The new compaction scheme (*COMPAC*; pink line in Fig. 3), which accounts for wind-induced increases in snow compaction, has the most significant impact on the simulated snow depth, snow density, and soil temperatures at the Arctic sites, while it has a negligible effect at most SnowMIP sites. This new scheme substantially reduces the snow depth bias at Bylot, from about 7.5 cm to nearly zero (Fig. 5a and b, pink line). It also improves simulated snow density and thermal conditions,

https://doi.org/10.5194/egusphere-2026-492
Preprint. Discussion started: 23 April 2026

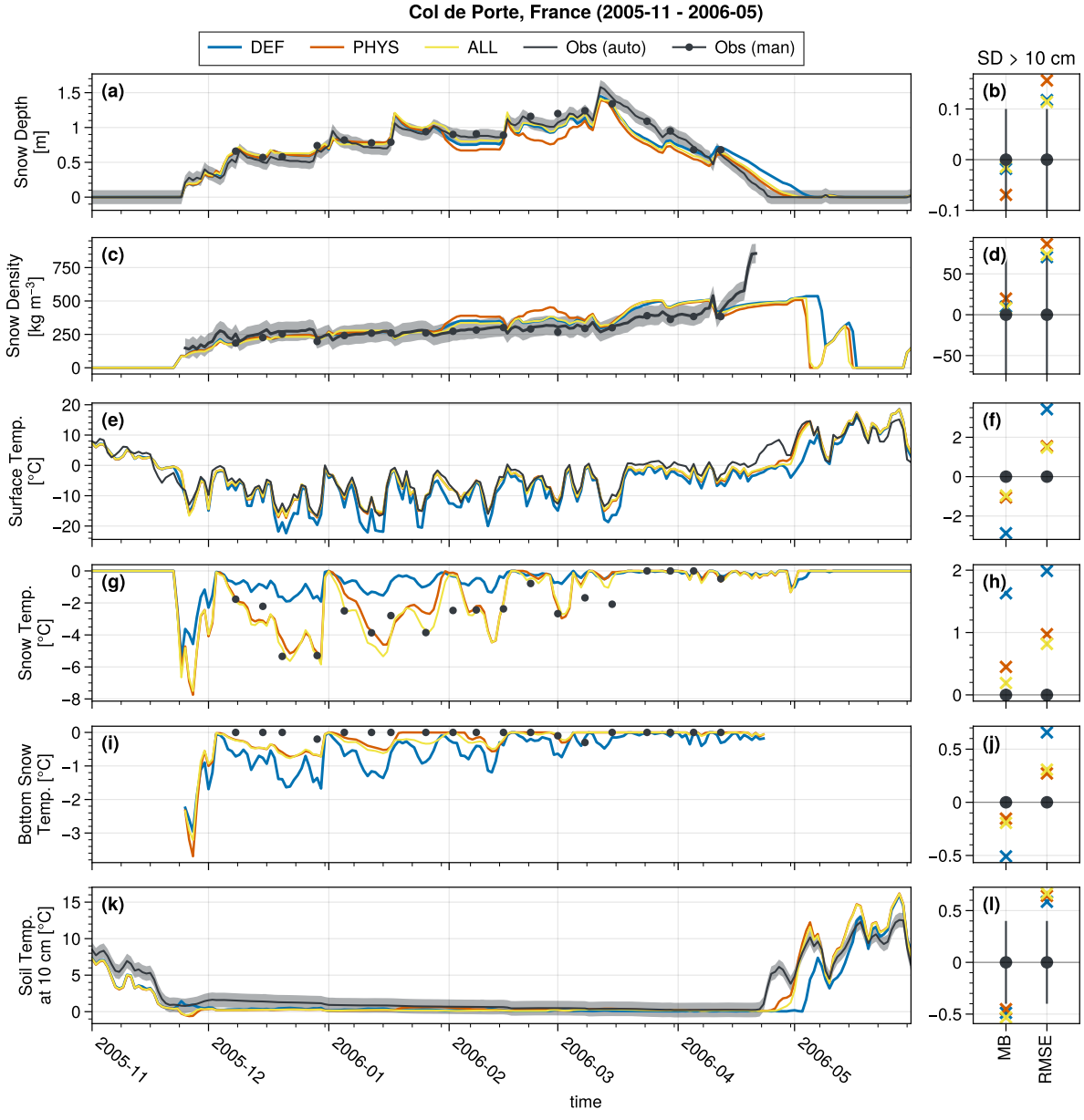

Figure 4. Example of time series of the snow depth (a), snow density (c), surface temperature (e), snow temperature (g), bottom snow temperature (i), and soil temperature at 10 cm (k) at Col de Porte during the 2005-2006 snow season. Automatic (black line) and manual (black dots) measurements are shown when available. The black shading represents the average uncertainty derived from Lejeune et al. (2019). The snow density uncertainty σ_ρ was derived from the median value of the automatic snow depth d_s, SWE measurements, and their associated uncertainties (σ_{d_s} and σ_{SWE}) as follows: $\sigma_\rho = \rho\sqrt{(\sigma_{\mathrm{SWE}}/\mathrm{SWE})^2 + (\sigma_{d_s}/d_s)^2}$ over the whole period. The right panels indicate the mean error and RMSE over the example period (2005-2006) for snow depth > 10 cm. The simulated time series correspond to the default configuration (*DEF*; blue), the physics improvements (*PHYS*; orange), and the physics and Arctic modifications (*ALL*; yellow). See Table 2 for the description of the experiments.

https://doi.org/10.5194/egusphere-2026-492
Preprint. Discussion started: 23 April 2026

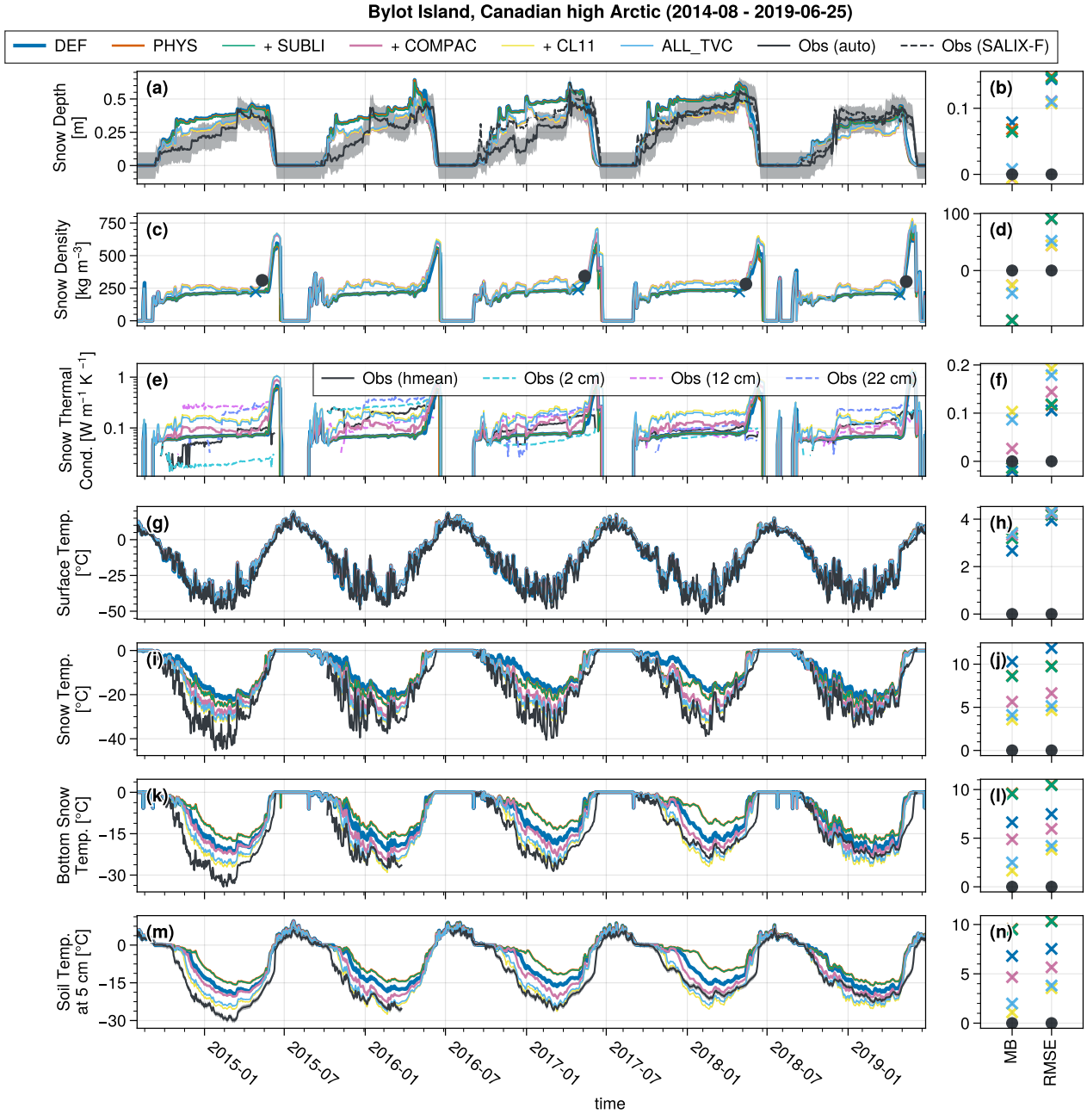

Figure 5. Time series of snow depth (a), snow density (c), snow thermal conductivity (e), snow surface temperature (g), bulk snowpack temperature (i), bottom snowpack temperature (k), and soil temperatures at 5 cm (m) at Bylot from August 2014 to end of June 2019 for all experiments. Automatic measurements are shown in black, and alternative snow depth measurements from a nearby site (SALIX-F; 9 km away) are shown as dashed lines in panel (a). The black shading corresponds to measurement uncertainties derived at Col de Porte (Lejeune et al., 2019) as an indicative reference. Panel (e) displays the measured snow thermal conductivities at various heights (dashed lines), and the black line represents the weighted harmonic average of those values. The snow density measurements are derived from snow pits in 2015, 2017, 2018, and 2019. Because of early melt in the model (see panel a), the observed snow density is compared to the simulated values 2 weeks before (blue cross). The right panels correspond to the mean error and RMSE over the period 2014–2019 for snow depth $>$ 10 cm.

https://doi.org/10.5194/egusphere-2026-492
Preprint. Discussion started: 23 April 2026

with snow density reaching values closer to observations (around 300 kg m^{-3}; Fig. 5c and d, pink line) and reduced biases in snow, bottom snow, and soil temperatures (mean bias decreasing from about 10 to 5 °C between the *PHYS* and *COMPAC* experiments; Fig. 5i—n, orange and pink lines, respectively).

Similar improvements are observed at TVC, with decreased snow depth, increased snow density, and reduced soil temperatures, which are in better agreement with observations (Fig. D2, pink line). In contrast, a slight deterioration in simulated snow depth is found at Umiujaq (Fig. D1a and b, pink line), where it becomes underestimated by about 10 cm relative to observations, likely due to earlier simulated melt and/or the absence of snow trapping by shrubs, which can locally increase snow depth in reality (further discussed in Sect. 4). Moreover, an improvement in simulated snow depth is also observed at Senator Beck, a site subject to strong wind conditions (Fig. 3k, pink line), while the remaining overestimation is likely related to wind-induced snow erosion that is not accounted for in the model.

The implementation of the new snow thermal conductivity parameterization (*CL11*; yellow line in Fig. 3) improves the simulated soil temperatures compared to observations at Bylot and to a lesser extent at Umiujaq (Fig. 3nn and ss), whereas they are slightly underestimated at TVC (panel xx). In the *CL11* experiment, the simulated snow thermal conductivity at Bylot and TVC is, on average, overestimated by about 0.1 W m^{-1} K^{-1} relative to the bulk snow thermal conductivity inferred from observations (Figs. 5e and f, and D2c, yellow line). These values approach those typically associated with wind slabs, as indicated by the dark blue horizontal shading at TVC (Fig. D2c) and the dashed lines at Bylot (Fig. 5e), which will be further discussed in Sect. 4.3. The new snow thermal conductivity parameterization also improves the simulated snow and bottom snow temperatures at Bylot (Fig. 5i–l).

The adjusted parameters of the compaction scheme, including TVC (*ALL_TVC*; light blue line in Fig. 3), do not significantly affect most sites. The *ALL_TVC* experiment includes a slight reduction of the impact of the wind-induced compaction in Eq. 12 by setting U_0 to 3.5 m s^{-1} instead of 2.5 m s^{-1} from the *COMPAC* experiment, leading to increased snow depths of a few centimeters at the Arctic sites. *ALL_TVC* improves the simulated soil temperatures at TVC by about 1 °C and slightly worsens them at Bylot and Umiujaq (∼0.5 °C), due to a marginally thicker snowpack (by a few centimeters) and, therefore, enhanced soil insulation.

3.2 Experiment ranking

Figures 6 and 7 show the RMSE and mean bias for each variable and site and their normalized values (i.e., divided by the standard deviation of the observations) to better compare between the different sites with varying amplitudes.

3.2.1 Snow depth and SWE

The largest snow depth and SWE errors are observed at Swamp Angel (red cross), with RMSE values ranging from 45 to 65 cm and from 200 to 225 mm, respectively, across all experiments and for both manual and automatic measurements (Fig. 6a—h). These errors primarily reflect a strong underestimation of snow depth and SWE (about 50 cm and 200 mm, respectively), already apparent in Fig. 3. This systematic underestimation could be related to snow trapping in this subalpine forest environment, which is located downstream of Senator Beck (green cross). In contrast, the highest snow depth NRMSE (exceeding 1) is

https://doi.org/10.5194/egusphere-2026-492
Preprint. Discussion started: 23 April 2026

found at Bylot (gray triangle; Fig. 6b), reflecting the relatively thin snowpack at this site, for which even small absolute errors translate into large relative errors.

Overall, the new physics (*PHYS*; second x-axis tick) degrades the simulated snow depths by about 5 % compared to the *DEF* experiment (first x-axis tick), with an average RMSE across all sites of 25.0 cm compared to 23.8 cm in the *DEF* experiment, with respect to the automatic measurements (Fig. 6a; red plain circles excluding TVC). Similar results are observed for the manual snow depth and SWE measurements (with slightly larger errors). The addition of the blowing-snow sublimation loss parameterization (*SUBLI*; third x-axis tick) has no significant impact on average across all sites, owing to its limited influence at only a few sites (as mentioned in Sect. 3.1.3). The new compaction scheme (*COMPAC* experiment; fourth x-axis tick) and the inclusion of the new thermal conductivity (*CL11* experiment; fifth x-axis tick) improve the results with mean snow depth RMSEs across all sites of 22.8 cm and 21.5 cm, respectively. Results are improved at both SnowMIP (black circles) and Arctic (blue plain circles) sites, with snow depth RMSE decreasing from 25.1 to 23.3 cm (NRMSE from 0.54 to 0.50) at SnowMIP sites and from 19.4 to 15.1 cm (NRMSE from 1.05 to 0.79) at Arctic sites between the *DEF* and *CL11* experiments (Fig. 6a and b). Including TVC (empty circles) in the evaluation does not significantly affect the average snow depth NRMSE across all sites for the *CL11* and *ALL_TVC* experiments (fifth and last x-axis ticks, respectively).

3.2.2 Snow albedo and surface temperature

Impacts on snow albedo are limited, with an average RMSE ranging between 0.07 and 0.08 at the SnowMIP sites for all the experiments (Fig. 6i and j). Snow albedo measurements at Arctic sites are prone to errors (due to gap-filling, frost, etc.) and are therefore not shown. The implementation of the new physics (*PHYS*) improves the simulated surface temperature at all SnowMIP sites by decreasing the RMSE from 3.41 °C to 1.51 °C and the mean bias from -2.20 °C to -0.25 °C (Figs. 6 and 7k and l), mainly due to the implementation of the windless exchange coefficient in the sensible heat flux (*EZERO*; Figs. C2 and C3k and l). The simulated surface temperature worsens slightly at Bylot; however, given the larger temperature amplitude at Arctic sites, the NRMSE increases only from 0.29 to 0.30. Overall, considering the Arctic and SnowMIP sites, the average NRMSE decreases from 0.60 to 0.30 (although the Arctic sites are underrepresented).

3.2.3 Soil temperatures

Soil temperature RMSEs and mean biases show large dispersion, especially at the Arctic sites, due to large warm biases in the model for the *DEF*, *PHYS*, and *SUBLI* experiments (Figs. 6 and 7m and n; first to third x-axis ticks). The *DEF* experiment has a mean RMSE (MB) of 5.78 °C (5.10 °C) and NRMSE (NMB) of 1.06 (0.93) at the Arctic sites and 0.63 °C (0.09 °C) and 0.81 (0.07) at the SnowMIP sites. The normalized RMSEs and mean biases show smaller differences between the Arctic and SnowMIP sites because of the larger (smaller) soil temperature amplitudes at the Arctic (SnowMIP) sites. Implementing the new bottom snow temperature formulation degrades overall model performance, as discussed in Sect. 3.1 and illustrated in Figs. C2 and C3m and n (*TSNBOT*; third x-axis tick). This is reflected in the *PHYS* experiment (Fig. 6m and n; second x-axis tick) with an increase of the RMSE (NRMSE) to 8.08 °C (1.49) and 0.76 °C (0.93) on average at the Arctic and SnowMIP sites, respectively.

https://doi.org/10.5194/egusphere-2026-492
Preprint. Discussion started: 23 April 2026

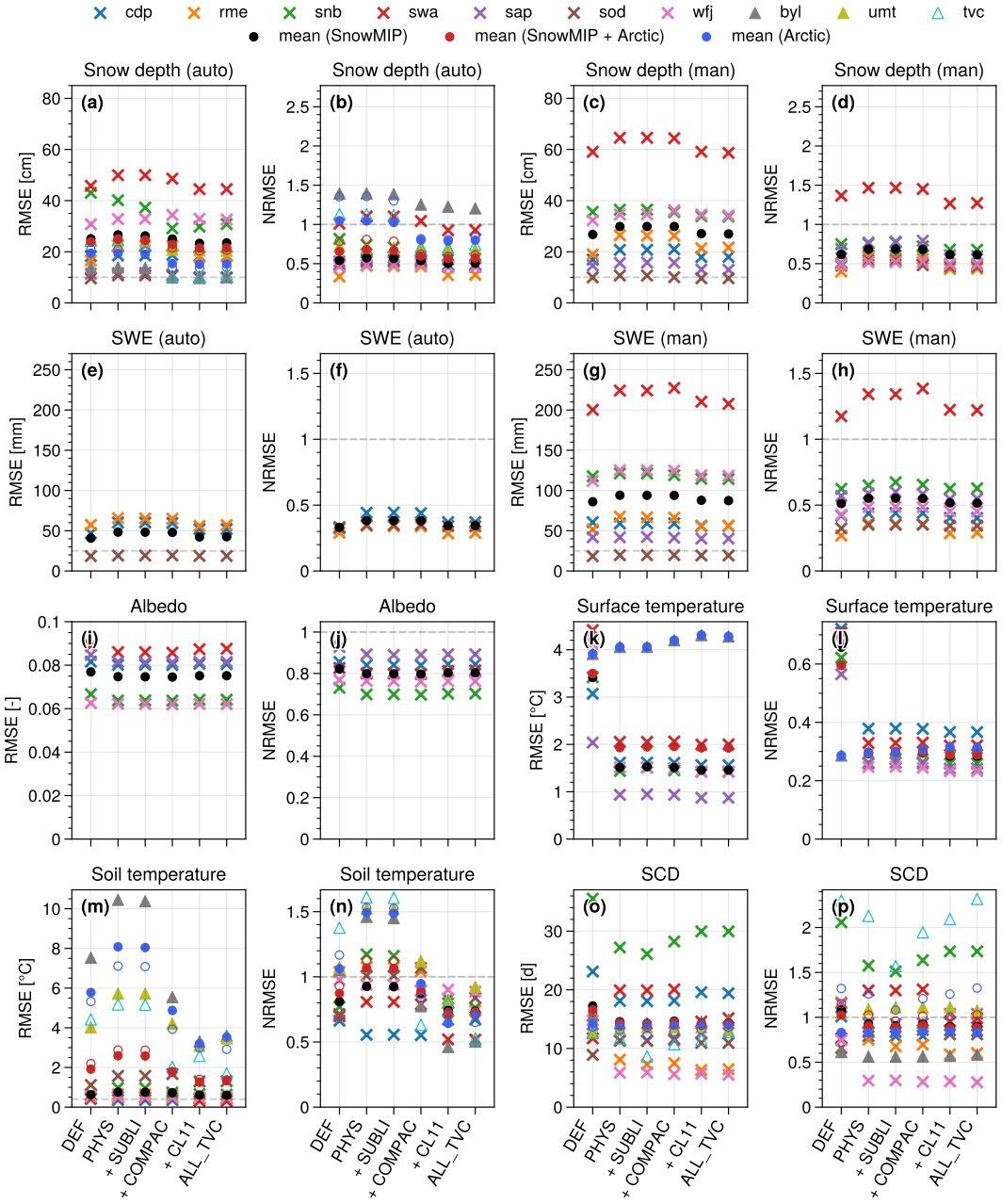

Figure 6. RMSE and normalized RMSE (NRMSE; normalized by the standard deviation of the observations) computed for daily time series of snow depth (automatic and manual; a—d), SWE (automatic and manual; e—h), snow albedo (i, j), surface temperature (k, l), soil temperature at the first measured depth (m, n), and snow cover duration (SCD; snow depth > 10 cm; o, p) for the experiments listed in Table 2, over the available analysis period at each site. The SnowMIP sites are shown as crosses, and the Arctic sites as triangles. The black, red, and blue circles represent, respectively, the mean RMSE/NRMSE of all the SnowMIP sites, the SnowMIP and Arctic sites, and the Arctic sites only. The full circles exclude TVC (independent validation site), and the empty circles include TVC. The black dotted lines correspond to the observation uncertainties estimated at Col de Porte (Lejeune et al., 2019), applied to the other sites as an indicative reference for the RMSE, and to 1 standard deviation of the observations for the NRMSE. All metrics are computed only over the period of snow depths greater than 10 cm in the automatic measurements for each site.

https://doi.org/10.5194/egusphere-2026-492
Preprint. Discussion started: 23 April 2026

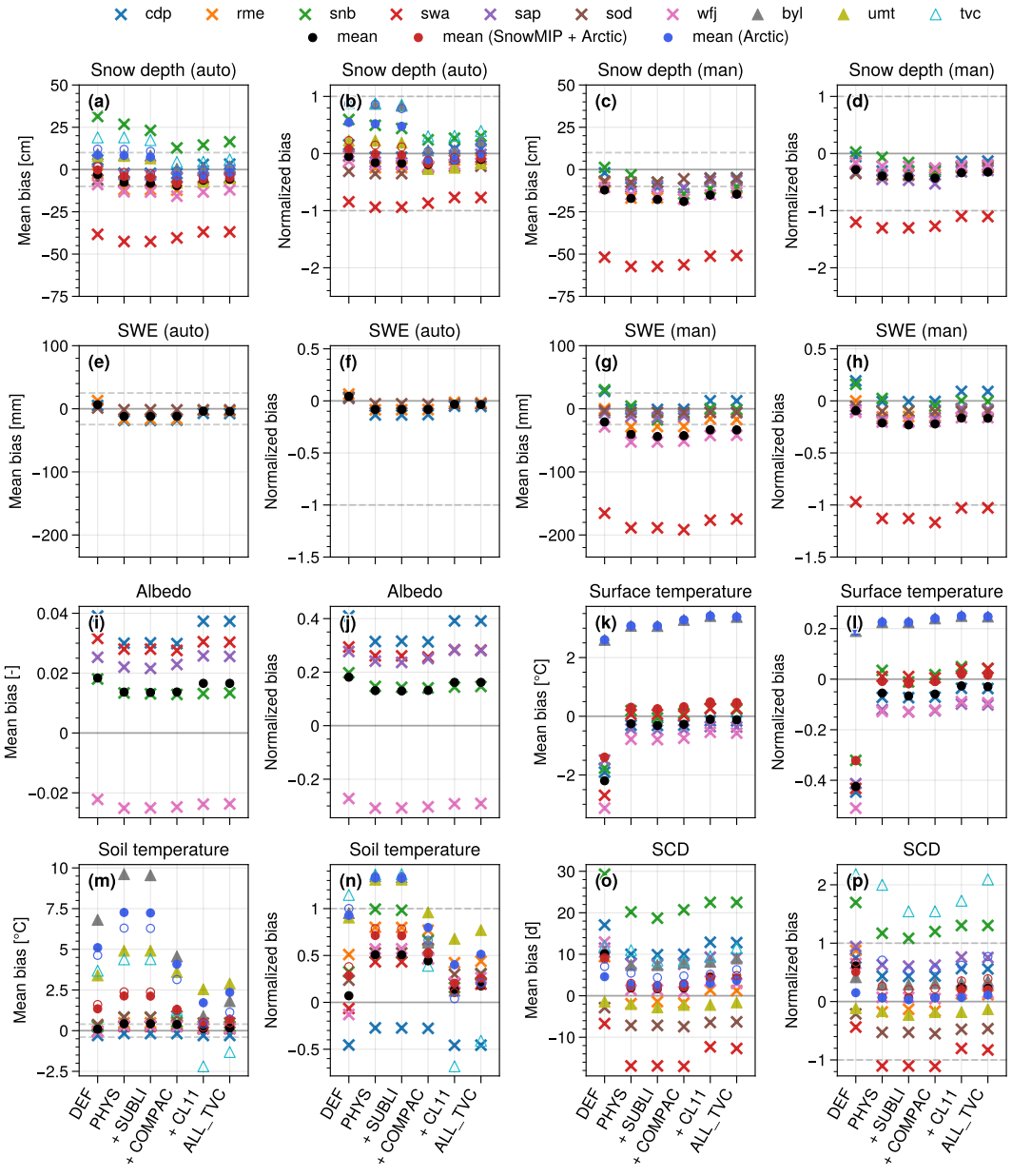

Figure 7. Same as Fig. 6 but for the mean bias (MB) and normalized mean bias (NMB; divided by the standard deviation of the observations).

The addition of the new compaction scheme (*COMPAC*) and the snow thermal conductivity parameterization (*CL11*) improves simulated soil temperatures (Fig. 6m and n; fourth and fifth x-axis ticks). At Arctic sites, the RMSE (NRMSE) decreases to 4.88 °C (0.95) with *COMPAC* and to 3.20 °C (0.64) with *CL11*. At SnowMIP sites, the corresponding RMSE (NRMSE) values are 0.73 °C (0.87) and 0.61 °C (0.74), respectively. Including TVC slightly improves the performance of the simulated

https://doi.org/10.5194/egusphere-2026-492
Preprint. Discussion started: 23 April 2026

soil temperature in the *CL11* experiment to an RMSE (NRMSE) of 2.99 °C (0.70) at the Arctic sites (Fig. 6m and n; blue empty circles), despite a negative soil temperature bias of -2.19 °C at TVC (Fig. 7m; light blue empty triangle). The adjusted compaction scheme, including TVC (*ALL_TVC*; blue empty circles, last x-axis tick in Fig. 6m and n), further reduces the RMSE (NRMSE) on average at all Arctic sites to 2.92 °C (0.65). However, a persistent cold bias of -1.31 °C remains at TVC, while warm biases increase at Bylot and Umiujaq, from 0.89 to 1.81 °C and from 2.31 to 2.70 °C, respectively (Fig. 7m; triangles).

3.2.4 Snow cover days

The average SCD RMSE (NRMSE) improves at both SnowMIP (black circles) and Arctic sites (including TVC; empty blue circles) from 16.2 days (1.2) for the *DEF* experiment to 14.1 days (1.0) for the *ALL_TVC* experiment (Fig. 6o and p; first and last x-axis ticks, respectively). However, the model performance worsens at some sites by a few days (e.g., TVC). Early and late melts span from about ± 20 days depending on sites, and around ± 10 days if we exclude Senator Beck and Swamp Angel (Fig. 7o).

3.2.5 Scores

The overall scores (Eq. 20) at all sites excluding TVC incrementally improve from 0.284 (*DEF*) to 0.380 (*CL11*; Table 3). The model performs better at the SnowMIP than at the Arctic sites, although the new snow model developments (*CL11*) yield larger improvements at the Arctic sites (where the model performed poorly compared to the SnowMIP sites). Indeed, scores increase between the *DEF* and *CL11* experiments from 0.309 to 0.391 at the SnowMIP sites and from 0.119 to 0.306 at the Arctic sites (excluding TVC). Including TVC degrades model performance across all sites, with scores decreasing to 0.140 for the Arctic-only sites and to 0.347 when considering all sites in the *CL11* experiment. Including the adapted compaction scheme with TVC (*ALL_TVC*) does not improve the overall score. Indeed, no overall calibration with TVC was performed, but only an adjustment of the compaction parameters (in Eq. 12), with the main aim of improving soil temperatures without significantly worsening the simulated snow depth (Sect. 2.6).

Table 3. Scores (Eq. 20) computed for each experiment at the SnowMIP, Arctic, and all sites (with and without TVC) for all variables. The last two rows exclude the SCD in the score computation.

Experiment	DEF	PHYS	SUBLI	COMPAC	CL11	ALL_TVC
SnowMIP	0.309	0.333	0.337	0.345	0.391	0.391
Arctic (without TVC)	0.119	-0.003	0.001	0.217	0.306	0.286
SnowMIP + Arctic (without TVC)	0.284	0.290	0.294	0.329	0.380	0.377
Arctic (with TVC)	-0.181	-0.274	-0.202	0.109	0.140	0.124
SnowMIP + Arctic (with TVC)	0.223	0.227	0.242	0.304	0.347	0.344
Arctic (with TVC; SCD excluded)	-0.121	-0.280	-0.254	0.245	0.311	0.317
SnowMIP + Arctic (with TVC; SCD excluded)	0.303	0.280	0.285	0.371	0.421	0.423

https://doi.org/10.5194/egusphere-2026-492
Preprint. Discussion started: 23 April 2026

For the Arctic sites, the scores were computed using only the following available variables: automatic snow depth, soil temperature, and SCD (in addition to surface temperature at Bylot). Therefore, the scores are more sensitive to variations in individual variables. The SCD metric at TVC spans only two snow seasons and exhibits a large NRMSE (> 2.0 for the *CL11* and *ALL_TVC* experiments), whereas the NRMSEs for the other variables are generally below 1.5 (Fig. 6b, n, and p; last two x-axis ticks; triangles). As a result, SCD contributes substantially to the overall score at TVC. Nevertheless, the seasonal evolution of snow depth at TVC is reasonably well captured by the model, and the low score may arise from a low standard deviation due to similar SCDs over the two snow seasons and from an early simulated snow onset in 2017 relative to observations leading to high NRMSE, which may be related to forcing uncertainties (Fig. D2a). Consequently, the strong weight given to SCD in the score computation at TVC may overemphasize this metric and does not necessarily reflect a generally poor model performance at this site. Excluding SCD from the score computation yields scores of 0.311 and 0.317 for the *CL11* and *ALL_TVC* experiments, respectively, at the Arctic sites, and 0.421 and 0.423 when considering all sites. These results highlight the improved performance of the TVC-adjusted compaction parameters for simulating snow depth and soil temperatures.

4 Discussion

In this study, we introduce six new snow model developments in the CLASSIC LSM—three physics improvements and three Arctic-specific adaptations. These developments are evaluated using 1D site simulations at seven SnowMIP and three Arctic sites. The discussion is organized as follows. Sect. 4.1 interprets the site-specific biases and discusses their likely links to unresolved or simplified snow processes. Sect. 4.2 discusses limitations related to unresolved spatial heterogeneities in snow accumulation and melt processes. Sect. 4.3 focuses on limitations associated with energy transfer and vertical (1-D) processes within the snowpack. Sect. 4.4 focuses on uncertainties related to meteorological forcing and observations. Finally, Sect. 4.5 addresses limitations arising from interactions between snow, soil, vegetation, and carbon fluxes.

4.1 Site-specific limitations related to unresolved processes

The discrepancies in simulated snow depth with respect to observation at Senator Beck and Swamp Angels (Fig. 3k and p) could be due to the lack of representations of wind-driven snow redistribution in the model. Indeed, Senator Beck is located at 3714 m a.s.l. in an alpine tundra with thin soils and exposed bedrock, subject to strong winds that favor snow erosion, whereas Swamp Angel is located in a sheltered meadow surrounded by subalpine forest at 3371 m a.s.l., lower down in the same watershed. Therefore, Swamp Angel could trap some snow during wind events (not reflected in the snowfall measurements), leading to higher observed snow depths than simulated, while wind-driven snow erosion at Senator Beck—not accounted in the model—could lead to an overestimation of simulated snow depth at this site. Alternatively, the current snow compaction scheme could not be adapted to the conditions at these sites. Further investigation would be needed to unravel this uncertainty, especially since most models underestimate the simulated SWE at this site (Menard et al., 2021, their Fig 2).

The early melt at Weissfluhjoch (Fig. 3ee) could be due to the lack of representation of the effects of LAPs on snow albedo in our simulations. Indeed, the model uses a single time constant for the albedo decay for dry snow and cannot capture differences

https://doi.org/10.5194/egusphere-2026-492
Preprint. Discussion started: 23 April 2026

in albedo decay due to differences in LAP deposition. For example, the snow albedo tends to be overestimated at Col de Porte and Sapporo (Fig. 3c and w) during the ablation period (among other sites), where they are known to be affected by LAPs (e.g., Niwano et al., 2012; Réveillet et al., 2022). Niwano et al. (2012) show that the snow albedo can be reduced by up to 0.18 during the ablation period at Sapporo due to the deposition of LAPs on the snow surface, which corresponds to the discrepancies between the simulated and observed snow albedo in our simulations (Fig. 3w). At Weissfluhjoch, the simulated albedo is closer to observations during the ablation period, suggesting that this site is likely less subject to LAPs. However, because the CLASSIC snow scheme was calibrated to fit sites, including Col de Porte (Brown et al., 2006, unpublished manuscript, 2001), it indirectly takes into account the LAPs, which could partly explain the good performance at the Col de Porte and early melt at Weissfluhjoch. Alternatively, this early melt at Weissfluhjoch could result from an underestimated simulated albedo during the accumulation period (Fig. 3gg), leading to excessive absorption of solar radiation and, in turn, a warmer snowpack, which could trigger an earlier onset of melt. Further investigation will be needed by including LAPs and/or adapting the albedo scheme to distinguish the contribution of these respective phenomena to those discrepancies, especially since early melt is also observed at other sites (discussed in other sections below).

4.2 Spatial heterogeneities

A key limitation of this study is the use of point-scale simulations at Arctic sites, where snow processes are strongly influenced by spatial heterogeneity (e.g., Mohammadzadeh Khani et al., 2023). Arctic environments are subjected to harsh conditions, including strong winds that induce significant snow drifting and sublimation losses, which are difficult to quantify. As a result, simulated snow depth is not necessarily correlated with observed precipitation (e.g., strong snowstorms can erode an entire snowfall event). For instance, on 12 April 2018, Lackner et al. (2022) conducted 172 distributed snow depth measurements within a 100 m radius of the Umiujaq TUNDRA site. Observed snow depths ranged from 50 to 210 cm, with a mean value of 109 cm, which is within 8 cm of the value measured by the automatic station on the same day (117 cm). This suggests that we can reasonably assume the station is representative of the surrounding snow depth, although it demonstrates the intrinsic spatial heterogeneity of snow characteristics in these environments. Large-scale LSMs such as CLASSIC are designed to represent processes at grid-cell scales of tens to hundreds of kilometers. Consequently, our simulations are not intended to reproduce the exact snowpack evolution at a specific site affected by wind-driven redistribution, but rather to capture its key characteristics over multiple snow seasons.

Enabling or deactivating SCF parameterizations is also a thorny question for point-scale simulations. Krinner et al. (2018) and Menard et al. (2021) advise deactivating the SCF parameterizations in the ESM-SnowMIP exercise, as they assume that snow cover is either present or absent in site simulations. Indeed, SCF parameterizations are generally designed to represent large-scale spatial heterogeneities (e.g., Niu and Yang, 2007; Swenson and Lawrence, 2012; Lalande et al., 2023). However, time-lapse camera observations at Arctic sites (e.g., Bylot and Umiujaq) reveal small-scale spatial variability at meter or sub-meter scales, driven by microtopography, vegetation, and surface roughness, particularly during the ablation period or at the onset of the snow season. In addition, the presence of instruments themselves can locally enhance melt around the measurement station (e.g., Morin et al., 2012, their Fig. 3). Such small-scale snow cover heterogeneities can affect the surface

https://doi.org/10.5194/egusphere-2026-492
Preprint. Discussion started: 23 April 2026

energy budget, soil temperatures, and measurements of upward long- and shortwave radiation, whose instruments have larger spatial footprints than automatic snow depth sensors, thereby influencing the measured albedo, for example. A 10 cm snow depth threshold is usually applied—excluding periods with shallow snow cover—to limit those uncertainties in point-scale snow studies; however, it is not obvious whether considering a complete snow cover for point-scale simulations is always relevant. Further investigation should be conducted at specific sites, including with cameras, to clarify this issue. Estimating the average snow depth and SCF around a station could help develop site-dependent SCF parameterizations, which could alternatively be inferred indirectly from albedo measurements using known snow and snow-free albedo values at those sites (e.g., Essery et al., 2013, their Eq. 54).

In CLASSIC, the model imposes a minimum snow depth of 10 cm—when snow is present—over the snow-covered subfraction of the grid cell to ensure numerical stability of the time-stepping scheme. Consequently, the snow cover parameterization cannot be deactivated without compromising numerical stability at snow depths below 10 cm. We tested minimum snow depth thresholds ranging from 5 to 20 cm at a subset of sites where such experiments could be performed without compromising numerical stability. These tests showed limited impacts on simulated soil temperatures, except during occasional periods characterized by strong temperature gradients between the soil and the atmosphere, combined with thin snowpacks. Overall, these effects were transient and smaller than those associated with the new snow model developments (not shown); however, they may still affect model tuning parameters. Furthermore, the choice of SCF parameterization (e.g., Swenson and Lawrence, 2012; Lalande et al., 2023; Wang et al., 2025) is expected to exert a stronger influence in spatial simulations and will be investigated in future studies using the new snow model developments.

4.3 Energy transfer and vertical snowpack processes

The vertical energy and water fluxes are modeled separately in CLASSIC for the four subareas in each grid cell: vegetated and bare soil surfaces, each with and without snow cover. However, at each model time step, all variables of each subarea are averaged together. Therefore, the separate energy budgets of each subarea do not persist over time. This assumption is particularly critical for snow because the presence or absence of snow cover strongly modifies the surface energy balance (e.g., albedo, insulation, and latent heat exchanges). Averaging the subareas may artificially smooth sharp contrasts between snow-covered and snow-free fractions, which can in turn affect simulated snow accumulation and melt rates. Further investigation could assess whether this assumption is realistic and at which spatial scales it applies.

Furthermore, the current hypothesis of quadratic temperature profiles within the snowpack could reach some limitations. On the one hand, it allows for an indirect representation of multilayer heat transfer within the snowpack, which may be more realistic than a simple linear profile in a single-layer snow model. On the other hand, it is known that snowpack temperature profiles may be more complex (e.g., Fierz, 2011, their Fig. 1). For instance, cold temperatures accumulated during the night can persist in the mid-upper layers of the snowpack, while the surface warms during the day and the bottom remains relatively warm due to ground heat flux, resulting in a temperature profile that deviates from a simple quadratic curve. Therefore, when the surface and soil temperatures simulated by CLASSIC both approach 0 °C, the modelled average snowpack temperature will also approach 0 °C, whereas in reality the bulk snowpack could still be colder. Despite its good overall performance, this

https://doi.org/10.5194/egusphere-2026-492
Preprint. Discussion started: 23 April 2026

may be a limitation of the single-layer CLASSIC snowpack and could be one of the causes of the early melt observed at a few sites, especially at the Arctic ones (e.g., Figs. 5, D1, and D2a).

Some limitations in the representation of bulk snow properties may also arise from the use of a single-layer snow model. As shown in Sect. 3.1.3, the simulated bulk snow thermal conductivity in the *CL11* experiment is overestimated at Bylot and TVC by about 0.1 W m^{-1} K^{-1} relative to observations (Fig. 5e and f; Fig. D2c). Generally, estimating an effective snow thermal conductivity from the mean snow density can be misleading in a single-layer framework. Indeed, the relationship between density and thermal conductivity is nonlinear, and thermal resistances—not conductivities—combine in series in vertically stratified snowpacks. As a result, applying a density-dependent snow thermal conductivity parameterization to the mean snow density cannot reproduce the equivalent conductivity of a multilayer snowpack. This limitation may partly explain why the model reproduces observed snow density reasonably well while still exhibiting deviations in simulated snow thermal conductivity. Although heated-needle probe measurements are also known to underestimate snow thermal conductivity due to contact resistance effects and assumptions inherent to the heating method (Fourteau et al., 2022), which may partly explain discrepancies between simulated and observed snow thermal conductivities. Some discrepancies may also stem from the estimation of bulk snow thermal conductivity using a limited number of point measurements, as the harmonic mean does not fully capture the effects of snow stratigraphy. Further evaluation using vertically resolved snow thermal conductivity measurements and alternative parameterizations (e.g., Calonne et al., 2019; Fourteau et al., 2021) could help better constrain these processes.

Despite the model improvements, persistent warm biases remain in the simulated snowpack and snow surface temperatures at some Arctic sites (e.g., at Bylot; Fig. 5c–j), which may contribute to an early onset of melt. A first possible explanation is related to the treatment of meltwater refreezing in CLASSIC: meltwater can refreeze entirely within the snowpack if the available heat sink is sufficient, thereby releasing latent heat and warming the snowpack. However, in reality, preferential flow pathways may allow some of the meltwater to reach the soil without fully refreezing, even when the snowpack heat sink would be sufficient to refreeze it. This effect may be particularly important in Arctic environments, where the formation of depth hoar at the base of the snowpack can enhance water drainage due to its larger grain size (e.g., Marsh and Woo, 1984; Wever et al., 2018). Alternatively, the simulated early melt at Arctic sites may also arise from uncertainties in the forcing datasets, especially in spring when radiative sensors are often affected by frost (e.g., Domine et al., 2019), or from limitations of the albedo scheme, since light-absorbing particles are not represented (as discussed for the Weissfluhjoch site in Sect. 4.1). Furthermore, warm biases may arise from radiative heating of near-surface air temperature sensors under high incoming and reflected shortwave radiation combined with weak wind conditions, which can lead to air temperature overestimations of several degrees Celsius (e.g., Georges and Kaser, 2002; Genthon et al., 2011)—conditions that could occur at Bylot given its relatively low wind speeds (e.g., Domine et al., 2018a). A sensitivity test applying a radiation-dependent correction to spring air temperatures could help assess its contribution to the simulated early melt (e.g., Huwald et al., 2009; Yang et al., 2016; Morino et al., 2021).

Ultimately, the new wind-dependent compaction scheme could be further refined using additional datasets in future work. The most sensitive parameters in Eq. 12 are U_0 and the wind speed threshold triggering enhanced wind compaction. In this study, the latter was fixed at 2.5 m s^{-1}, while a range of U_0 values between 2.5 and 3.5 m s^{-1} was explored. Additional Arctic sites and improved forcing data would help reassess these values and better constrain the center ($d_0 = 0.8$ m) and width

https://doi.org/10.5194/egusphere-2026-492
Preprint. Discussion started: 23 April 2026

($\sigma = 1.0$ m) of the Gaussian function controlling wind-enhanced compaction. More generally, better constraining fresh snow density, maximum snow density, and compaction rates will likely require dedicated experimental and field studies—such as wind tunnel experiments (e.g., Walter et al., 2024) and targeted in situ observations—to jointly inform and disentangle the effects of snowfall properties, wind redistribution, and mechanical compaction in Arctic snowpacks. The formulation of the wind threshold itself could also be made more process-based, for instance by analogy with blowing-snow sublimation schemes (Eq. 6) or by allowing it to depend on surface snow grain type or density (e.g., Liston et al., 2007; Vionnet et al., 2012; Amory et al., 2021).

4.4 Forcing and observation uncertainties

Large uncertainties can also arise from forcing and observation data. Indeed, arctic field sites often face extreme conditions, including prolonged polar nights and harsh weather, which can impact sensor reliability and data collection, especially due to frost and solid precipitation wind undercatch (e.g. Pan et al., 2016; Domine et al., 2021a). The remote nature of these sites also makes it difficult to perform regular maintenance and verification of instruments. Therefore, the measurements can have many gaps, which are often filled with data from nearby stations and/or reanalysis products. For example, at Bylot, the Geonor 200 measurements are complemented with data from nearby Geonor gauge stations at Pond Inlet (84.1 km to the southeast) and Cape Liverpool (79.5 km to the northeast; Domine et al., 2021a), which adds further uncertainties. An alternative precipitation gap-filling method was tested at Bylot (Mohammadzadeh Khani, 2024), resulting in significant differences in simulated snow and soil temperatures, reaching up to 10 cm and a few degrees, respectively, within a few years (not shown). Although those differences were, on average, of lower magnitude than the impact of our model developments, they could affect parameter optimization.

At TVC, large uncertainties arise because the station itself may act as a snow trap (Brampton Dakin, personal communication, 2023), further complicating the interpretation of snow depth measurements. In addition, the site lacks direct snowfall measurements, and the available precipitation data are inconsistent with the simulated snowpack evolution, as discussed in Sect. 2.1. In particular, the initial simulated snow depth is too low, and snow density is underestimated relative to snow pit measurements (Fig. S1a—c; *DEF (1xSnowf)*, blue line in the Sect. 3 of the Supplement). To address this, we doubled the snowfall rates (Sect. 2.1) to obtain more realistic simulated snow depth, density, and soil temperature values in better agreement with observations when using our new model developments (Fig. S1a—c; *ALL_TVC (2xSnowf)*, green line). This adjustment, however, introduces additional uncertainties into the analysis and may bias the tuning applied at TVC in the *TVC_ALL* experiment. More refined precipitation corrections, such as those that explicitly account for wind effects (e.g., Lackner et al., 2022), may be more appropriate. However, because snow drifting can occur even in the absence of precipitation, it remains challenging to determine which correction approach is most accurate. In this context, the forthcoming 32-year dataset at TVC (Woolley et al., 2024; Tutton et al., 2025) will be particularly valuable for better constraining these model developments and ascertaining whether the two snow seasons currently available from Dutch et al. (2022) are representative, or whether snow redistribution processes compensate over longer time scales.

https://doi.org/10.5194/egusphere-2026-492
Preprint. Discussion started: 23 April 2026

4.5 Soil, vegetation, and carbon fluxes

Using CLASSIC enables the simulation of carbon fluxes and dynamically evolving vegetation. However, simulated vegetation height can differ from observations at specific sites. For example, at Col de Porte, grass is regularly mowed (Lejeune et al., 2019), which is not represented in the model and leads to overestimated vegetation height, affecting simulated albedo when vegetation is not yet fully buried by snow (Figs. 3 and S2c). In addition, CLASSIC does not account for vegetation bending under snow load (e.g., Ménard et al., 2014), further increasing uncertainty in the representation of vegetation height. As a result, simulated surface albedos (Fig. S3, third column in Sect. 7 of the Supplement) differ substantially from observations, particularly at the beginning of the snow season at Col de Porte, Senator Beck, and Swamp Angel, with underestimations exceeding 0.2 (Fig. S3c, m, and r). This bias is partly related to unrealistic vegetation heights, which can reach 50 cm to 1 m in the model, even at Arctic sites, where the vegetation is in reality dominated by short grasses, mosses, and lichens. Sensitivity tests comparing bare-ground and grass configurations showed only minor impacts on snowpack evolution in these offline simulations, despite noticeable albedo differences during transition periods (not shown). However, such effects are expected to be more pronounced in land–atmosphere coupled simulations, where albedo biases can feed back on surface energy fluxes, near-surface temperatures, and snow evolution.

Uncertainties in simulated soil temperatures at Arctic sites may also partly arise from the thermal bridge effect associated with shrubs, which is not represented in CLASSIC. This effect can enhance heat exchange between the atmosphere and the ground and reduce soil temperatures by up to 4 °C during cold spells compared to shrub-free areas (Domine et al., 2023). Its absence in the model could therefore contribute to the limited improvement and remaining warm biases in simulated soil temperatures at Umiujaq TUNDRA, where broadleaf deciduous cold shrubs are present (e.g., Fig. 3ss). Consistent with this interpretation, Meyer et al. (2021) reported that simulated soil temperatures in shrub-dominated environments were generally slightly warmer in winter and slightly cooler in summer than observations (their Fig. 1). However, this effect may yet be weak at Umiujaq TUNDRA, as shrubs are short relative to snow depth, largely bent under the snow, and characterized by very small branch diameters, all of which strongly limit the efficiency of thermal bridging. Uncertainties may also stem from the pedotransfer functions used in CLASSIC (Cosby et al., 1984), which are calibrated over a broad range of soil types and may perform poorly for extreme cases (e.g., nearly pure sand; Wösten et al., 2001; Vereecken et al., 2010; Van Looy et al., 2017). Such limitations can affect the estimation of key soil properties, such as soil moisture at saturation, and consequently influence simulated soil water content and soil temperatures.

Using a peat layer to compensate for the absence of explicit moss and lichen representation at Arctic sites (Sect. 2.1) also highlights important model limitations. Mosses and lichens exhibit distinct behaviors in terms of water drainage, heat transfer, and carbon fluxes (Beringer et al., 2001; Gornall et al., 2007), which are not fully captured by this simplified approach. This may introduce additional uncertainties in our simulations, even if its impact appears limited in winter and mainly leads to improved summer albedo, soil temperatures, and soil moisture (not shown). However, remaining biases in simulated volumetric water content persist (Fig. S4 in Sect. 8 of the Supplement) and may still affect winter soil temperatures, particularly during zero-curtain periods when excess liquid water delays soil freezing. Previous studies that explicitly implemented mosses in land

https://doi.org/10.5194/egusphere-2026-492
Preprint. Discussion started: 23 April 2026

surface models, such as JSBACH and JULES, reported notable improvements, particularly for permafrost dynamics (Ekici et al., 2014; Chadburn et al., 2015).

Additional analyses of Arctic carbon budgets are presented in Sect. 9 of the Supplement. They show that improved simulation of winter soil temperatures can substantially affect modeled net ecosystem exchange (NEE), particularly by reducing winter CO_2 emissions at sites with the largest soil temperature biases (e.g., Bylot and TVC). In these cases, lower winter soil temperatures reduce heterotrophic respiration and shift the annual carbon balance toward weaker sources or net sinks (Fig. S5a and c in Sect. 9 of the Supplement). In contrast, changes in NEE at Umiujaq are limited, consistent with the smaller soil temperature differences simulated at this site (Fig. S5b). While simulated NEE amplitudes remain smaller than observed (Fig. S6), large uncertainties in winter flux measurements and limitations in Arctic vegetation representation complicate a direct evaluation. Overall, these results highlight the strong coupling between snow processes, soil thermal regimes, and Arctic carbon fluxes, and emphasize the need to improve the representation of Arctic snowpacks and their interactions with vegetation—such as vegetation bending, thermal bridging in shrubs, and explicit moss and lichen plant functional types—to achieve more consistent simulations of energy, water, and carbon budgets in Arctic environments.

Another source of uncertainty arises from the lack of detailed information on soil composition and measurement locations at some sites (e.g., soil temperature sensors and snow pits), which hampers accurate simulation of snow–soil interactions. This is particularly relevant at TVC, where hummock and inter-hummock zones can exhibit markedly different thermal properties (Brampton Dakin, personal communication, 2023). More broadly, the absence of standardized, homogenized Arctic snow datasets comparable to those of SnowMIP (Menard and Essery, 2019) remains a major challenge for Arctic snow model evaluation and intercomparison. Expanded and more comprehensive observations—including snow temperature, snow thermal conductivity, and camera-based monitoring—are also needed to better constrain and evaluate snow processes in Arctic environments.

5 Conclusions

This study introduces three physics-based snow model improvements in the Canadian Land Surface Scheme including Biogeochemical Cycles (CLASSIC; Melton et al., 2020): (1) a correction to the computation of thermal conductivity at the top of the first soil layer, (2) a revised formulation for bottom snow temperature, and (3) the inclusion of a windless exchange coefficient in the sensible heat flux calculation. In addition, three Arctic-specific snowpack adaptations are implemented: (1) the representation of blowing-snow sublimation losses, (2) a revised snow compaction scheme, and (3) a modification of the snow thermal conductivity parameterization.

To assess the new model developments, seven sites from the Snow Model Intercomparison Project (SnowMIP; Krinner et al., 2018; Ménard et al., 2019; Menard et al., 2021) are used, together with three Arctic sites: Bylot Island (Domine et al., 2021a), Umiujaq TUNDRA (Domine et al., 2024b), and Trail Valley Creek (TVC; Dutch et al., 2022) (Fig. 1). The model is evaluated against automatic and manual measurements of snow depth and SWE, albedo, surface temperature, soil temperature, and snow cover duration (SCD) at all sites except TVC. When available, snow thermal conductivity, bulk snow temperature, and bottom

https://doi.org/10.5194/egusphere-2026-492
Preprint. Discussion started: 23 April 2026

snow temperature are also used to provide additional process-level insights at selected sites. Trail Valley Creek is retained as an independent evaluation site; however, an adjusted version of the new compaction scheme that includes TVC is additionally proposed.

The revised computation of bottom snow temperature (Sect. 2.3.2), combined with the updated snow thermal conductivity parameterization of Calonne et al. (2011) (Sect. 2.4.3), alleviates a bias compensation that previously led to an overestimation of heat storage within the snowpack (e.g., Fig. 4g–j and Sect. B in Appendix). The new formulation of the bottom snow temperature (Eq. 3) reduces the mean simulated snow temperature bias at Col de Porte over 2002—2014 from 0.8 to 0.3 °C (RMSE from 1.4 to 1.2 °C), and the bottom snow temperature bias from -0.4 to -0.1 °C (RMSE from 0.5 to 0.3 °C). It also substantially improves bottom snow temperature estimates at Bylot, with the RMSE decreasing from 4.2 to 0.9 °C (Fig. B2).

The addition of a windless exchange coefficient in the sensible heat flux calculation (Sect. 2.3.3) improves the simulated surface temperature at all SnowMIP sites, reducing the RMSE from 3.41 to 1.51 °C (Fig. 6k) and the mean bias from -2.20 to -0.25 °C (Fig. 7k). At Bylot, surface temperature performance is slightly degraded; however, given the larger temperature amplitude at Arctic sites, the corresponding NRMSE increases only marginally, from 0.29 to 0.30. Overall, when considering both Arctic and SnowMIP sites, the average NRMSE decreases from 0.60 to 0.30 (Fig. 6l).

The snow sublimation scheme (Sect. 2.4.1) has a negligible impact at most sites, except at Umiujaq, TVC, and Senator Beck, where it leads to an average snow depth reduction of 2—4 cm. Large uncertainties remain in the estimation of snow sublimation losses, owing to snow drifting processes and the difficulty of accurately measuring snowfall rates.

The revised snow compaction scheme (Sect. 2.4.2), which accounts for wind effects, has the most pronounced impact at the Arctic sites. Indeed, the previous compaction formulation (Brown et al., 2006) constrained the maximum dry-snow density to values lower than those observed in Arctic environments, leading to an underestimation of bulk snow density by more than 50 kg m^{-3} and, consequently, to an overestimation of simulated snow depth (e.g., Figs. 2 and 5a–d blue line). The new scheme allows higher maximum snow densities during strong wind events for snowpacks around 80 cm (corresponding to the center of the Gaussian formulation of Eq. 12; Fig. 2, red line), while avoiding impacts on deeper mid-latitude snowpacks, where compaction is primarily governed by gravity and metamorphism. As a result, the mean snow depth bias at the Arctic sites (including TVC) is reduced from 12.0 to -1.0 cm, and the associated warm bias in simulated soil temperatures decreases from 4.6 to 3.1 °C from the *DEF* to the *COMPACT* experiment (Fig. 7a and m, blue empty circles; Table 2).

The inclusion of the snow thermal conductivity parameterization of Calonne et al. (2011) (Sect. 2.4.3) further improves model performance. At the SnowMIP sites, the overall soil temperature RMSE remains stable at about 0.6 °C between the *DEF* and *CL11* experiments (Fig. 6m, black circles; Table 2). In contrast, at the Arctic sites (including TVC), the soil temperature RMSE decreases substantially from 5.3 to 3.0 °C, and the mean bias is further reduced to 0.41 °C (Fig. 6 and 7m, blue empty circles). Incorporating TVC-adjusted parameters in the compaction scheme (*ALL_TVC*) yields a modest additional improvement in soil temperature RMSE across all sites (SnowMIP and Arctic), from 1.40 to 1.37 °C (Fig. 6m, red empty circles). Meanwhile, the snow depth RMSE remains close to 20 cm across all sites (Fig. 6a, red empty circles), and the mean snow depth bias at the Arctic sites is reduced to 0.9 cm (Fig. 7a, blue empty circles).

https://doi.org/10.5194/egusphere-2026-492
Preprint. Discussion started: 23 April 2026

The improved simulated soil temperatures induced by the new snow model physics yield changes in simulated net ecosystem exchange (NEE)—the net flux of CO_2 between the land surface and the atmosphere—at all Arctic sites (especially in the winter land surface respiration), which can trigger a switch from carbon sources to sinks (Sect. 9 of the Supplement). Accurate representation of Arctic snowpacks and soil thermal regimes is therefore essential for robust estimates of Arctic carbon fluxes. Such improvements are especially important in the context of climate change and Arctic amplification (e.g., Serreze and Barry, 2011; Arctic Monitoring and Assessment Programme (AMAP), 2024), as well as for Arctic carbon budget assessments, which remain highly uncertain (e.g., McGuire et al., 2012; Natali et al., 2019).

Despite inherent limitations to the CLASSIC snow model (Sect. 4), this study demonstrates the ability of a single-layer snow model to reproduce the bulk characteristics of an Arctic snowpack. In particular, we introduce a novel wind-dependent compaction scheme (Sect. 2.4.2) that enables the simulated snowpack to perform as well at Arctic sites as at mid-latitude sites. Furthermore, the substantial variability in simulated snow depth and soil temperature across the three Arctic sites highlights the need to calibrate and evaluate snow models using multiple Arctic sites, rather than relying on a single location, as has often been the case in previous studies (e.g., Barrere et al., 2017; Gouttevin et al., 2018; Lackner et al., 2022).

Uncertainties remain in the forcing and evaluation datasets, particularly owing to the harsh Arctic environments—characterized by strong winds, frost-affected sensors, polar night conditions, and wind-driven snow redistribution. Overall, there is a crucial need for more measurements in Arctic environments and standardized quality-controlled snow datasets to enable modeling teams to incorporate Arctic sites into their model assessments. To further improve the representation of energy, water, and carbon fluxes in Arctic environments in CLASSIC, future work should incorporate moss and lichen dynamics, along with a more refined assessment of carbon fluxes. Integrating vegetation bending may also be important, as non-buried protruding vegetation may significantly bias surface albedo and the energy budget, particularly in autumn and spring (Sect. 4.5). Accounting for light-absorbing particles on the snowpack and revising the compaction and/or albedo scheme accordingly should also be considered (e.g., Gaillard et al., 2025). Future work will focus on performing spatial simulations to evaluate the 1D snow model developments of this study over the Arctic, in addition to assessing new snow cover fraction parameterizations to better account for spatial snow heterogeneities.

Code and data availability. All scripts to produce the figures and results are available at: https://doi.org/10.5281/zenodo.18154779 (Lalande, 2026a). The CLASSIC code used for this study can be accessed at https://doi.org/10.5281/zenodo.18175772 (Lalande, 2026b). The SnowMIP data used in this paper are available in the data repository PANGAEA: https://doi.org/10.1594/PANGAEA.897575 (Menard and Essery, 2019). Additional snow temperatures were extracted from Lejeune et al. (2019). The Bylot driving and validating data, are available on the Nordicana D repository: https://doi.org/10.5885/45693CE-02685A5200DD4C38 (Domine et al., 2021b). The Umiujaq TUNDRA data are available in the PANGAEA repository at https://doi.org/10.1594/PANGAEA.964743 (Domine et al., 2024a). Trail Valley Creek data are available at https://github.com/V-Dutch/TVCSnowCLM and https://doi.org/10.5281/zenodo.7137729 (V-Dutch, 2022).

https://doi.org/10.5194/egusphere-2026-492
Preprint. Discussion started: 23 April 2026

Appendix A: Snow depth time series

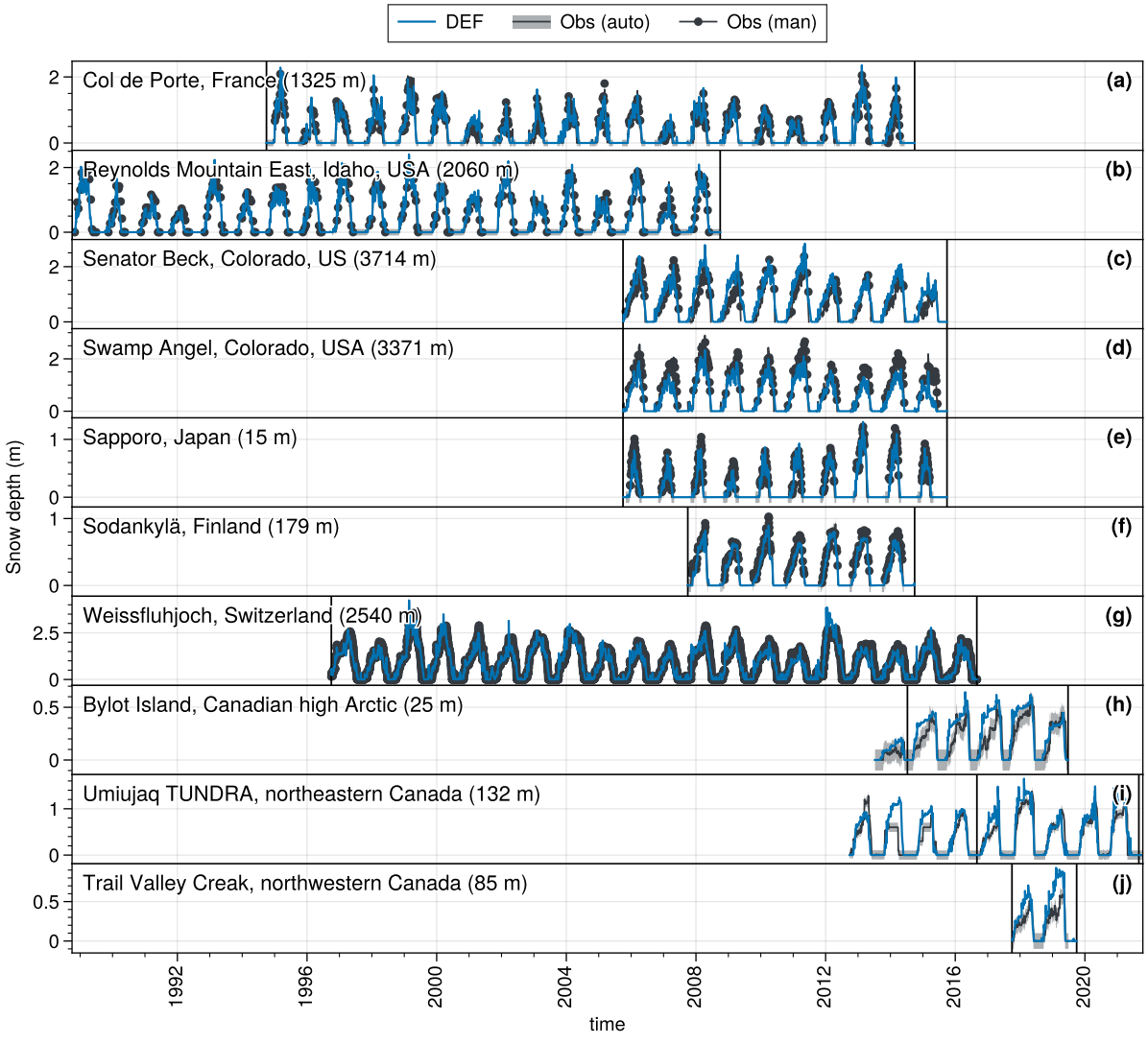

Figure A1. Snow depth time series for the *DEF* experiment (blue line), and the automatic (black line) and manual (black dots) observations. The black shading represents the snow depth uncertainty of ±10 cm estimated at Col de Porte (Lejeune et al., 2019) and applied to the other sites as an indicative reference. The black vertical lines correspond to the analysis period for each site.

https://doi.org/10.5194/egusphere-2026-492
Preprint. Discussion started: 23 April 2026

Appendix B: Bottom snow temperature

The snow and bottom snow temperatures were estimated at Col de Porte and Bylot. At Col de Porte, weekly snow profiles have been available since 1993. A trapezoidal integration was applied to obtain the bulk snow temperature and density. The evaluation period was chosen between 2002 and 2014 to compare with the automatic SWE measurements. The bottom snow temperature was derived from the lowest snow measurement (typically at 0 cm). Two example snow seasons are shown in Figs. 4 and B1 of simulated versus observed variables. The metrics (bias and RMSE) mentioned in Sect. 2.3.2 are computed over the whole period.

At Bylot, because the initial model version (*DEF*) did not simulate correct snow depth and densities (e.g., Fig 5a–d), the observed bottom snow temperature was directly compared to the theoretical Eqs. 2 and 3 in Fig. B2. The observed bulk snow temperature is estimated by integrating (trapezoidal method) the measured snow temperatures at 2, 7, 17, 27, and 37 cm or at 0, 5, 15, 25, 35 cm after July 2018 (Domine et al., 2021a), considering only the sensors when the snow depth exceeds their respective height. The bottom snow temperature is estimated as the average of the shallowest soil and snow temperature measurements, i.e., at ± 2 cm before July 2018, and the snow temperature measurement at 0 cm is taken after. The automatic snow depth measurement was used to estimate the snow depth. A data gap is present at the end of the 2016 snow season, but the available period for that year is still used for the comparison.

https://doi.org/10.5194/egusphere-2026-492
Preprint. Discussion started: 23 April 2026

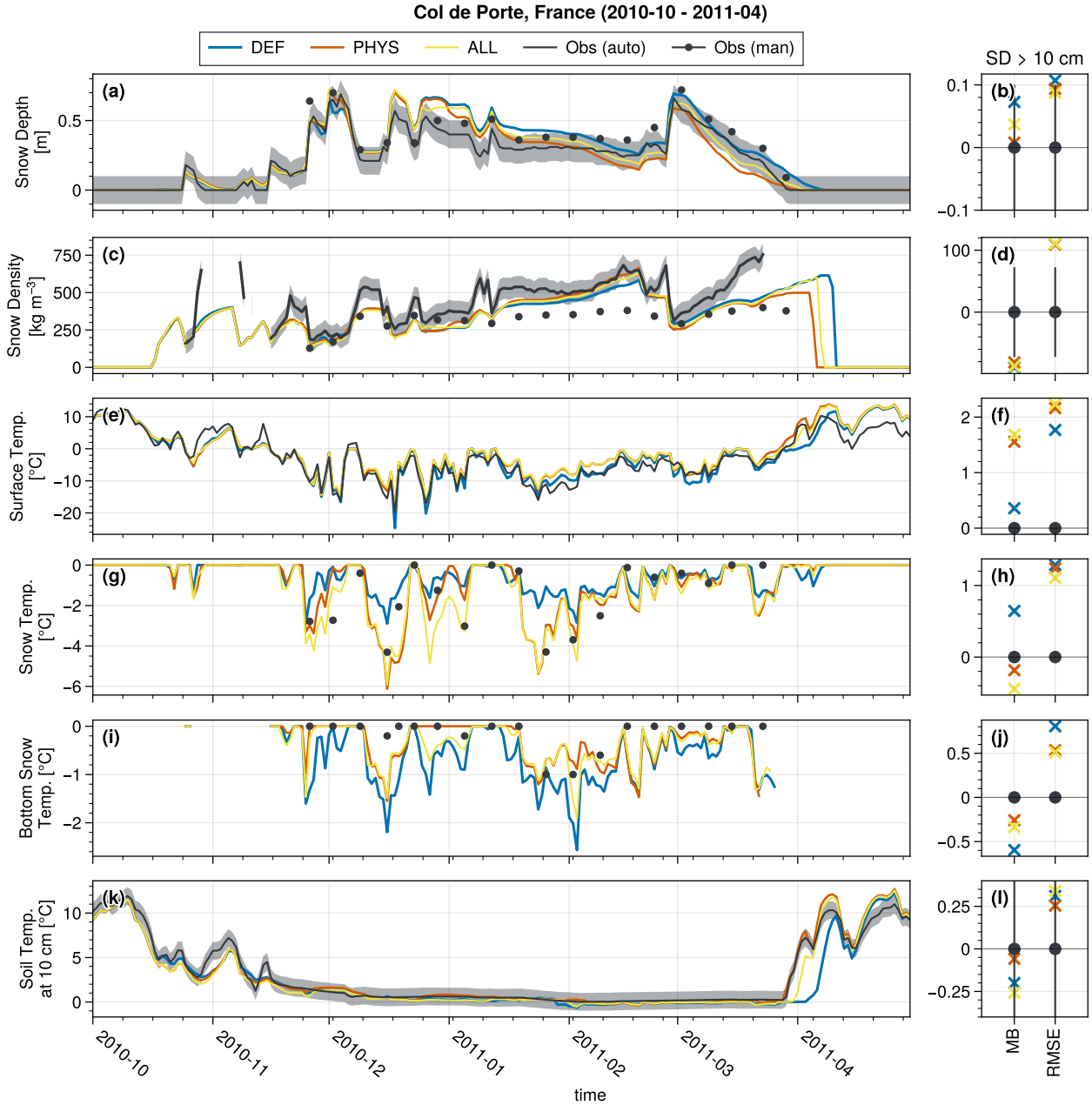

Figure B1. Same as Fig. 4 but for the period 2010-2011.

https://doi.org/10.5194/egusphere-2026-492
Preprint. Discussion started: 23 April 2026

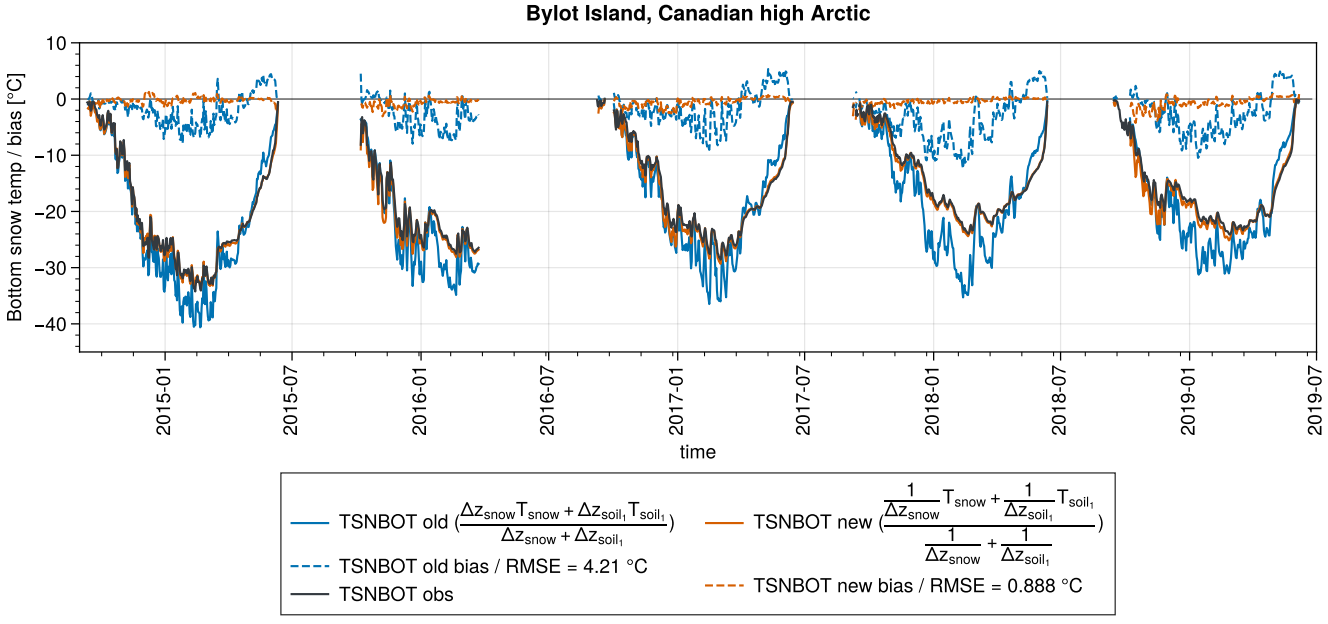

Figure B2. Daily time series of the observed bottom snow temperature (black line), and its theoretical estimation with Eqs. 2 and 3 (blue and orange lines respectively) at Bylot over the period 2015-2019. The dashed lines correspond to the differences between the theoretical estimate and the observed bottom snow temperature. The averaged RMSE is also indicated in the legend.

https://doi.org/10.5194/egusphere-2026-492
Preprint. Discussion started: 23 April 2026

Appendix C: Physics improvements

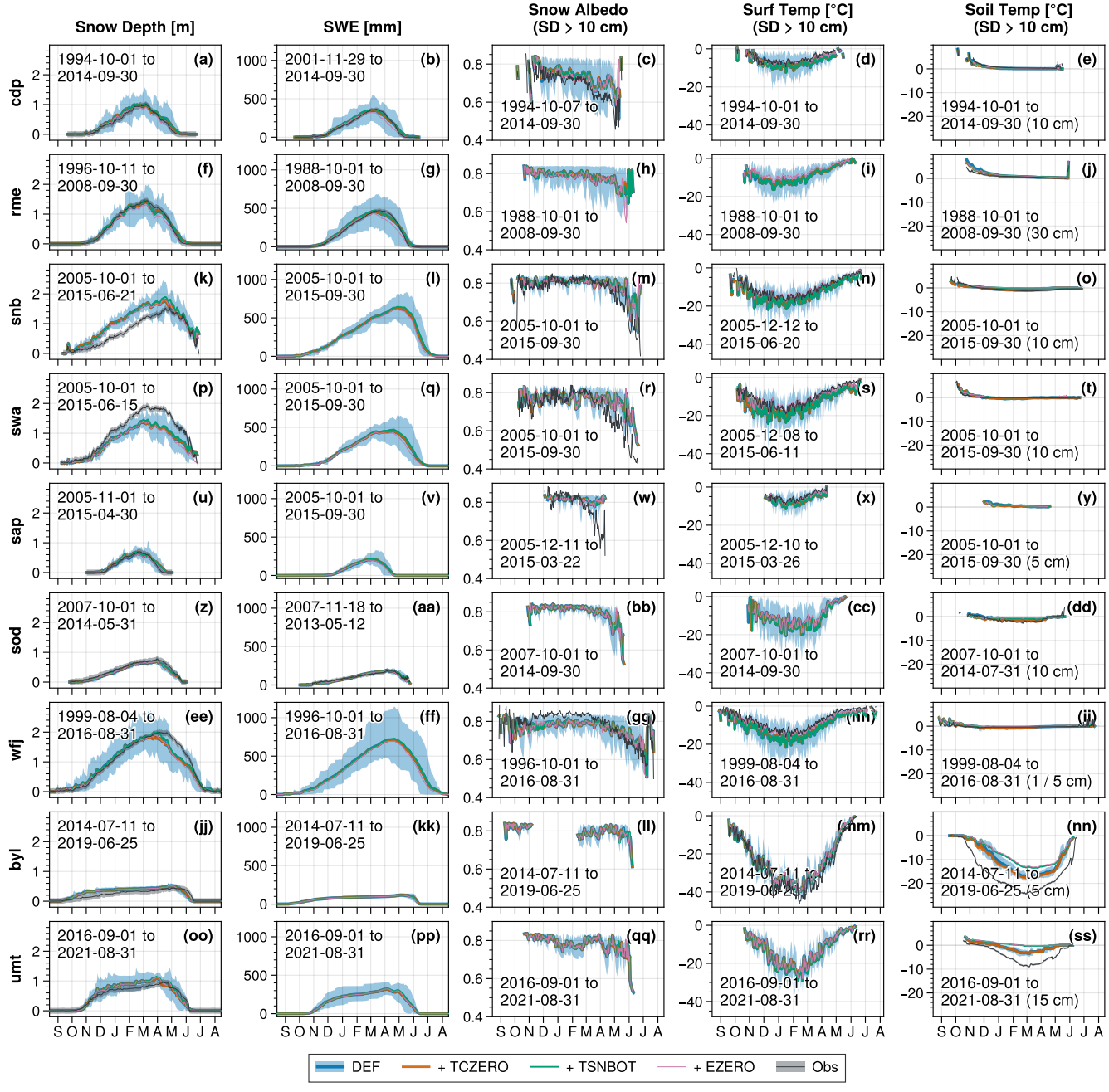

Figure C1. Same as Fig. 3 but for the *DEF*, *TCZERO*, *TSNBOT*, and *EZERO* experiments (without TVC).

https://doi.org/10.5194/egusphere-2026-492
Preprint. Discussion started: 23 April 2026

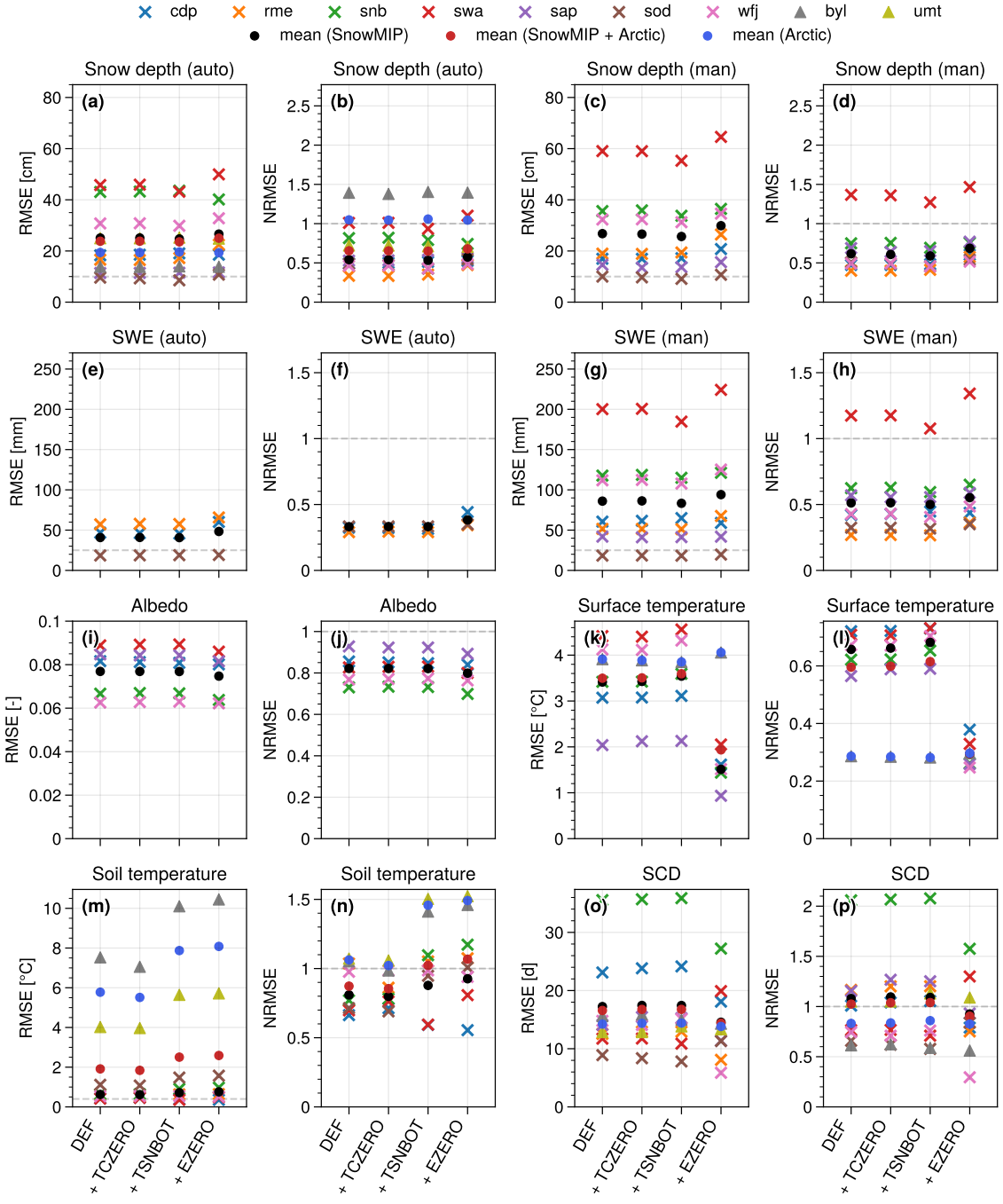

Figure C2. Same as Fig. 6 but for the *DEF*, *TCZERO*, *TSNBOT*, and *EZERO* experiments (without TVC)

https://doi.org/10.5194/egusphere-2026-492
Preprint. Discussion started: 23 April 2026

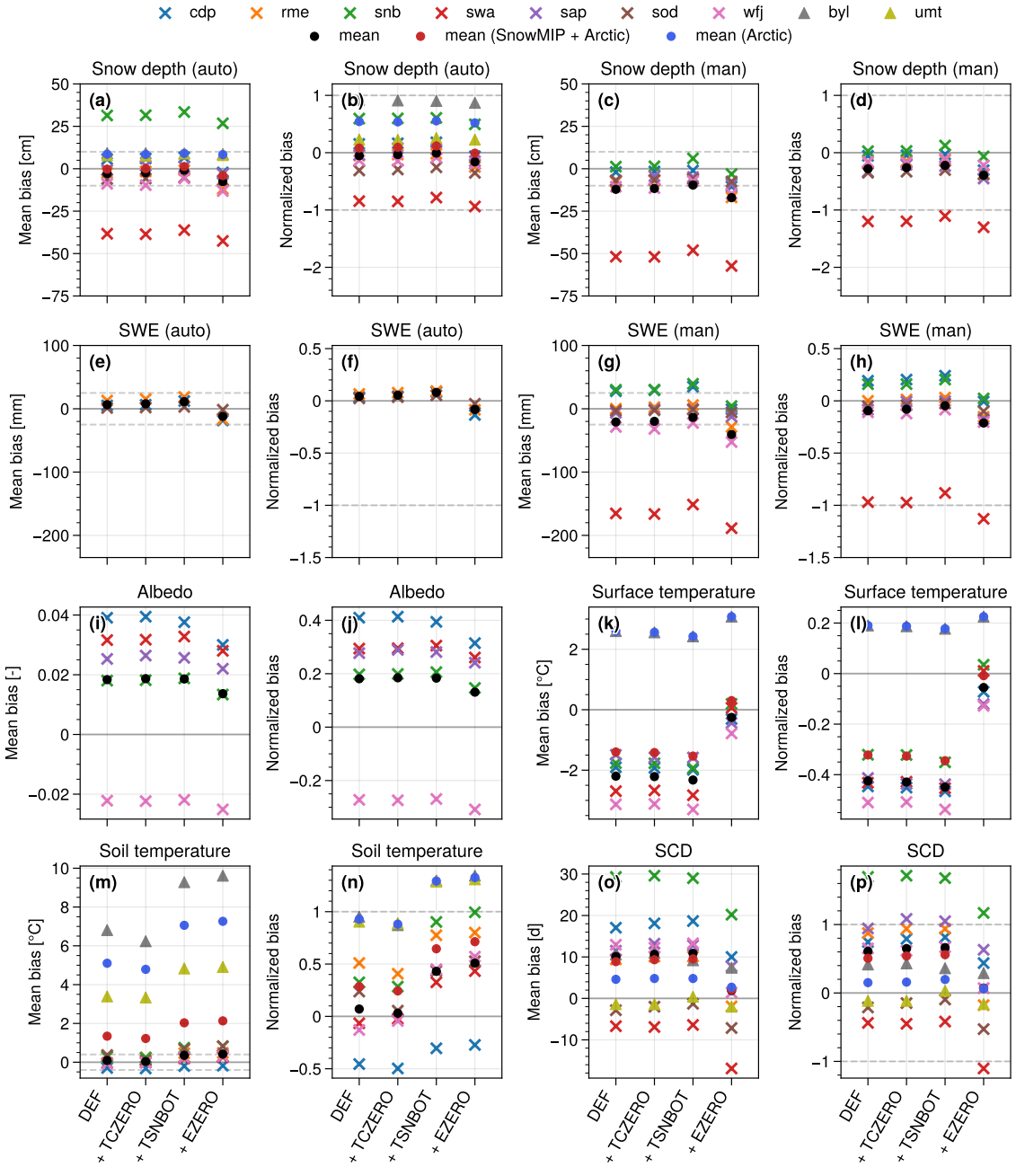

Figure C3. Same as Fig. 7 but for the *DEF*, *TCZERO*, *TSNBOT*, and *EZERO* experiments (without TVC).

https://doi.org/10.5194/egusphere-2026-492
Preprint. Discussion started: 23 April 2026

Appendix D: Arctic sites time series

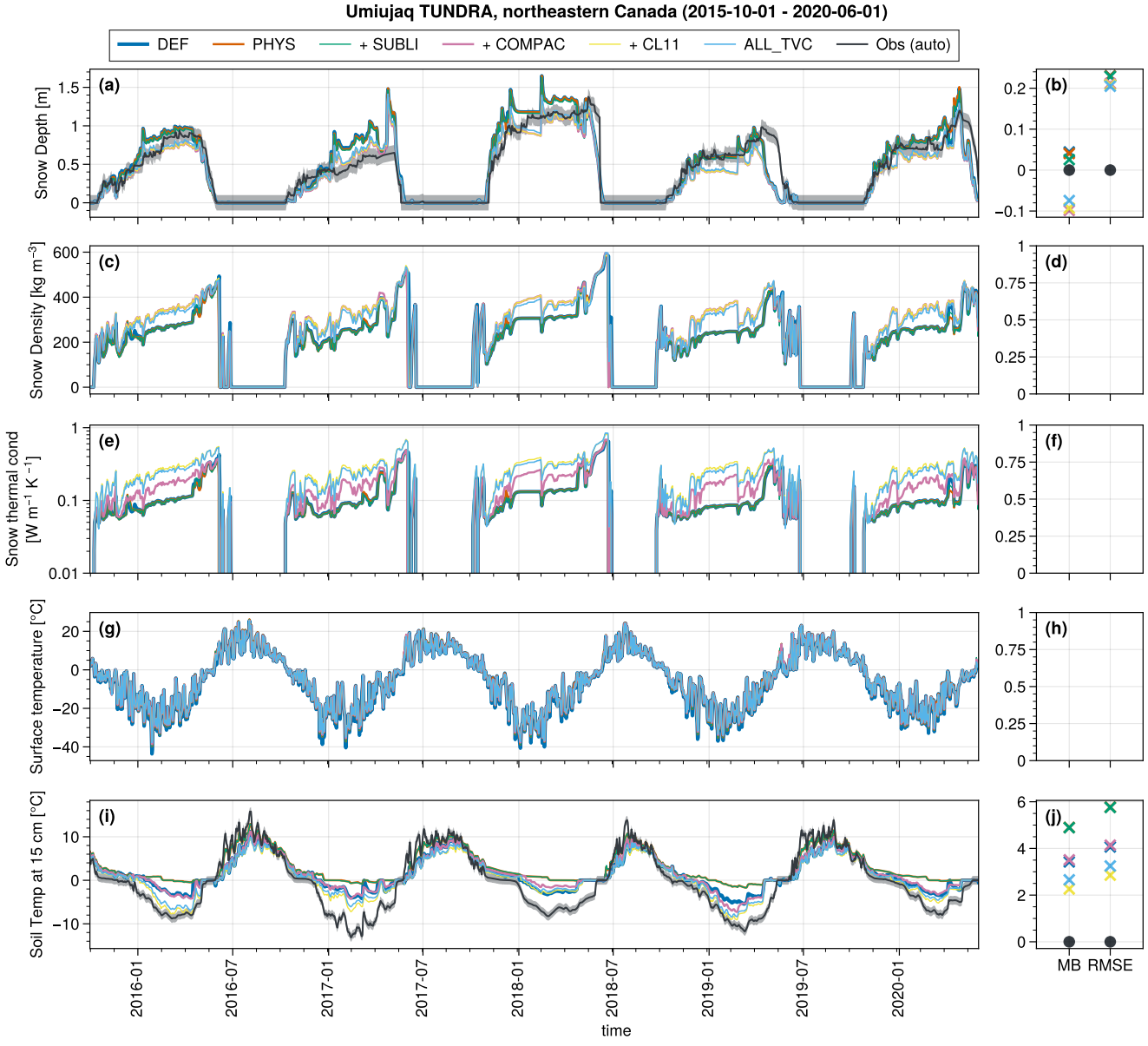

Figure D1. Same as Fig. 5 but only for the snow depth (a), snow density (c), snow thermal conductivity (e), snow surface temperature (g), and soil temperatures at 15 cm (i) at Umiujaq TUNDRA from October 2015 to the end of June 2020.

https://doi.org/10.5194/egusphere-2026-492
Preprint. Discussion started: 23 April 2026

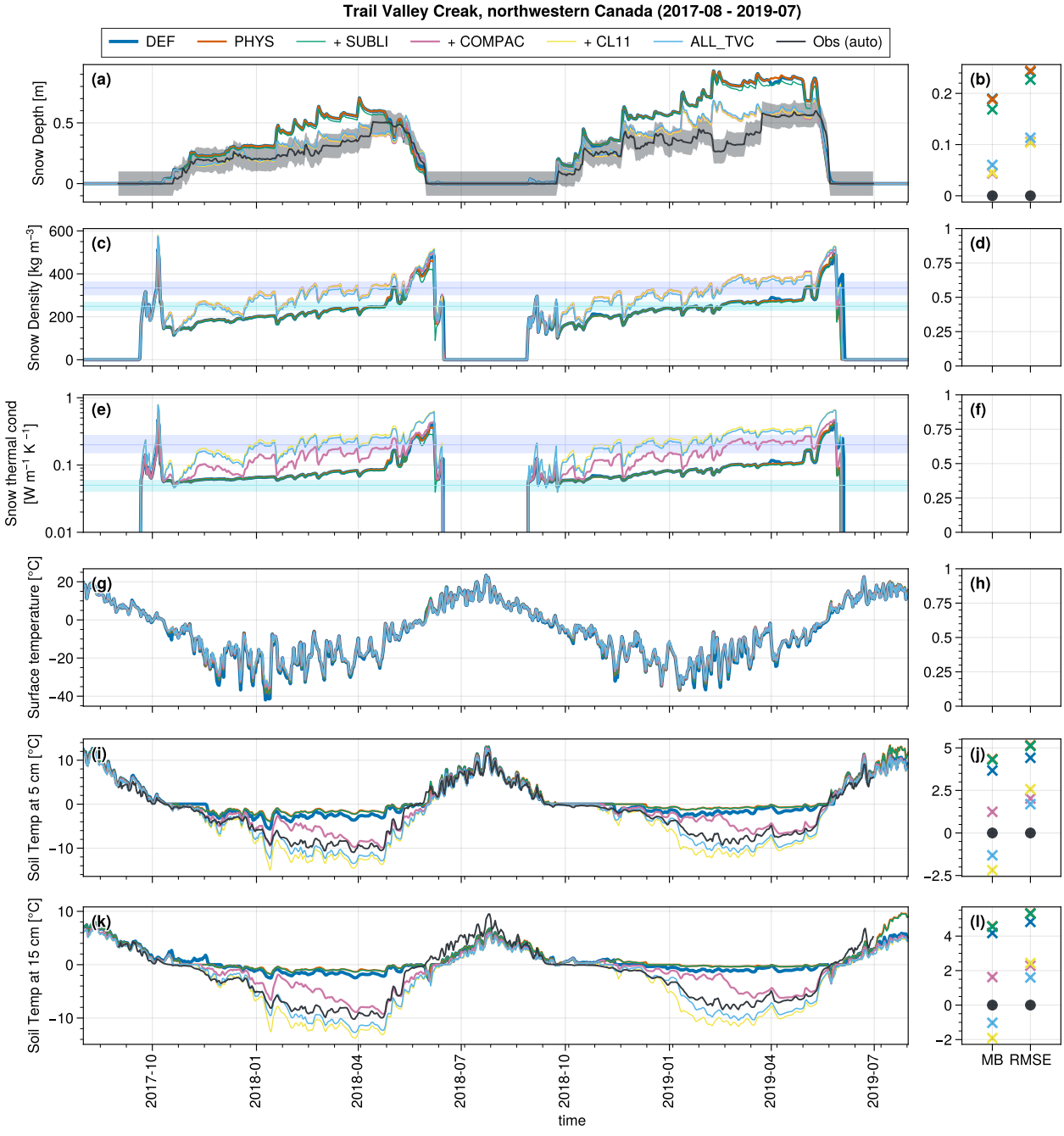

Figure D2. Same as Fig. 5 but for the snow depth (a), snow density (c), snow thermal conductivity (e), snow surface temperature (g), and soil temperatures at 5 and 15 cm (i, k) at TVC from September 2017 to the end of June 2019. The dark and light horizontal blue shadings on panels (c) and (e) correspond to average snow densities and thermal conductivities of the wind slab and depth hoar, respectively, over multiple snow pits around the simulation site (Dutch et al., 2022, their Table 2).

https://doi.org/10.5194/egusphere-2026-492
Preprint. Discussion started: 23 April 2026

Author contributions. ML, CK, and AR designed the study. ML implemented the model developments, performed the simulations, and produced the figures. LW, DV, and VV provided valuable insights, ideas, and critical perspectives on the new snow model developments. FD helped set up Arctic sites and provided expertise in Arctic snow and field observations. ML wrote the manuscript, and all co-authors contributed through revisions, comments, and suggestions. All authors discussed the results and provided critical feedback.

Competing interests. The authors declare that they have no conflict of interest.

Acknowledgements. We acknowledge Mark D. Gordon for sharing his expertise on the implementation of the snow sublimation loss parameterization. We are grateful to Ross Brown for providing valuable insights into previous CLASS snow model developments, particularly regarding the snow compaction scheme. We thank Brampton Dakin and Georgina J. Woolley for sharing additional information on the Trail Valley Creek (TVC) site, as well as Oliver Sonnentag for providing the meteorological forcing data used in this study, made available through the dataset compiled by Victoria Dutch. We also thank Paul Bartlett for providing the latest configuration of the SnowMIP experiments. We are grateful to Joe R. Melton and Gesa Meyer for their extensive help with the CLASSIC model and simulation setup, as well as for their valuable comments that helped improve this study. Finally, we thank Anna Maria Trofaier and Clément Albergel for supervising the European Space Agency (ESA) Climate Change Initiative Research Fellowships project: *Snow cover heterogeneity and its impact on the Climate and Carbon cycle of Arctic regions (SnowC^2)*, which supported this work.

https://doi.org/10.5194/egusphere-2026-492
Preprint. Discussion started: 23 April 2026

References

Amory, C., Kittel, C., Le Toumelin, L., Agosta, C., Delhasse, A., Favier, V., and Fettweis, X.: Performance of MAR (v3.11) in Simulating the Drifting-Snow Climate and Surface Mass Balance of Adélie Land, East Antarctica, Geoscientific Model Development, 14, 3487–3510, https://doi.org/10.5194/gmd-14-3487-2021, 2021.

Arctic Monitoring and Assessment Programme (AMAP): Arctic Climate Change Update 2024: Key Trends and Impacts. Summary for Policy-Makers, Tech. rep., Arctic Monitoring and Assessment Programme (AMAP), Tromsø, Norway, 2024.

Augas, J., Abbasnezhadi, K., Rousseau, A. N., and Baraer, M.: What Is the Trade-Off between Snowpack Stratification and Simulated Snow Water Equivalent in a Physically-Based Snow Model?, Water, 12, 3449, https://doi.org/10.3390/w12123449, 2020.

Barnett, T. P., Adam, J. C., and Lettenmaier, D. P.: Potential Impacts of a Warming Climate on Water Availability in Snow-Dominated Regions, Nature, 438, 303–309, https://doi.org/10.1038/nature04141, 2005.

Barrere, M., Domine, F., Decharme, B., Morin, S., Vionnet, V., and Lafaysse, M.: Evaluating the Performance of Coupled Snow–Soil Models in SURFEXv8 to Simulate the Permafrost Thermal Regime at a High Arctic Site, Geoscientific Model Development, 10, 3461–3479, https://doi.org/10.5194/gmd-10-3461-2017, 2017.

Bartelt, P. and Lehning, M.: A Physical SNOWPACK Model for the Swiss Avalanche Warning: Part I: Numerical Model, Cold Regions Science and Technology, 35, 123–145, https://doi.org/10.1016/S0165-232X(02)00074-5, 2002.

Bartlett, P. A. and Verseghy, D. L.: Modified Treatment of Intercepted Snow Improves the Simulated Forest Albedo in the Canadian Land Surface Scheme, Hydrological Processes, 29, 3208–3226, https://doi.org/10.1002/hyp.10431, 2015.

Bartlett, P. A., MacKay, M. D., and Verseghy, D. L.: Modified Snow Algorithms in the Canadian Land Surface Scheme: Model Runs and Sensitivity Analysis at Three Boreal Forest Stands, Atmosphere-Ocean, 44, 207–222, https://doi.org/10.3137/ao.440301, 2006.

Beringer, J., Lynch, A. H., Chapin, F. S., Mack, M., and Bonan, G. B.: The Representation of Arctic Soils in the Land Surface Model: The Importance of Mosses, Journal of Climate, 14, 3324–3335, https://doi.org/10.1175/1520-0442(2001)014<3324:TROASI>2.0.CO;2, 2001.

Best, M. J., Pryor, M., Clark, D. B., Rooney, G. G., Essery, R. L. H., Ménard, C. B., Edwards, J. M., Hendry, M. A., Porson, A., Gedney, N., Mercado, L. M., Sitch, S., Blyth, E., Boucher, O., Cox, P. M., Grimmond, C. S. B., and Harding, R. J.: The Joint UK Land Environment Simulator (JULES), Model Description – Part 1: Energy and Water Fluxes, Geoscientific Model Development, 4, 677–699, https://doi.org/10.5194/gmd-4-677-2011, 2011.

Boike, J., Miesner, F., Bornemann, N., Cable, W. L., and Grünberg, I.: Trail Valley Creek, NWT, Canada Soil Moisture and Temperature 2016 et Seq, PANGAEA [Data Set], https://doi.pangaea.de/10.1594/PANGAEA.962726, https://doi.org/10.1594/PANGAEA.962726, 2023.

Bokhorst, S., Pedersen, S. H., Brucker, L., Anisimov, O., Bjerke, J. W., Brown, R. D., Ehrich, D., Essery, R. L. H., Heilig, A., Ingvander, S., Johansson, C., Johansson, M., Jónsdóttir, I. S., Inga, N., Luojus, K., Macelloni, G., Mariash, H., McLennan, D., Rosqvist, G. N., Sato, A., Savela, H., Schneebeli, M., Sokolov, A., Sokratov, S. A., Terzago, S., Vikhamar-Schuler, D., Williamson, S., Qiu, Y., and Callaghan, T. V.: Changing Arctic Snow Cover: A Review of Recent Developments and Assessment of Future Needs for Observations, Modelling, and Impacts, Ambio, 45, 516–537, https://doi.org/10.1007/s13280-016-0770-0, 2016.

Boone, A. and Etchevers, P.: An Intercomparison of Three Snow Schemes of Varying Complexity Coupled to the Same Land Surface Model: Local-Scale Evaluation at an Alpine Site, Journal of Hydrometeorology, 2, 374–394, https://doi.org/10.1175/1525-7541(2001)002<0374:AIOTSS>2.0.CO;2, 2001.

https://doi.org/10.5194/egusphere-2026-492
Preprint. Discussion started: 23 April 2026

Bring, A., Fedorova, I., Dibike, Y., Hinzman, L., Mård, J., Mernild, S. H., Prowse, T., Semenova, O., Stuefer, S. L., and Woo, M.-K.: Arctic Terrestrial Hydrology: A Synthesis of Processes, Regional Effects, and Research Challenges, Journal of Geophysical Research: Biogeosciences, 121, 621–649, https://doi.org/10.1002/2015JG003131, 2016.

Brondex, J., Fourteau, K., Dumont, M., Hagenmuller, P., Calonne, N., Tuzet, F., and Löwe, H.: A Finite-Element Framework to Explore the Numerical Solution of the Coupled Problem of Heat Conduction, Water Vapor Diffusion, and Settlement in Dry Snow (IvoriFEM v0.1.0), Geoscientific Model Development, 16, 7075–7106, https://doi.org/10.5194/gmd-16-7075-2023, 2023.

Brown, R., Bartlett, P., MacKay, M., and Verseghy, D.: Evaluation of Snow Cover in CLASS for SnowMIP, Atmosphere-Ocean, 44, 223–238, https://doi.org/10.3137/ao.440302, 2006.

Bruce, J. P. and Clark, R. H.: Introduction to Hydrometeorology, Elsevier Science & Technology, ISBN 978-0-08-011714-0, 1966.

Burke, E. J., Ekici, A., Huang, Y., Chadburn, S. E., Huntingford, C., Ciais, P., Friedlingstein, P., Peng, S., and Krinner, G.: Quantifying Uncertainties of Permafrost Carbon–Climate Feedbacks, Biogeosciences, 14, 3051–3066, https://doi.org/10.5194/bg-14-3051-2017, 2017.

Calonne, N., Flin, F., Morin, S., Lesaffre, B., du Roscoat, S. R., and Geindreau, C.: Numerical and Experimental Investigations of the Effective Thermal Conductivity of Snow, Geophysical Research Letters, 38, L23 501, https://doi.org/10.1029/2011GL049234, 2011.

Calonne, N., Milliancourt, L., Burr, A., Philip, A., Martin, C. L., Flin, F., and Geindreau, C.: Thermal Conductivity of Snow, Firn, and Porous Ice From 3-D Image-Based Computations, Geophysical Research Letters, 46, 13 079–13 089, https://doi.org/10.1029/2019GL085228, 2019.

Campbell, J. L. and Laudon, H.: Carbon Response to Changing Winter Conditions in Northern Regions: Current Understanding and Emerging Research Needs, Environmental Reviews, 27, 545–566, https://doi.org/10.1139/er-2018-0097, 2019.

Chadburn, S., Burke, E., Essery, R., Boike, J., Langer, M., Heikenfeld, M., Cox, P., and Friedlingstein, P.: An Improved Representation of Physical Permafrost Dynamics in the JULES Land-Surface Model, Geoscientific Model Development, 8, 1493–1508, https://doi.org/10.5194/gmd-8-1493-2015, 2015.

Cohen, J. L., Furtado, J. C., Barlow, M. A., Alexeev, V. A., and Cherry, J. E.: Arctic Warming, Increasing Snow Cover and Widespread Boreal Winter Cooling, Environmental Research Letters, 7, 014 007, https://doi.org/10.1088/1748-9326/7/1/014007, 2012.

Comyn-Platt, E., Hayman, G., Huntingford, C., Chadburn, S. E., Burke, E. J., Harper, A. B., Collins, W. J., Webber, C. P., Powell, T., Cox, P. M., Gedney, N., and Sitch, S.: Carbon Budgets for 1.5 and 2 °C Targets Lowered by Natural Wetland and Permafrost Feedbacks, Nature Geoscience 2018 11:8, 11, 568–573, https://doi.org/10.1038/s41561-018-0174-9, 2018.

Cook, B. I., Bonan, G. B., Levis, S., and Epstein, H. E.: The Thermoinsulation Effect of Snow Cover within a Climate Model, Climate Dynamics, 31, 107–124, https://doi.org/10.1007/s00382-007-0341-y, 2008.

Cosby, B. J., Hornberger, G. M., Clapp, R. B., and Ginn, T. R.: A Statistical Exploration of the Relationships of Soil Moisture Characteristics to the Physical Properties of Soils, Water Resources Research, 20, 682–690, https://doi.org/10.1029/WR020i006p00682, 1984.

Cristea, N. C., Bennett, A., Nijssen, B., and Lundquist, J. D.: When and Where Are Multiple Snow Layers Important for Simulations of Snow Accumulation and Melt?, Water Resources Research, 58, e2020WR028 993, https://doi.org/10.1029/2020WR028993, 2022.

Dai, Y., Zeng, X., Dickinson, R. E., Baker, I., Bonan, G. B., Bosilovich, M. G., Denning, A. S., Dirmeyer, P. A., Houser, P. R., Niu, G., Oleson, K. W., Schlosser, C. A., and Yang, Z.-L.: The Common Land Model, Bulletin of the American Meteorological Society, 84, 1013–1024, https://doi.org/10.1175/BAMS-84-8-1013, 2003.

Decharme, B., Brun, E., Boone, A., Delire, C., Le Moigne, P., and Morin, S.: Impacts of Snow and Organic Soils Parameterization on Northern Eurasian Soil Temperature Profiles Simulated by the ISBA Land Surface Model, The Cryosphere, 10, 853–877, https://doi.org/10.5194/tc-10-853-2016, 2016.

https://doi.org/10.5194/egusphere-2026-492
Preprint. Discussion started: 23 April 2026

Domine, F., Barrere, M., Sarrazin, D., Morin, S., and Arnaud, L.: Automatic Monitoring of the Effective Thermal Conductivity of Snow in a Low-Arctic Shrub Tundra, The Cryosphere, 9, 1265–1276, https://doi.org/10.5194/tc-9-1265-2015, 2015.

Domine, F., Barrere, M., and Sarrazin, D.: Seasonal Evolution of the Effective Thermal Conductivity of the Snow and the Soil in High Arctic Herb Tundra at Bylot Island, Canada, The Cryosphere, 10, 2573–2588, https://doi.org/10.5194/tc-10-2573-2016, 2016.

Domine, F., Belke-Brea, M., Sarrazin, D., Arnaud, L., Barrere, M., and Poirier, M.: Soil Moisture, Wind Speed and Depth Hoar Formation in the Arctic Snowpack, Journal of Glaciology, 64, 990–1002, https://doi.org/10.1017/jog.2018.89, 2018a.

Domine, F., Gauthier, G., Vionnet, V., Fauteux, D., Dumont, M., and Barrere, M.: Snow Physical Properties May Be a Significant Determinant of Lemming Population Dynamics in the High Arctic, Arctic Science, 4, 813–826, https://doi.org/10.1139/as-2018-0008, 2018b.

Domine, F., Picard, G., Morin, S., Barrere, M., Madore, J.-B., and Langlois, A.: Major Issues in Simulating Some Arctic Snowpack Properties Using Current Detailed Snow Physics Models: Consequences for the Thermal Regime and Water Budget of Permafrost, Journal of Advances in Modeling Earth Systems, 11, 34–44, https://doi.org/10.1029/2018MS001445, 2019.

Domine, F., Lackner, G., Sarrazin, D., Poirier, M., and Belke-Brea, M.: Meteorological, Snow and Soil Data (2013–2019) from a Herb Tundra Permafrost Site at Bylot Island, Canadian High Arctic, for Driving and Testing Snow and Land Surface Models, Earth System Science Data, 13, 4331–4348, https://doi.org/10.5194/essd-13-4331-2021, 2021a.

Domine, F., Lackner, G., Sarrazin, D., Poirier, M., and Belke-Brea, M.: Meteorological, Snow and Soil Data from Bylot Island, Canadian High Arctic, for Driving and Testing Snow and Land Surface Models, v. 1.100000 (2013-2019), Nordicana D86 [Data Set], https://doi.org/10.5885/45693CE-02685A5200DD4C38, 2021b.

Domine, F., Fourteau, K., and Choler, P.: Exploration of Thermal Bridging Through Shrub Branches in Alpine Snow, Geophysical Research Letters, 50, e2023GL105 100, https://doi.org/10.1029/2023GL105100, 2023.

Domine, F., Sarrazin, D., Nadeau, D., Lackner, G., and Belke-Brea, M.: Hydrometeorological, Snow and Soil Data from a Low-Arctic Valley in the Forest-Tundra Ecotone in Northern Quebec, PANGAEA [Data Set], https://doi.org/10.1594/PANGAEA.964743, 2024a.

Domine, F., Sarrazin, D., Nadeau, D. F., Lackner, G., and Belke-Brea, M.: Meteorological, Snow and Soil Data, CO_2, Water and Energy Fluxes from a Low-Arctic Valley of Northern Quebec, Earth System Science Data, 16, 1523–1541, https://doi.org/10.5194/essd-16-1523-2024, 2024b.

Douville, H., Royer, J. F., and Mahfouf, J. F.: A New Snow Parameterization for the Météo-France Climate Model, Climate Dynamics, 12, 21–35, https://doi.org/10.1007/BF00208760, 1995.

Dutch, V. R., Rutter, N., Wake, L., Sandells, M., Derksen, C., Walker, B., Hould Gosselin, G., Sonnentag, O., Essery, R., Kelly, R., Marsh, P., King, J., and Boike, J.: Impact of Measured and Simulated Tundra Snowpack Properties on Heat Transfer, The Cryosphere, 16, 4201–4222, https://doi.org/10.5194/tc-16-4201-2022, 2022.

Dutra, E., Balsamo, G., Viterbo, P., Miranda, P. M. A., Beljaars, A., Schär, C., and Elder, K.: An Improved Snow Scheme for the ECMWF Land Surface Model: Description and Offline Validation, Journal of Hydrometeorology, 11, 899–916, https://doi.org/10.1175/2010JHM1249.1, 2010.

Ekici, A., Beer, C., Hagemann, S., Boike, J., Langer, M., and Hauck, C.: Simulating High-Latitude Permafrost Regions by the JSBACH Terrestrial Ecosystem Model, Geoscientific Model Development, 7, 631–647, https://doi.org/10.5194/gmd-7-631-2014, 2014.

Essery, R., Morin, S., Lejeune, Y., and B Ménard, C.: A Comparison of 1701 Snow Models Using Observations from an Alpine Site, Advances in Water Resources, 55, 131–148, https://doi.org/10.1016/J.ADVWATRES.2012.07.013, 2013.

https://doi.org/10.5194/egusphere-2026-492
Preprint. Discussion started: 23 April 2026

Essery, R., Kontu, A., Lemmetyinen, J., Dumont, M., and Ménard, C. B.: A 7-Year Dataset for Driving and Evaluating Snow Models at an Arctic Site (Sodankylä, Finland), Geoscientific Instrumentation, Methods and Data Systems, 5, 219–227, https://doi.org/10.5194/gi-5-219-2016, 2016.

Etchevers, P., Martin, E., Brown, R., Fierz, C., Lejeune, Y., Bazile, E., Boone, A., Dai, Y.-J., Essery, R., Fernandez, A., Gusev, Y., Jordan, R., Koren, V., Kowalczyk, E., Nasonova, N. O., Pyles, R. D., Schlosser, A., Shmakin, A. B., Smirnova, T. G., Strasser, U., Verseghy, D., Yamazaki, T., and Yang, Z.-L.: Validation of the Energy Budget of an Alpine Snowpack Simulated by Several Snow Models (Snow MIP Project), Annals of Glaciology, 38, 150–158, https://doi.org/10.3189/172756404781814825, 2004.

Eyring, V., Bony, S., Meehl, G. A., Senior, C. A., Stevens, B., Stouffer, R. J., and Taylor, K. E.: Overview of the Coupled Model Intercomparison Project Phase 6 (CMIP6) Experimental Design and Organization, Geoscientific Model Development, 9, 1937–1958, https://doi.org/10.5194/gmd-9-1937-2016, 2016.

Fierz, C.: Temperature Profile of Snowpack, in: Encyclopedia of Snow, Ice and Glaciers, edited by Singh, V. P., Singh, P., and Haritashya, U. K., pp. 1151–1154, Springer Netherlands, Dordrecht, ISBN 978-90-481-2642-2, https://doi.org/10.1007/978-90-481-2642-2_569, 2011.

Flanner, M. G., Shell, K. M., Barlage, M., Perovich, D. K., and Tschudi, M. A.: Radiative Forcing and Albedo Feedback from the Northern Hemisphere Cryosphere between 1979 and 2008, Nature Geoscience, 4, 151–155, https://doi.org/10.1038/ngeo1062, 2011.

Fourteau, K., Domine, F., and Hagenmuller, P.: Impact of Water Vapor Diffusion and Latent Heat on the Effective Thermal Conductivity of Snow, The Cryosphere, 15, 2739–2755, https://doi.org/10.5194/tc-15-2739-2021, 2021.

Fourteau, K., Hagenmuller, P., Roulle, J., and Domine, F.: On the Use of Heated Needle Probes for Measuring Snow Thermal Conductivity, Journal of Glaciology, 68, 705–719, https://doi.org/10.1017/jog.2021.127, 2022.

Friedlingstein, P., O'Sullivan, M., Jones, M. W., Andrew, R. M., Bakker, D. C. E., Hauck, J., Landschützer, P., Le Quéré, C., Luijkx, I. T., Peters, G. P., Peters, W., Pongratz, J., Schwingshackl, C., Sitch, S., Canadell, J. G., Ciais, P., Jackson, R. B., Alin, S. R., Anthoni, P., Barbero, L., Bates, N. R., Becker, M., Bellouin, N., Decharme, B., Bopp, L., Brasika, I. B. M., Cadule, P., Chamberlain, M. A., Chandra, N., Chau, T.-T.-T., Chevallier, F., Chini, L. P., Cronin, M., Dou, X., Enyo, K., Evans, W., Falk, S., Feely, R. A., Feng, L., Ford, D. J., Gasser, T., Ghattas, J., Gkritzalis, T., Grassi, G., Gregor, L., Gruber, N., Gürses, Ö., Harris, I., Hefner, M., Heinke, J., Houghton, R. A., Hurtt, G. C., Iida, Y., Ilyina, T., Jacobson, A. R., Jain, A., Jarníková, T., Jersild, A., Jiang, F., Jin, Z., Joos, F., Kato, E., Keeling, R. F., Kennedy, D., Klein Goldewijk, K., Knauer, J., Korsbakken, J. I., Körtzinger, A., Lan, X., Lefèvre, N., Li, H., Liu, J., Liu, Z., Ma, L., Marland, G., Mayot, N., McGuire, P. C., McKinley, G. A., Meyer, G., Morgan, E. J., Munro, D. R., Nakaoka, S.-I., Niwa, Y., O'Brien, K. M., Olsen, A., Omar, A. M., Ono, T., Paulsen, M., Pierrot, D., Pocock, K., Poulter, B., Powis, C. M., Rehder, G., Resplandy, L., Robertson, E., Rödenbeck, C., Rosan, T. M., Schwinger, J., Séférian, R., Smallman, T. L., Smith, S. M., Sospedra-Alfonso, R., Sun, Q., Sutton, A. J., Sweeney, C., Takao, S., Tans, P. P., Tian, H., Tilbrook, B., Tsujino, H., Tubiello, F., van der Werf, G. R., van Ooijen, E., Wanninkhof, R., Watanabe, M., Wimart-Rousseau, C., Yang, D., Yang, X., Yuan, W., Yue, X., Zaehle, S., Zeng, J., and Zheng, B.: Global Carbon Budget 2023, Earth System Science Data, 15, 5301–5369, https://doi.org/10.5194/essd-15-5301-2023, 2023.

Gaillard, M., Vionnet, V., Lafaysse, M., Dumont, M., and Ginoux, P.: Improving Large-Scale Snow Albedo Modeling Using a Climatology of Light-Absorbing Particle Deposition, The Cryosphere, 19, 769–792, https://doi.org/10.5194/tc-19-769-2025, 2025.

Genthon, C., Six, D., Favier, V., Lazzara, M., and Keller, L.: Atmospheric Temperature Measurement Biases on the Antarctic Plateau, https://doi.org/10.1175/JTECH-D-11-00095.1, 2011.

https://doi.org/10.5194/egusphere-2026-492
Preprint. Discussion started: 23 April 2026

Georges, C. and Kaser, G.: Ventilated and Unventilated Air Temperature Measurements for Glacier-Climate Studies on a Tropical High Mountain Site, Journal of Geophysical Research: Atmospheres, 107, ACL 15–1–ACL 15–10, https://doi.org/10.1029/2002JD002503, 2002.

Gordon, M., Simon, K., and Taylor, P. A.: On Snow Depth Predictions with the Canadian Land Surface Scheme Including a Parametrization of Blowing Snow Sublimation, Atmosphere-Ocean, 44, 239–255, https://doi.org/10.3137/ao.440303, 2006.

Gornall, J. L., Jónsdóttir, I. S., Woodin, S. J., and Van der Wal, R.: Arctic Mosses Govern Below-Ground Environment and Ecosystem Processes, Oecologia, 153, 931–941, https://doi.org/10.1007/s00442-007-0785-0, 2007.

Gouttevin, I., Menegoz, M., Dominé, F., Krinner, G., Koven, C., Ciais, P., Tarnocai, C., and Boike, J.: How the Insulating Properties of Snow Affect Soil Carbon Distribution in the Continental Pan-Arctic Area, Journal of Geophysical Research: Biogeosciences, 117, G02 020, https://doi.org/10.1029/2011JG001916, 2012.

Gouttevin, I., Langer, M., Löwe, H., Boike, J., Proksch, M., and Schneebeli, M.: Observation and Modelling of Snow at a Polygonal Tundra Permafrost Site: Spatial Variability and Thermal Implications, The Cryosphere, 12, 3693–3717, https://doi.org/10.5194/tc-12-3693-2018, 2018.

Groffman, P. M., Driscoll, C. T., Fahey, T. J., Hardy, J. P., Fitzhugh, R. D., and Tierney, G. L.: Colder Soils in a Warmer World: A Snow Manipulation Study in a Northern Hardwood Forest Ecosystem, Biogeochemistry, 56, 135–150, 2001.

Hedstrom, N. R. and Pomeroy, J. W.: Measurements and Modelling of Snow Interception in the Boreal Forest, Hydrological Processes, 12, 1611–1625, https://doi.org/10.1002/(SICI)1099-1085(199808/09)12:10/11<1611::AID-HYP684>3.0.CO;2-4, 1998.

Hengl, T., de Jesus, J. M., Heuvelink, G. B. M., Gonzalez, M. R., Kilibarda, M., Blagotić, A., Shangguan, W., Wright, M. N., Geng, X., Bauer-Marschallinger, B., Guevara, M. A., Vargas, R., MacMillan, R. A., Batjes, N. H., Leenaars, J. G. B., Ribeiro, E., Wheeler, I., Mantel, S., and Kempen, B.: SoilGrids250m: Global Gridded Soil Information Based on Machine Learning, PLOS ONE, 12, e0169 748, https://doi.org/10.1371/journal.pone.0169748, 2017.

Huwald, H., Higgins, C. W., Boldi, M.-O., Bou-Zeid, E., Lehning, M., and Parlange, M. B.: Albedo Effect on Radiative Errors in Air Temperature Measurements, Water Resources Research, 45, https://doi.org/10.1029/2008WR007600, 2009.

IPCC: Summary for Policymakers, in: Climate Change 2021: The Physical Science Basis. Contribution of Working Group I to the Sixth Assessment Report of the Intergovernmental Panel on Climate Change, pp. 3–32, Cambridge University Press, Cambridge, United Kingdom and New York, NY, USA, https://doi.org/10.1017/9781009157896.001, 2021.

Jafari, M., Gouttevin, I., Couttet, M., Wever, N., Michel, A., Sharma, V., Rossmann, L., Maass, N., Nicolaus, M., and Lehning, M.: The Impact of Diffusive Water Vapor Transport on Snow Profiles in Deep and Shallow Snow Covers and on Sea Ice, Frontiers in Earth Science, 8, 249, https://doi.org/10.3389/feart.2020.00249, 2020.

Jafari, M., Sharma, V., and Lehning, M.: Convection of Water Vapour in Snowpacks, Journal of Fluid Mechanics, 934, A38, https://doi.org/10.1017/jfm.2021.1146, 2022.

Jordan, R. E., Andreas, E. L., and Makshtas, A. P.: Heat Budget of Snow-Covered Sea Ice at North Pole 4, Journal of Geophysical Research: Oceans, 104, 7785–7806, https://doi.org/10.1029/1999JC900011, 1999.

King, J. C.: Some Measurements of Turbulence over an Antarctic Ice Shelf, Quarterly Journal of the Royal Meteorological Society, 116, 379–400, https://doi.org/10.1002/qj.49711649208, 1990.

Krinner, G., Derksen, C., Essery, R., Flanner, M., Hagemann, S., Clark, M., Hall, A., Rott, H., Brutel-Vuilmet, C., Kim, H., Ménard, C. B., Mudryk, L., Thackeray, C., Wang, L., Arduini, G., Balsamo, G., Bartlett, P., Boike, J., Boone, A., Chéruy, F., Colin, J., Cuntz, M., Dai, Y., Decharme, B., Derry, J., Ducharne, A., Dutra, E., Fang, X., Fierz, C., Ghattas, J., Gusev, Y., Haverd, V., Kontu, A., Lafaysse, M., Law, R.,

https://doi.org/10.5194/egusphere-2026-492
Preprint. Discussion started: 23 April 2026

Lawrence, D., Li, W., Marke, T., Marks, D., Ménégoz, M., Nasonova, O., Nitta, T., Niwano, M., Pomeroy, J., Raleigh, M. S., Schaedler, G., Semenov, V., Smirnova, T. G., Stacke, T., Strasser, U., Svenson, S., Turkov, D., Wang, T., Wever, N., Yuan, H., Zhou, W., and Zhu, D.: ESM-SnowMIP: Assessing Snow Models and Quantifying Snow-Related Climate Feedbacks, Geoscientific Model Development, 11, 5027–5049, https://doi.org/10.5194/gmd-11-5027-2018, 2018.

Lackner, G., Domine, F., Sarrazin, D., Nadeau, D., and Belke-Brea, M.: Hydrometeorological, Snow and Soil Data from a Low-Arctic Valley in the Forest-Tundra Ecotone in Northern Quebec, https://doi.org/10.1594/PANGAEA.946538, 2022.

Lalande, M.: SnowC2-CLASSIC-1D-analysis: Analysis and Figure-Generation Code (v0.1.0), Zenodo [code], https://doi.org/10.5281/zenodo.18154779, 2026a.

Lalande, M.: SnowC2-CLASSIC-1D: Model Configuration, Forcing Data, and Simulation Outputs, Zenodo [Data Set], https://doi.org/10.5281/zenodo.18175772, 2026b.

Lalande, M., Ménégoz, M., Krinner, G., Ottlé, C., and Cheruy, F.: Improving Climate Model Skill over High Mountain Asia by Adapting Snow Cover Parameterization to Complex-Topography Areas, The Cryosphere, 17, 5095–5130, https://doi.org/10.5194/tc-17-5095-2023, 2023.

Landry, C. C., Buck, K. A., Raleigh, M. S., and Clark, M. P.: Mountain System Monitoring at Senator Beck Basin, San Juan Mountains, Colorado: A New Integrative Data Source to Develop and Evaluate Models of Snow and Hydrologic Processes, Water Resources Research, 50, 1773–1788, https://doi.org/10.1002/2013WR013711, 2014.

Langlois, A., Bergeron, J., Brown, R., Royer, A., Harvey, R., Roy, A., Wang, L., and Thériault, N.: Evaluation of CLASS 2.7 and 3.5 Simulations of Snow Properties from the Canadian Regional Climate Model (CRCM4) over Québec, Canada*, Journal of Hydrometeorology, 15, 1325–1343, https://doi.org/10.1175/JHM-D-13-055.1, 2014.

Lehning, M., Bartelt, P., Brown, B., and Fierz, C.: A Physical SNOWPACK Model for the Swiss Avalanche Warning: Part III: Meteorological Forcing, Thin Layer Formation and Evaluation, Cold Regions Science and Technology, 35, 169–184, https://doi.org/10.1016/S0165-232X(02)00072-1, 2002a.

Lehning, M., Bartelt, P., Brown, B., Fierz, C., and Satyawali, P.: A Physical SNOWPACK Model for the Swiss Avalanche Warning: Part II. Snow Microstructure, Cold Regions Science and Technology, 35, 147–167, https://doi.org/10.1016/S0165-232X(02)00073-3, 2002b.

Lejeune, Y., Dumont, M., Panel, J.-M., Lafaysse, M., Lapalus, P., Le Gac, E., Lesaffre, B., and Morin, S.: 57 Years (1960–2017) of Snow and Meteorological Observations from a Mid-Altitude Mountain Site (Col de Porte, France, 1325 m of Altitude), Earth System Science Data, 11, 71–88, https://doi.org/10.5194/essd-11-71-2019, 2019.

Lemke, P., Ren, J., Alley, R., Allison, I., Carrasco, J., Flato, G., Fujii, Y., Kaser, G., Mote, P., Thomas, R., and Zhang, T.: Observations: Changes in Snow, Ice and Frozen Ground., in: Climate Change 2007: The Physical Science Basis. Contribution of Working Group I to the Fourth Assessment Report of the Intergovernmental Panel on Climate Change [Solomon, S., D. Qin, M. Manning, Z. Chen, M. Marquis, K.B. Averyt, M. Tignor and H.L. Miller, January 2007, Cambridge University Press, Cambridge, United Kingdom and New York, NY, USA., 2007.

Letts, M. G., Roulet, N. T., Comer, N. T., Skarupa, M. R., and Verseghy, D. L.: Parametrization of Peatland Hydraulic Properties for the Canadian Land Surface Scheme, Atmosphere-Ocean, 38, 141–160, https://doi.org/10.1080/07055900.2000.9649643, 2000.

Liston, G. E. and Hiemstra, C. A.: The Changing Cryosphere: Pan-Arctic Snow Trends (1979–2009), Journal of Climate, 24, 5691–5712, https://doi.org/10.1175/JCLI-D-11-00081.1, 2011.

Liston, G. E., Haehnel, R. B., Sturm, M., Hiemstra, C. A., Berezovskaya, S., and Tabler, R. D.: Simulating Complex Snow Distributions in Windy Environments Using SnowTran-3D, Journal of Glaciology, 53, 241–256, https://doi.org/10.3189/172756507782202865, 2007.

https://doi.org/10.5194/egusphere-2026-492
Preprint. Discussion started: 23 April 2026

Liston, G. E., Itkin, P., Stroeve, J., Tschudi, M., Stewart, J. S., Pedersen, S. H., Reinking, A. K., and Elder, K.: A Lagrangian Snow-Evolution System for Sea-Ice Applications (SnowModel-LG): Part I—Model Description, Journal of Geophysical Research: Oceans, 125, e2019JC015 913, https://doi.org/10.1029/2019JC015913, 2020.

Loth, B., Graf, H.-F., and Oberhuber, J. M.: Snow Cover Model for Global Climate Simulations, Journal of Geophysical Research, 98, 10 451, https://doi.org/10.1029/93JD00324, 1993.

Lynch-Stieglitz, M.: The Development and Validation of a Simple Snow Model for the GISS GCM, Journal of Climate, 7, 1842–1855, https://doi.org/10.1175/1520-0442(1994)007<1842:TDAVOA>2.0.CO;2, 1994.

Magnusson, J., Wever, N., Essery, R., Helbig, N., Winstral, A., and Jonas, T.: Evaluating Snow Models with Varying Process Representations for Hydrological Applications, Water Resources Research, 51, 2707–2723, https://doi.org/10.1002/2014WR016498, 2015.

Manabe, S.: CLIMATE AND THE OCEAN CIRCULATION: I. THE ATMOSPHERIC CIRCULATION AND THE HYDROLOGY OF THE EARTH'S SURFACE, Monthly Weather Review, 97, 739–774, https://doi.org/10.1175/1520-0493(1969)097<0739:CATOC>2.3.CO;2, 1969.

Marsh, P. and Woo, M.-K.: Wetting Front Advance and Freezing of Meltwater within a Snow Cover: 1. Observations in the Canadian Arctic, Water Resources Research, 20, 1853–1864, https://doi.org/10.1029/WR020i012p01853, 1984.

Martin, E. and Lejeune, Y.: Turbulent Fluxes above the Snow Surface, Annals of Glaciology, 26, 179–183, https://doi.org/10.3189/1998AoG26-1-179-183, 1998.

Mavrovic, A., Sonnentag, O., Lemmetyinen, J., Voigt, C., Rutter, N., Mann, P., Sylvain, J.-D., and Roy, A.: Environmental Controls of Winter Soil Carbon Dioxide Fluxes in Boreal and Tundra Environments, Biogeosciences, 20, 5087–5108, https://doi.org/10.5194/bg-20-5087-2023, 2023.

McGuire, A. D., Christensen, T. R., Hayes, D., Heroult, A., Euskirchen, E., Kimball, J. S., Koven, C., Lafleur, P., Miller, P. A., Oechel, W., Peylin, P., Williams, M., and Yi, Y.: An Assessment of the Carbon Balance of Arctic Tundra: Comparisons among Observations, Process Models, and Atmospheric Inversions, Biogeosciences, 9, 3185–3204, https://doi.org/10.5194/bg-9-3185-2012, 2012.

Melton, J. R. and Arora, V. K.: Competition between Plant Functional Types in the Canadian Terrestrial Ecosystem Model (CTEM) v. 2.0, Geoscientific Model Development, 9, 323–361, https://doi.org/10.5194/gmd-9-323-2016, 2016.

Melton, J. R., Arora, V. K., Wisernig-Cojoc, E., Seiler, C., Fortier, M., Chan, E., and Teckentrup, L.: CLASSIC v1.0: The Open-Source Community Successor to the Canadian Land Surface Scheme (CLASS) and the Canadian Terrestrial Ecosystem Model (CTEM) – Part 1: Model Framework and Site-Level Performance, Geoscientific Model Development, 13, 2825–2850, https://doi.org/10.5194/gmd-13-2825-2020, 2020.

Menard, C. and Essery, R.: ESM-SnowMIP Meteorological and Evaluation Datasets at Ten Reference Sites (in Situ and Bias Corrected Reanalysis Data), PANGAEA [Data Set], https://doi.org/10.1594/PANGAEA.897575, 2019.

Ménard, C. B., Essery, R., Pomeroy, J., Marsh, P., and Clark, D. B.: A Shrub Bending Model to Calculate the Albedo of Shrub-Tundra, Hydrological Processes, 28, 341–351, https://doi.org/10.1002/hyp.9582, 2014.

Ménard, C. B., Essery, R., Barr, A., Bartlett, P., Derry, J., Dumont, M., Fierz, C., Kim, H., Kontu, A., Lejeune, Y., Marks, D., Niwano, M., Raleigh, M., Wang, L., and Wever, N.: Meteorological and Evaluation Datasets for Snow Modelling at 10 Reference Sites: Description of in Situ and Bias-Corrected Reanalysis Data, Earth System Science Data, 11, 865–880, https://doi.org/10.5194/essd-11-865-2019, 2019.

Menard, C. B., Essery, R., Krinner, G., Arduini, G., Bartlett, P., Boone, A., Brutel-Vuilmet, C., Burke, E., Cuntz, M., Dai, Y., Decharme, B., Dutra, E., Fang, X., Fierz, C., Gusev, Y., Hagemann, S., Haverd, V., Kim, H., Lafaysse, M., Marke, T., Nasonova, O., Nitta, T., Niwano, M., Pomeroy, J., Schädler, G., Semenov, V. A., Smirnova, T., Strasser, U., Swenson, S., Turkov, D., Wever, N., and Yuan,

https://doi.org/10.5194/egusphere-2026-492
Preprint. Discussion started: 23 April 2026

H.: Scientific and Human Errors in a Snow Model Intercomparison, Bulletin of the American Meteorological Society, 102, E61–E79, https://doi.org/10.1175/BAMS-D-19-0329.1, 2021.

Meyer, G., Humphreys, E. R., Melton, J. R., Cannon, A. J., and Lafleur, P. M.: Simulating Shrubs and Their Energy and Carbon Dioxide Fluxes in Canada's Low Arctic with the Canadian Land Surface Scheme Including Biogeochemical Cycles (CLASSIC), Biogeosciences, 18, 3263–3283, https://doi.org/10.5194/bg-18-3263-2021, 2021.

Miner, K. R., Turetsky, M. R., Malina, E., Bartsch, A., Tamminen, J., McGuire, A. D., Fix, A., Sweeney, C., Elder, C. D., and Miller, C. E.: Permafrost Carbon Emissions in a Changing Arctic, Nature Reviews Earth & Environment, 3, 55–67, https://doi.org/10.1038/s43017-021-00230-3, 2022.

Mohammadzadeh Khani, H.: Sensitivity of the Snow Cover and the Active Layer to Landscape Spatial Heterogeneity and Climate Change over a Canadian High Arctic Tundra Environment = Sensibilité de La Couverture de Neige et de La Couche Active à l'hétérogénéité Spatiale Du Paysage et Aux Changements Climatiques Sur Un Environnement Canadien de Toundra Dans Le Haut Arctique, Ph.D. thesis, Université du Québec à Montréal;Université du Québec à Trois-Rivières, Montréal;Trois-Rivières, 2024.

Mohammadzadeh Khani, H., Kinnard, C., and Lévesque, E.: Historical Trends and Projections of Snow Cover over the High Arctic: A Review, Water, 14, 587, https://doi.org/10.3390/w14040587, 2022.

Mohammadzadeh Khani, H., Kinnard, C., Gascoin, S., and Lévesque, E.: Fine-Scale Environment Control on Ground Surface Temperature and Thaw Depth in a High Arctic Tundra Landscape, Permafrost and Periglacial Processes, 34, 467–480, https://doi.org/10.1002/ppp.2203, 2023.

Morin, S., Lejeune, Y., Lesaffre, B., Panel, J.-M., Poncet, D., David, P., and Sudul, M.: An 18-Yr Long (1993–2011) Snow and Meteorological Dataset from a Mid-Altitude Mountain Site (Col de Porte, France, 1325 m Alt.) for Driving and Evaluating Snowpack Models, Earth System Science Data, 4, 13–21, https://doi.org/10.5194/essd-4-13-2012, 2012.

Morino, S., Kurita, N., Hirasawa, N., Motoyama, H., Sugiura, K., Lazzara, M., Mikolajczyk, D., Welhouse, L., Keller, L., and Weidner, G.: Comparison of Ventilated and Unventilated Air Temperature Measurements in Inland Dronning Maud Land on the East Antarctic Plateau, https://doi.org/10.1175/JTECH-D-21-0107.1, 2021.

Morris, E. M., Anderson, P. S., Bader, H.-P., Weilnmann, P., and Blight, C.: Modelling Mass and Energy Exchange over Polar Snow Using the DAISY Model, 223, pp. 53–60, International Association of Hydrological Sciences, Wallingford, 1994.

Mudryk, L., Santolaria-Otín, M., Krinner, G., Ménégoz, M., Derksen, C., Brutel-Vuilmet, C., Brady, M., and Essery, R.: Historical Northern Hemisphere Snow Cover Trends and Projected Changes in the CMIP6 Multi-Model Ensemble, The Cryosphere, 14, 2495–2514, https://doi.org/10.5194/tc-14-2495-2020, 2020.

Mudryk, L. R., Derksen, C., Howell, S., Laliberté, F., Thackeray, C., Sospedra-Alfonso, R., Vionnet, V., Kushner, P. J., and Brown, R.: Canadian Snow and Sea Ice: Historical Trends and Projections, The Cryosphere, 12, 1157–1176, https://doi.org/10.5194/tc-12-1157-2018, 2018.

Natali, S. M., Watts, J. D., Rogers, B. M., Potter, S., Ludwig, S. M., Selbmann, A.-k., Sullivan, P. F., Abbott, B. W., Arndt, K. A., Birch, L., Björkman, M. P., Bloom, A. A., Celis, G., Christensen, T. R., Christiansen, C. T., Commane, R., Cooper, E. J., Crill, P., Czimczik, C., Davydov, S., Du, J., Egan, J. E., Elberling, B., Euskirchen, E. S., Friborg, T., Genet, H., Göckede, M., Goodrich, J. P., Grogan, P., Helbig, M., Jafarov, E. E., Jastrow, J. D., Kalhori, A. A. M., Kim, Y., Kimball, J. S., Kutzbach, L., Lara, M. J., Larsen, K. S., Lee, B.-y., Liu, Z., Loranty, M. M., Lund, M., Lupascu, M., Madani, N., Malhotra, A., Matamala, R., McFarland, J., McGuire, A. D., Michelsen, A., Minions, C., Oechel, W. C., Olefeldt, D., Parmentier, F.-J. W., Pirk, N., Poulter, B., Quinton, W., Rezanezhad, F., Risk, D., Sachs, T., Schaefer, K., Schmidt, N. M., Schuur, E. A. G., Semenchuk, P. R., Shaver, G., Sonnentag, O., Starr, G., Treat, C. C., Waldrop, M. P., Wang, Y., Welker,

https://doi.org/10.5194/egusphere-2026-492
Preprint. Discussion started: 23 April 2026

J., Wille, C., Xu, X., Zhang, Z., Zhuang, Q., and Zona, D.: Large Loss of CO2 in Winter Observed across the Northern Permafrost Region, Nature Climate Change, 9, 852–857, https://doi.org/10.1038/s41558-019-0592-8, 2019.

Niu, G.-Y. and Yang, Z.-L.: An Observation-Based Formulation of Snow Cover Fraction and Its Evaluation over Large North American River Basins, Journal of Geophysical Research, 112, D21 101, https://doi.org/10.1029/2007JD008674, 2007.

Niwano, M., Aoki, T., Kuchiki, K., Hosaka, M., and Kodama, Y.: Snow Metamorphism and Albedo Process (SMAP) Model for Climate Studies: Model Validation Using Meteorological and Snow Impurity Data Measured at Sapporo, Japan, Journal of Geophysical Research: Earth Surface, 117, F03 008, https://doi.org/10.1029/2011JF002239, 2012.

Pan, X., Yang, D., Li, Y., Barr, A., Helgason, W., Hayashi, M., Marsh, P., Pomeroy, J., and Janowicz, R. J.: Bias Corrections of Precipitation Measurements across Experimental Sites in Different Ecoclimatic Regions of Western Canada, The Cryosphere, 10, 2347–2360, https://doi.org/10.5194/tc-10-2347-2016, 2016.

Park, H., Fedorov, A. N., Zheleznyak, M. N., Konstantinov, P. Y., and Walsh, J. E.: Effect of Snow Cover on Pan-Arctic Permafrost Thermal Regimes, Climate Dynamics, 44, 2873–2895, https://doi.org/10.1007/s00382-014-2356-5, 2015.

Pedersen, S. H., Bentzen, T. W., Reinking, A. K., Liston, G. E., Elder, K., Lenart, E. A., Prichard, A. K., and Welker, J. M.: Quantifying Effects of Snow Depth on Caribou Winter Range Selection and Movement in Arctic Alaska, Movement Ecology, 9, 48, https://doi.org/10.1186/s40462-021-00276-4, 2021.

Pomeroy, J. and Gray, D.: Snowcover: Accumulation, Relocation, and Management, vol. 7 of *NHRI Science Report*, ISBN 0-660-15816-7, 1995.

Pomeroy, J., Gray, D., and Landine, P.: The Prairie Blowing Snow Model: Characteristics, Validation, Operation, Journal of Hydrology, 144, 165–192, https://doi.org/10.1016/0022-1694(93)90171-5, 1993.

Pomeroy, J. W., Gray, D. M., Shook, K. R., Toth, B., Essery, R. L. H., Pietroniro, A., and Hedstrom, N.: An Evaluation of Snow Accumulation and Ablation Processes for Land Surface Modelling, Hydrological Processes, 12, 2339–2367, https://doi.org/10.1002/(SICI)1099-1085(199812)12:15<2339::AID-HYP800>3.0.CO;2-L, 1998.

Pulliainen, J., Aurela, M., Laurila, T., Aalto, T., Takala, M., Salminen, M., Kulmala, M., Barr, A., Heimann, M., Lindroth, A., Laaksonen, A., Derksen, C., Mäkelä, A., Markkanen, T., Lemmetyinen, J., Susiluoto, J., Dengel, S., Mammarella, I., Tuovinen, J.-P., and Vesala, T.: Early Snowmelt Significantly Enhances Boreal Springtime Carbon Uptake, Proceedings of the National Academy of Sciences, 114, 11 081–11 086, https://doi.org/10.1073/pnas.1707889114, 2017.

Pulliainen, J., Luojus, K., Derksen, C., Mudryk, L., Lemmetyinen, J., Salminen, M., Ikonen, J., Takala, M., Cohen, J., Smolander, T., and Norberg, J.: Patterns and Trends of Northern Hemisphere Snow Mass from 1980 to 2018, Nature, 581, 294–298, https://doi.org/10.1038/s41586-020-2258-0, 2020.

Rantanen, M., Karpechko, A. Y., Lipponen, A., Nordling, K., Hyvärinen, O., Ruosteenoja, K., Vihma, T., and Laaksonen, A.: The Arctic Has Warmed Nearly Four Times Faster than the Globe since 1979, Communications Earth & Environment, 3, 168, https://doi.org/10.1038/s43247-022-00498-3, 2022.

Reba, M. L., Marks, D., Seyfried, M., Winstral, A., Kumar, M., and Flerchinger, G.: A Long-Term Data Set for Hydrologic Modeling in a Snow-Dominated Mountain Catchment, Water Resources Research, 47, W07 702, https://doi.org/10.1029/2010WR010030, 2011.

Réveillet, M., Dumont, M., Gascoin, S., Lafaysse, M., Nabat, P., Ribes, A., Nheili, R., Tuzet, F., Ménégoz, M., Morin, S., Picard, G., and Ginoux, P.: Black Carbon and Dust Alter the Response of Mountain Snow Cover under Climate Change, Nature Communications, 13, 5279, https://doi.org/10.1038/s41467-022-32501-y, 2022.

https://doi.org/10.5194/egusphere-2026-492
Preprint. Discussion started: 23 April 2026

Robinson, D. and Frei, A.: Seasonal Variability of Northern Hemisphere Snow Extent Using Visible Satellite Data, The Professional Geographer, 52, 307–315, https://doi.org/10.1111/0033-0124.00226, 2000.

Royer, A., Domine, F., Roy, A., Langlois, A., Marchand, N., and Davesne, G.: New Northern Snowpack Classification Linked to Vegetation Cover on a Latitudinal Mega-Transect across Northeastern Canada, Écoscience, 28, 225–242, https://doi.org/10.1080/11956860.2021.1898775, 2021a.

Royer, A., Picard, G., Vargel, C., Langlois, A., Gouttevin, I., and Dumont, M.: Improved Simulation of Arctic Circumpolar Land Area Snow Properties and Soil Temperatures, Frontiers in Earth Science, 9, 1–19, https://doi.org/10.3389/feart.2021.685140, 2021b.

Schuur, E. A., Abbott, B. W., Commane, R., Ernakovich, J., Euskirchen, E., Hugelius, G., Grosse, G., Jones, M., Koven, C., Leshyk, V., Lawrence, D., Loranty, M. M., Mauritz, M., Olefeldt, D., Natali, S., Rodenhizer, H., Salmon, V., Schädel, C., Strauss, J., Treat, C., and Turetsky, M.: Permafrost and Climate Change: Carbon Cycle Feedbacks From the Warming Arctic, Annual Review of Environment and Resources, 47, 343–371, https://doi.org/10.1146/annurev-environ-012220-011847, 2022.

Seiler, C., Melton, J. R., Arora, V. K., and Wang, L.: CLASSIC v1.0: The Open-Source Community Successor to the Canadian Land Surface Scheme (CLASS) and the Canadian Terrestrial Ecosystem Model (CTEM) – Part 2: Global Benchmarking, Geoscientific Model Development, 14, 2371–2417, https://doi.org/10.5194/gmd-14-2371-2021, 2021.

Serreze, M. C. and Barry, R. G.: Processes and Impacts of Arctic Amplification: A Research Synthesis, Global and Planetary Change, 77, 85–96, https://doi.org/10.1016/j.gloplacha.2011.03.004, 2011.

Shangguan, W., Hengl, T., Mendes de Jesus, J., Yuan, H., and Dai, Y.: Mapping the Global Depth to Bedrock for Land Surface Modeling, Journal of Advances in Modeling Earth Systems, 9, 65–88, https://doi.org/10.1002/2016MS000686, 2017.

Shrestha, M., Wang, L., Koike, T., Xue, Y., and Hirabayashi, Y.: Improving the Snow Physics of WEB-DHM and Its Point Evaluation at the SnowMIP Sites, Hydrology and Earth System Sciences, 14, 2577–2594, https://doi.org/10.5194/hess-14-2577-2010, 2010.

Simson, A., Löwe, H., and Kowalski, J.: Elements of Future Snowpack Modeling – Part 2: A Modular and Extendable Eulerian–Lagrangian Numerical Scheme for Coupled Transport, Phase Changes and Settling Processes, The Cryosphere, 15, 5423–5445, https://doi.org/10.5194/tc-15-5423-2021, 2021.

Still, C. J., Berry, J. A., Collatz, G. J., and DeFries, R. S.: Global Distribution of C3 and C4 Vegetation: Carbon Cycle Implications, Global Biogeochemical Cycles, 17, 6–1–6–14, https://doi.org/10.1029/2001GB001807, 2003.

Stuecker, M. F., Bitz, C. M., Armour, K. C., Proistosescu, C., Kang, S. M., Xie, S.-P., Kim, D., McGregor, S., Zhang, W., Zhao, S., Cai, W., Dong, Y., and Jin, F.-F.: Polar Amplification Dominated by Local Forcing and Feedbacks, Nature Climate Change, 8, 1076–1081, https://doi.org/10.1038/s41558-018-0339-y, 2018.

Sturm, M. and Benson, C. S.: Vapor Transport, Grain Growth and Depth-Hoar Development in the Subarctic Snow, Journal of Glaciology, 43, 42–59, https://doi.org/10.3189/S0022143000002793, 1997.

Sturm, M., Holmgren, J., König, M., and Morris, K.: The Thermal Conductivity of Seasonal Snow, Journal of Glaciology, 43, 26–41, https://doi.org/10.3189/S0022143000002781, 1997.

Sturm, M., Holmgren, J., McFadden, J. P., Liston, G. E., Chapin, F. S., and Racine, C. H.: Snow–Shrub Interactions in Arctic Tundra: A Hypothesis with Climatic Implications, Journal of Climate, 14, 336–344, https://doi.org/10.1175/1520-0442(2001)014<0336:SSIIAT>2.0.CO;2, 2001.

Sun, S., Jin, J., and Xue, Y.: A Simple Snow-Atmosphere-Soil Transfer Model, Journal of Geophysical Research: Atmospheres, 104, 19 587–19 597, https://doi.org/10.1029/1999JD900305, 1999.

https://doi.org/10.5194/egusphere-2026-492
Preprint. Discussion started: 23 April 2026

Swart, N. C., Cole, J. N. S., Kharin, V. V., Lazare, M., Scinocca, J. F., Gillett, N. P., Anstey, J., Arora, V., Christian, J. R., Hanna, S., Jiao, Y., Lee, W. G., Majaess, F., Saenko, O. A., Seiler, C., Seinen, C., Shao, A., Sigmond, M., Solheim, L., von Salzen, K., Yang, D., and Winter, B.: The Canadian Earth System Model Version 5 (CanESM5.0.3), Geoscientific Model Development, 12, 4823–4873, https://doi.org/10.5194/gmd-12-4823-2019, 2019.

Swenson, S. C. and Lawrence, D. M.: A New Fractional Snow-Covered Area Parameterization for the Community Land Model and Its Effect on the Surface Energy Balance, Journal of Geophysical Research: Atmospheres, 117, D21 107, https://doi.org/10.1029/2012JD018178, 2012.

Tabler, R. D., Benson, C. S., Santana, B. W., and Ganguly, P.: Estimating Snow Transport from Wind Speed Records: Estimates versus Measurements at Prudhoe Bay, Alaska, in: 58th Annual Western Snow Conference, Proceedings of the 58th Annual Western Snow Conference, Western Snow Conference, Sacramento, California, 1990.

Terzago, S., Andreoli, V., Arduini, G., Balsamo, G., Campo, L., Cassardo, C., Cremonese, E., Dolia, D., Gabellani, S., von Hardenberg, J., Morra di Cella, U., Palazzi, E., Piazzi, G., Pogliotti, P., and Provenzale, A.: Sensitivity of Snow Models to the Accuracy of Meteorological Forcings in Mountain Environments, Hydrology and Earth System Sciences, 24, 4061–4090, https://doi.org/10.5194/hess-24-4061-2020, 2020.

Tutton, R., Dakin, B., Essery, R., Griffith, J., Hould-Gosselin, G., Marsh, P., Sonnentag, O., Thorne, R., and Walker, B.: A hydrometeorological dataset from the taiga-tundra ecotone in the western Canadian Arctic: Trail Valley Creek, Northwest Territories, Borealis [data set], https://doi.org/10.5683/SP3/BXV4DE, 2025.

V-Dutch: V-Dutch/TVCSnowCLM (v1), Zenodo [Data Set], https://doi.org/10.5281/zenodo.7137729, 2022.

Van Looy, K., Bouma, J., Herbst, M., Koestel, J., Minasny, B., Mishra, U., Montzka, C., Nemes, A., Pachepsky, Y. A., Padarian, J., Schaap, M. G., Tóth, B., Verhoef, A., Vanderborght, J., van der Ploeg, M. J., Weihermüller, L., Zacharias, S., Zhang, Y., and Vereecken, H.: Pedotransfer Functions in Earth System Science: Challenges and Perspectives, Reviews of Geophysics, 55, 1199–1256, https://doi.org/10.1002/2017RG000581, 2017.

Vavrus, S.: The Role of Terrestrial Snow Cover in the Climate System, Climate Dynamics, 29, 73–88, https://doi.org/10.1007/s00382-007-0226-0, 2007.

Vereecken, H., Weynants, M., Javaux, M., Pachepsky, Y., Schaap, M. G., and van Genuchten, M.Th.: Using Pedotransfer Functions to Estimate the van Genuchten–Mualem Soil Hydraulic Properties: A Review, Vadose Zone Journal, 9, 795–820, https://doi.org/10.2136/vzj2010.0045, 2010.

Vernekar, A. D., Zhou, J., and Shukla, J.: The Effect of Eurasian Snow Cover on the Indian Monsoon, Journal of Climate, 8, 248–266, https://doi.org/10.1175/1520-0442(1995)008<0248:TEOESC>2.0.CO;2, 1995.

Verseghy, D., Brown, R., and Wang, L.: Evaluation of CLASS Snow Simulation over Eastern Canada, Journal of Hydrometeorology, 18, 1205–1225, https://doi.org/10.1175/JHM-D-16-0153.1, 2017.

Verseghy, D. L.: Class—A Canadian Land Surface Scheme for GCMS. I. Soil Model, International Journal of Climatology, 11, 111–133, https://doi.org/10.1002/joc.3370110202, 1991.

Vionnet, V., Brun, E., Morin, S., Boone, A., Faroux, S., Le Moigne, P., Martin, E., and Willemet, J. M.: The Detailed Snowpack Scheme Crocus and Its Implementation in SURFEX v7.2, Geoscientific Model Development, 5, 773–791, https://doi.org/10.5194/gmd-5-773-2012, 2012.

Walter, B., Weigel, H., Wahl, S., and Löwe, H.: Wind Tunnel Experiments to Quantify the Effect of Aeolian Snow Transport on the Surface Snow Microstructure, The Cryosphere, 18, 3633–3652, https://doi.org/10.5194/tc-18-3633-2024, 2024.

https://doi.org/10.5194/egusphere-2026-492
Preprint. Discussion started: 23 April 2026

Wang, L., Mudryk, L., Melton, J. R., Mortimer, C., Cole, J., Meyer, G., Bartlett, P., and Lalande, M.: Impact of Topography and Meteorological Forcing on Snow Simulation in the Canadian Land Surface Scheme Including Biogeochemical Cycles (CLASSIC), EGUsphere, pp. 1–37, https://doi.org/10.5194/egusphere-2025-1264, 2025.

Wang, T., Ottlé, C., Boone, A., Ciais, P., Brun, E., Morin, S., Krinner, G., Piao, S., and Peng, S.: Evaluation of an Improved Intermediate Complexity Snow Scheme in the ORCHIDEE Land Surface Model, Journal of Geophysical Research: Atmospheres, 118, 6064–6079, https://doi.org/10.1002/jgrd.50395, 2013.

Wever, N.: Weissfluhjoch Dataset for ESM-SnowMIP, EnviDat [Data Set], https://doi.org/10.16904/16, 2017.

Wever, N., Schmid, L., Heilig, A., Eisen, O., Fierz, C., and Lehning, M.: Verification of the Multi-Layer SNOWPACK Model with Different Water Transport Schemes, The Cryosphere, 9, 2271–2293, https://doi.org/10.5194/tc-9-2271-2015, 2015.

Wever, N., Vera Valero, C., and Techel, F.: Coupled Snow Cover and Avalanche Dynamics Simulations to Evaluate Wet Snow Avalanche Activity, Journal of Geophysical Research: Earth Surface, 123, 1772–1796, https://doi.org/10.1029/2017JF004515, 2018.

Woolley, G. J., Rutter, N., Wake, L., Vionnet, V., Derksen, C., Essery, R., Marsh, P., Tutton, R., Walker, B., Lafaysse, M., and Pritchard, D.: Multi-Physics Ensemble Modelling of Arctic Tundra Snowpack Properties, The Cryosphere, 18, 5685–5711, https://doi.org/10.5194/tc-18-5685-2024, 2024.

Wösten, J. H. M., Pachepsky, Ya. A., and Rawls, W. J.: Pedotransfer Functions: Bridging the Gap between Available Basic Soil Data and Missing Soil Hydraulic Characteristics, Journal of Hydrology, 251, 123–150, https://doi.org/10.1016/S0022-1694(01)00464-4, 2001.

Xu, L. and Dirmeyer, P.: Snow-Atmosphere Coupling Strength in a Global Atmospheric Model, Geophysical Research Letters, 38, L13 401, https://doi.org/10.1029/2011GL048049, 2011.

Xue, Y., Sun, S., Kahan, D. S., and Jiao, Y.: Impact of Parameterizations in Snow Physics and Interface Processes on the Simulation of Snow Cover and Runoff at Several Cold Region Sites, Journal of Geophysical Research: Atmospheres, 108, 2002JD003 174, https://doi.org/10.1029/2002JD003174, 2003.

Yang, J., Liu, Q., Dai, W., and Ding, R.: A Temperature Error Correction Method for a Naturally Ventilated Radiation Shield, Journal of Atmospheric and Solar-Terrestrial Physics, 149, 40–45, https://doi.org/10.1016/j.jastp.2016.09.010, 2016.

Yang, Z.-L. and Niu, G.-Y.: The Versatile Integrator of Surface and Atmosphere Processes, Global and Planetary Change, 38, 175–189, https://doi.org/10.1016/S0921-8181(03)00028-6, 2003.

Yen, Y.-C.: Sensible Heat Flux Measurements Near A Cold Surface, Tech. Rep. CRREL Report 95-22, U.S. Army Corps of Engineers, Hanover, New Hampshire, 1995.

Yokohata, T., Saito, K., Takata, K., Nitta, T., Satoh, Y., Hajima, T., Sueyoshi, T., and Iwahana, G.: Model Improvement and Future Projection of Permafrost Processes in a Global Land Surface Model, Progress in Earth and Planetary Science, 7, 69, https://doi.org/10.1186/s40645-020-00380-w, 2020.

Zhang, T.: Influence of the Seasonal Snow Cover on the Ground Thermal Regime: An Overview, Reviews of Geophysics, 43, RG4002, https://doi.org/10.1029/2004RG000157, 2005.